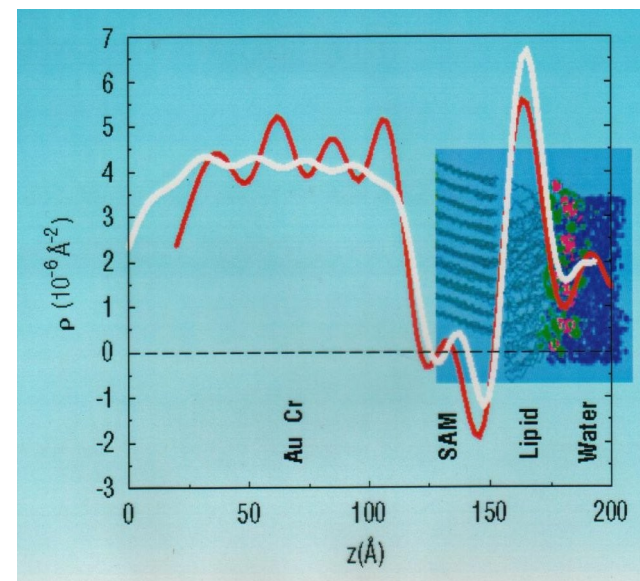
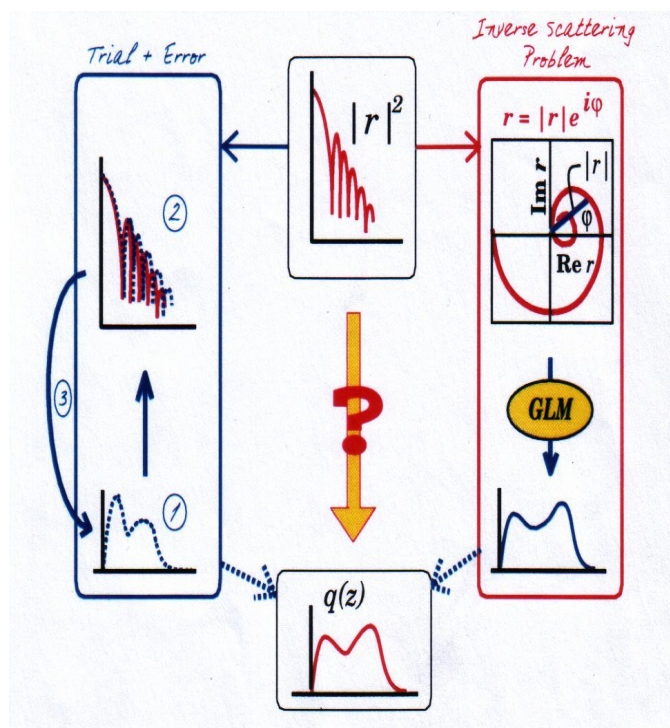
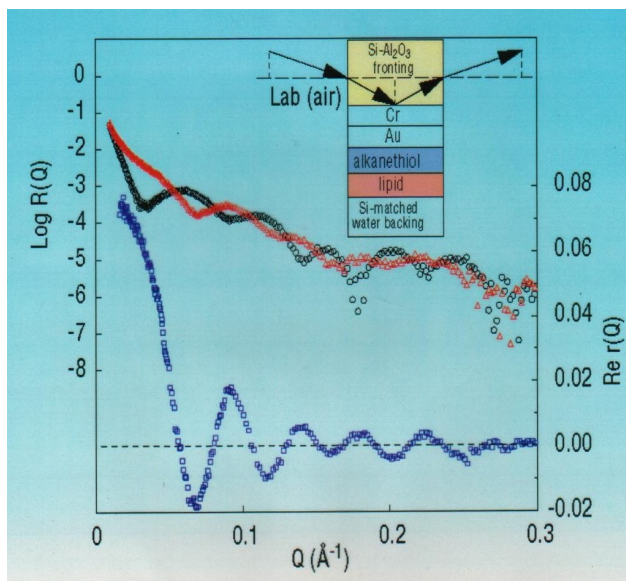


# Beauty is only skin deep; probing thin film and membrane structure by neutron reflection

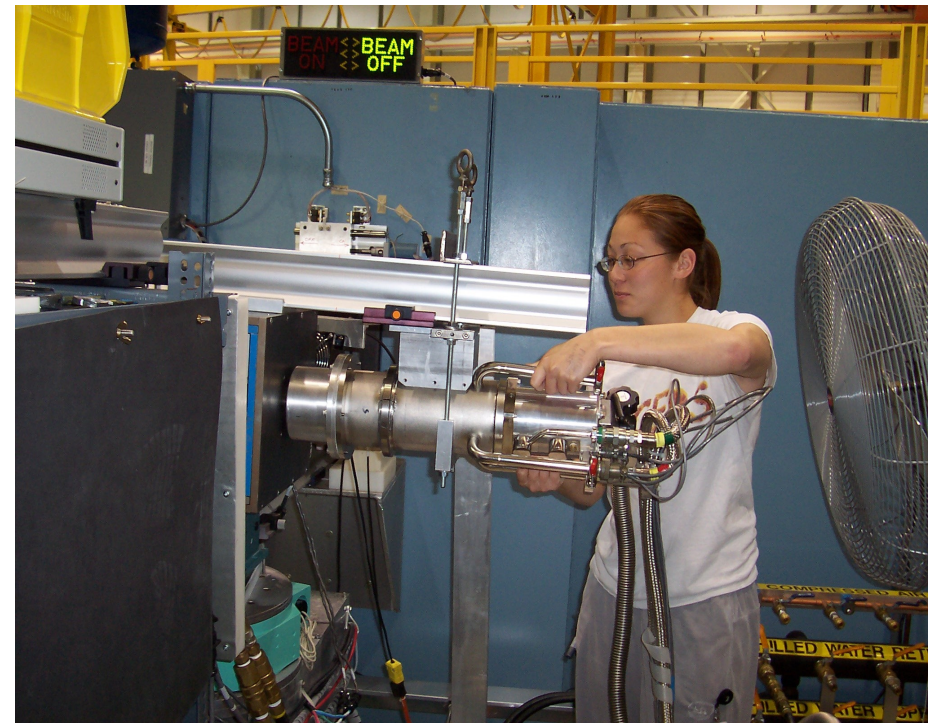
C.F.Majkrzak  
*NIST Center for Neutron Research*  
 September 10, 2010



# NIST Center for Neutron Research

## Surface and Interfacial Science Team

Bulent Akgun	Susan Krueger
Norm Berk	Kathryn Krycka
Julie Borchers	Brian Maranville
Joe Dura	Ella Mihailescu
Frank Heinrich	Sushil Satija
Paul Kienzle	Hirsh Nanda
Brian Kirby	
Chuck Majkrzak	



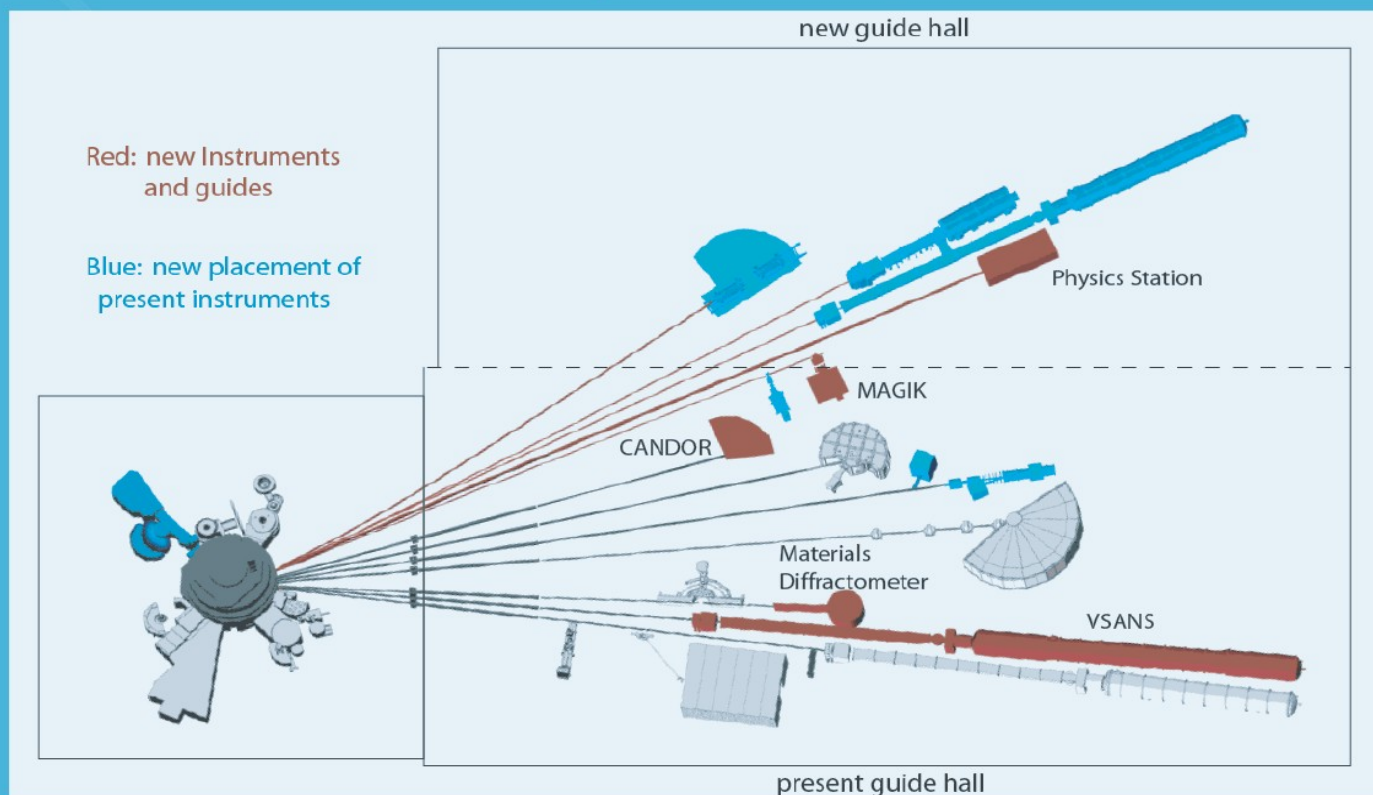
Former NCNR reflectometry team member Stephanie Moyerman prepares for a polarized neutron reflectivity measurement on the NG-1 instrument.

**Acknowledgements** -- many colleagues have contributed over the years to the development of neutron reflectometry. *Among* them:

Norm Berk, Susan Krueger, Ursula Perez-Salas, Paul Kienzle, Andreas Schreyer, Kevin O'Donovan, Stephen Holt, Jeremy Lakey, Anton Le Brun, Anne Plant, David Vanderah, Joe Dura, Michael Mackay, Jon Kiel, Brian Kirby, Brian Maranville, Frank Heinrich, Duncan McGillivray, Hirsh Nanda, Julie Borchers, Sushil Satija, . . .



# NCNR Expansion Activities in 2007



5 new instruments under development:  
**vSANS**: 40 m SANS for very small angle scattering measurements. **MAGIK**: multi-angle reflectometer with tagged beams: off-specular measurements of in-plane structure. **CANDOR**: chroma-

tic analysis of reflections at multiple specular angles: increased pattern resolution and rapid data acquisition.

**Materials Diffractometer**: for *in situ* reactions and real-time structure changes.

**Physics Station**: neutron imaging methods and precision neutron measurements.



## Outline of this presentation:

---

- <> Brief summary of specular neutron reflection theory
  - <> Phase-sensitive neutron reflection and direct inversion
  - <> Uncertainty due to data truncation and counting statistics
- 

- <> Example of phase-sensitive neutron reflectivity measurement -- organic photovoltaic films, lipid bilayer biomimetic membranes, giant magnetoresistive films
- 

- <> Interaction-free measurement -- can this quantum phenomenon be applied to neutron reflectivity measurements?
-

## Why is specular neutron reflectometry so special?

<> Neutron reflectometry (NR) is a valuable probe of the structure of both hard and soft condensed matter in thin film or multilayered form -- particularly for hydrogenous and magnetic materials. NR can see *beneath* the surface and provide quantitative structural information from *everywhere within* the film on a nanometer scale.

<> Both “forward” and “inverse” scattering problems for specular neutron reflection are mathematically solvable, exactly, from first-principles quantum theory. The mathematically unique solutions are thus far only possible in one dimension and for non-absorbing potentials of finite extent.

<> Phase-sensitive neutron specular reflectometry, employing references, enables direct inversion of composite reflectivity data sets to yield a unique scattering length density depth profile for an “unknown” film of interest, without fitting or any adjustable parameters.

<> The spatial resolution and accuracy of the SLD profile thereby obtained is limited only by the statistical uncertainty in the measured reflected intensities and truncation of the reflectivity data sets at the maximum value of wavevector transfer attainable.

# Principal Uses and Advantages of Neutron Reflectometry:

- \* For the specular condition, provides the chemical (isotopic) scattering length density (SLD) depth profile along the surface normal with a spatial resolution approaching half a nanometer.
- \* With polarized neutrons, provides the *vector* magnetization depth profile of a ferromagnetic material.
- \* Isotopic contrast, particularly applicable to hydrogen and deuterium.
- \* A non-destructive probe which can penetrate macroscopic distances through single crystalline substrates, making possible reflection studies of films in contact with liquids within a closed cell.
- \* As a consequence of the relatively weak interaction between the neutron and material, a remarkably accurate theoretical description of the reflection process and quantitative analysis of the data is possible, although the Born approximation is often not valid and an “exact” or “dynamical” formulation is required.

# **What distinguishes neutron reflectometry as a special diffraction technique?**

- > planar reflection geometry for scattering from thin films

## **What makes it a powerful probe for scientific investigations of condensed matter?**

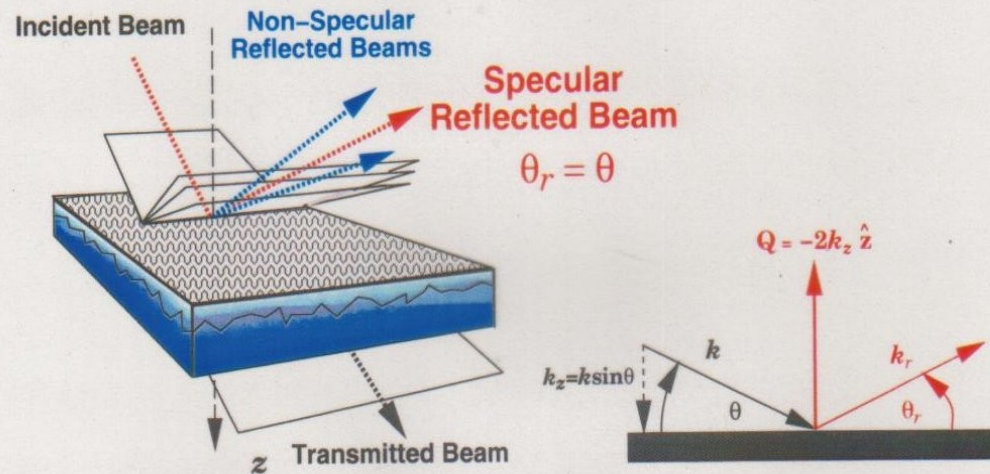
- > tailored samples synthesized by various deposition techniques (e.g., molecular beam epitaxy, chemical vapor deposition, Langmuir-Blodgett, self assembly, spin coating)
- > intense cold neutron sources and accurate and efficient measurement devices (e.g., for quantitative determination of wavevector transfer and polarization)
- > an accurate theoretical formalism for analysing reflectivity measurements
- > calculation capabilities (e.g., molecular dynamics simulation) for relating scattering length density profiles to corresponding compositional or magnetization distributions
- > the particular sensitivity of the neutron to different isotopes (notably hydrogen and deuterium) and atomic magnetic moments and also its high penetration length in condensed matter (the same properties that make the neutron so valuable in other scattering techniques)

> The great success in using neutron reflection/diffraction to study thin film systems of hard condensed matter, in particular the structures and fundamental interactions in magnetic materials, is largely due to the ability to tailor, with atomic-layer accuracy and precision, single-crystalline, layered sandwiches and superlattices (using vapor deposition techniques such as molecular beam epitaxy in ultra-high vacuum). Advances in film deposition techniques and lithography continue at a remarkable rate.

> Similarly, neutron reflectometry in principle can be applied as a probe to further our understanding of the structure and function of molecules in lipid membranes, of relevance in biology and bioengineering, when comparable control over the fabrication of model systems is achieved. Great progress has been made toward realizing this goal in practice. However, we are still at a relatively early stage of development in our ability to engineer soft condensed matter films on atomic and nanometer scales. Progress can be expected as efforts in creating and manipulating membrane / molecular systems accelerates.

> Employing phase-sensitive methods in reflectivity measurements ensures a unique scattering length density (SLD) depth profile. Additional application of hydrogen / deuterium substitution techniques and comparison with molecular dynamics calculations assures a correspondingly high degree of certainty of obtaining an unambiguous chemical composition depth profile.

$$\text{Reflectivity} = \frac{\text{Number of reflected neutrons}}{\text{Number of incident neutrons}} = |r|^2$$



**Specular reflection:**  $\bar{\rho}(z) = \langle \rho(x, y, z) \rangle_{xy}$

**Non-Specular reflection:**  $\Delta \rho(x, y, z) = \rho(x, y, z) - \bar{\rho}(z)$

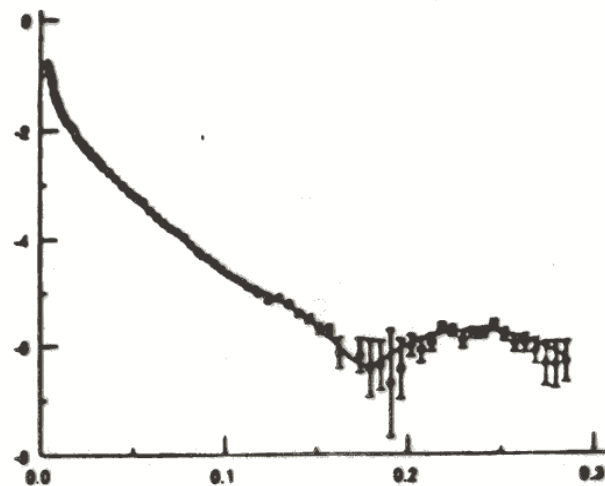
(AFTER N.F. BERK ET AL.)



Sedimentary rock layers in Pennsylvania (photo by Jerome Wyckoff):  
note biolayer at top and tethering structure at bottom.

$$Q = \frac{4\pi \sin \theta}{\lambda}$$

$\log_{10}(|r|^2)$



$$\vec{Q} = \vec{k}_f - \vec{k}_i$$

$\vec{k}_i$

$\theta$

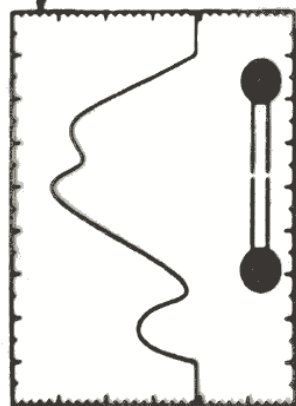
$\vec{k}_f$

$\theta$

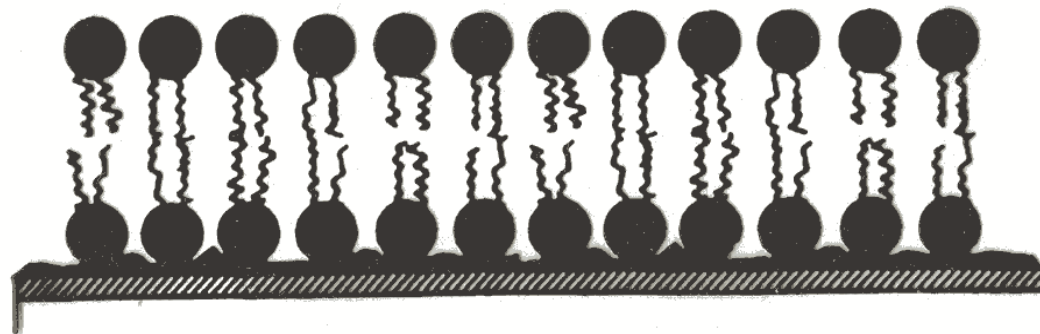
$$\rho = Nb$$

$$(\text{SLD}) = \left( \frac{\# \text{ ATOMS}}{\text{U. VOL.}} \right)$$

• (SCALAR  
SCATT. LENGTH)  
~ -2 → 10



$z$



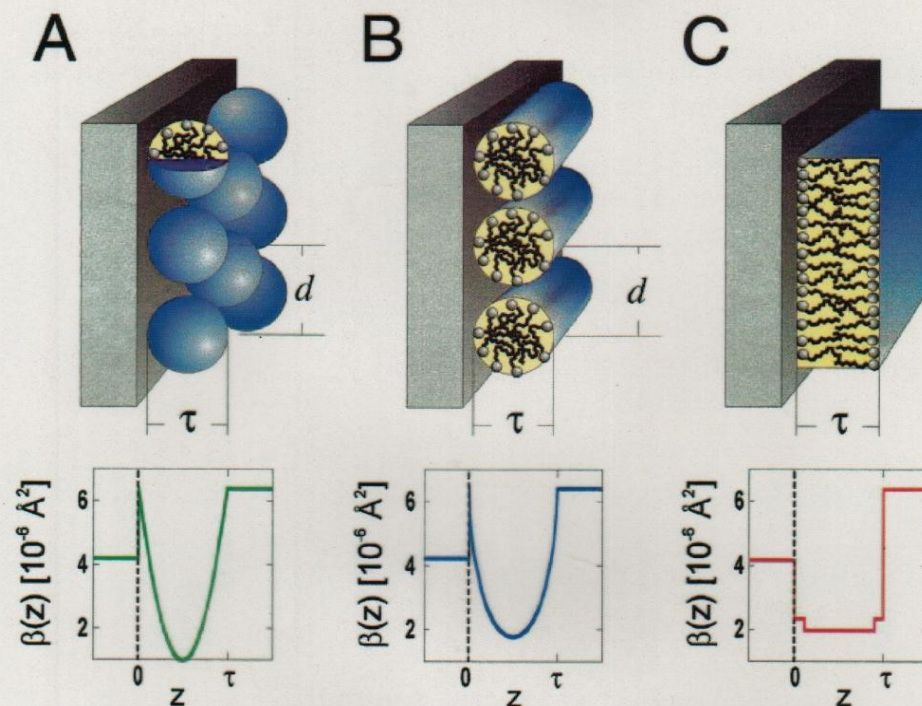


FIG. 1. (Color) Schematic diagram of adsorbed layer structures consisting of (A) spherical micelles, (B) cylindrical micelles, and (C) a bilayer, including the film thickness  $\tau$  and interaggregate spacing  $d$ . Also shown are examples of neutron scattering length density profiles normal to the interface,  $\beta(z)$ , corresponding to each structure at the quartz/D<sub>2</sub>O interface at a fractional surface coverage of 0.55. The head-group and alkyl tails of the surfactants have different scattering length densities, but because of the arrangement of the molecules this is only apparent in the bilayer  $\beta(z)$ .

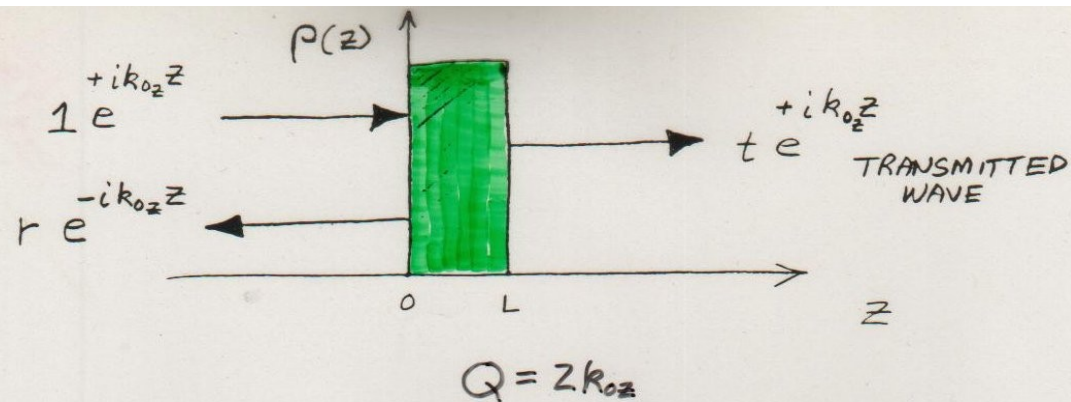
single-crystal quartz block and reflected from the quartz-solution interface were recorded as a function of angle of incidence. The off-specular background, including any signal due to scattering from the bulk solution [15], was subtracted to give the reflection coefficient of the surfactant-coated interface. All solutions used were above their critical micelle

or aggregation concentration, a condition which leads to a saturated adsorbed film at the solid-solution interface.

The cationic surfactant tetradecyltrimethylammonium bromide (TTAB) forms nearly spherical micellar aggregates consisting of approximately 80 molecules in bulk solution. Small angle neutron-scattering measurements [16] give mi-



FIG. 2. 200×200-nm<sup>2</sup> AFM tip deflection images of (A) spherical TTAB aggregates adsorbed onto quartz from water solution, (B) cylindrical TTAB aggregates adsorbed onto quartz from an aqueous 200mM NaBr solution, and (C) planar DDAB bilayer adsorbed onto quartz from water solution. Long-wavelength undulations visible in (B) and (C) arise from roughness in the underlying quartz.



FROM THE WAVE EQUATION,  
IT IS POSSIBLE TO FIND  
A SOLUTION FOR THE  
REFLECTION AMPLITUDE IN  
INTEGRAL FORM  
(SEE ARTICLE PAGES) :

$$r(Q) = \frac{4\pi}{iQ} \int_{-\infty}^{+\infty} \psi(z) p(z) e^{+ik_0z} dz$$

WHAT IS LOCALIZED AT  $z$  IN  
THE SLD PROFILE  $p(z)$  IN  
"REAL" SPACE, IS DISTRIBUTED  
OVER THE REFLECTION AMPLITUDE  
 $r(Q)$  IN THE RELATED SCATTERING  
OR "RECIPROCAL" SPACE

$\psi(z)$  INSIDE THE MEDIUM  
IS GENERALLY UNKNOWN:

BORN APPROXIMATION REPLACES  
 $\psi(z)$  WITH THE INCIDENT  
WAVE FUNCTION  $e^{+ik_0 z}$  BASED  
ON THE ASSUMPTION THAT  
 $\psi(z)$  IS NOT SIGNIFICANTLY  
DISTORTED FROM THE FREE  
SPACE FORM (WEAK  
INTERACTION): THEN

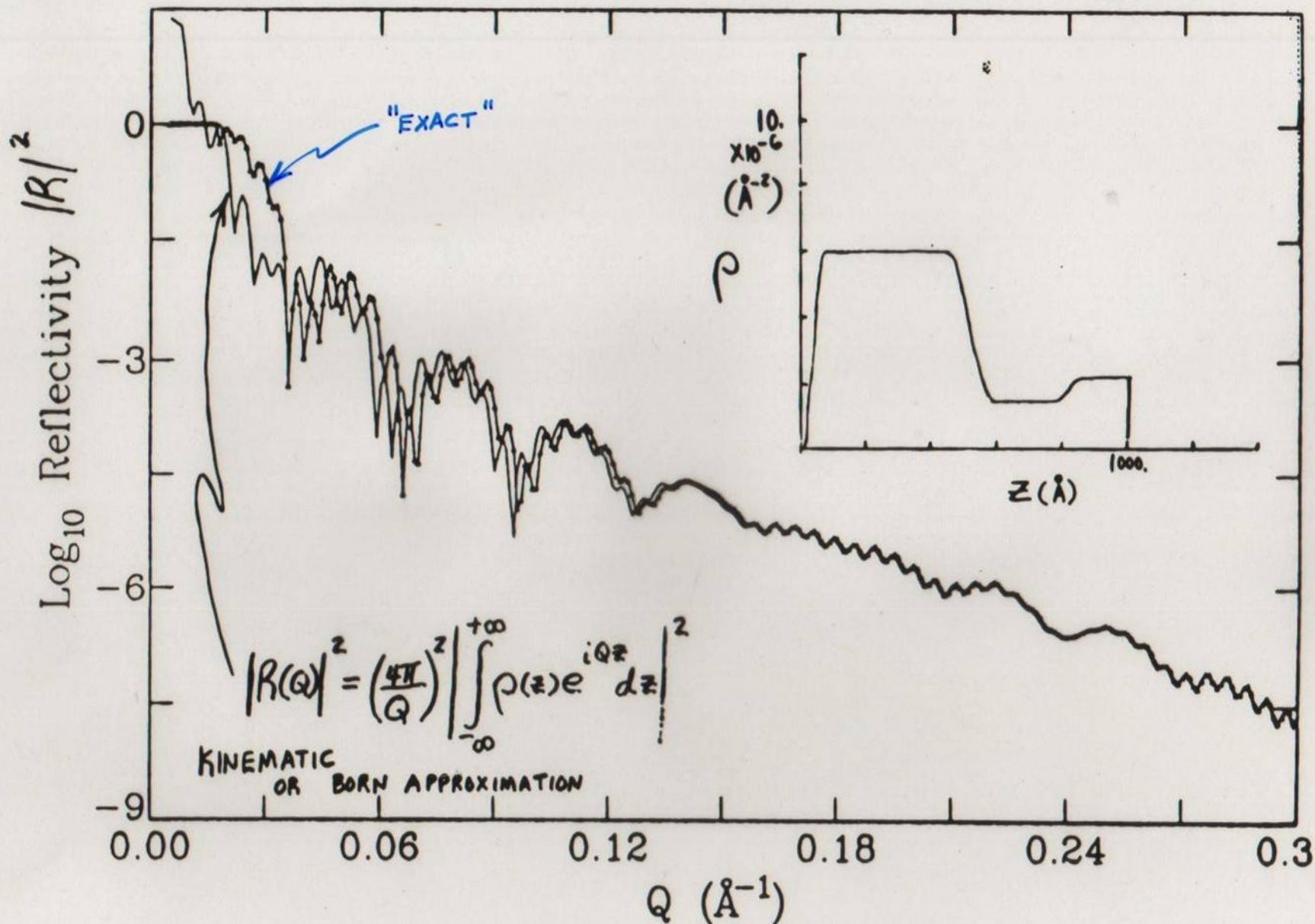
$$r(Q) \approx \frac{4\pi}{iQ} \int_{-\infty}^{+\infty} p(z) e^{iQz} dz$$

FOURIER  
TRANSFORM

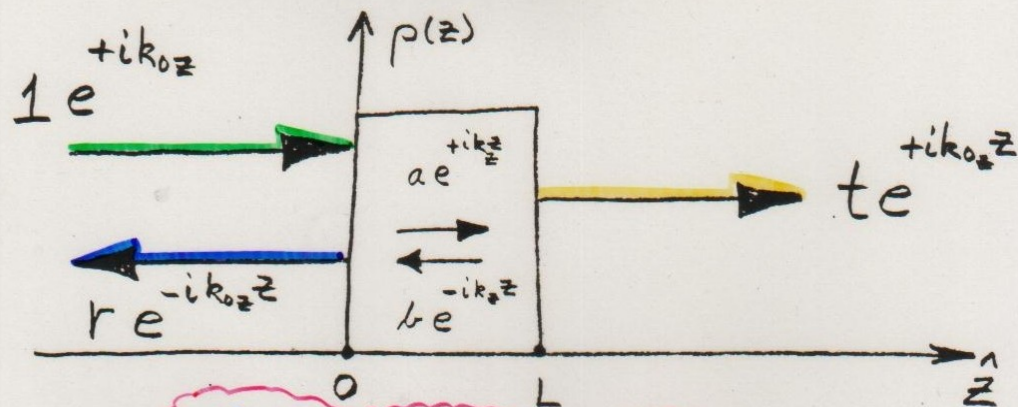
FOR A REAL POTENTIAL  $p(z)$

$$\text{Re } r(Q) \approx \frac{4\pi}{Q} \int_{-\infty}^{+\infty} p(z) \sin(Qz) dz$$

**PROBLEM:** BORN APPROXIMATION FAILS AT SUFFICIENTLY SMALL  $Q$  — MUST THEN USE EXACT THEORY



Comparison between kinematic (line) and dynamic (triangle + line) plus-state reflectivities for a density profile similar to that of Fig.2 as described in the text.

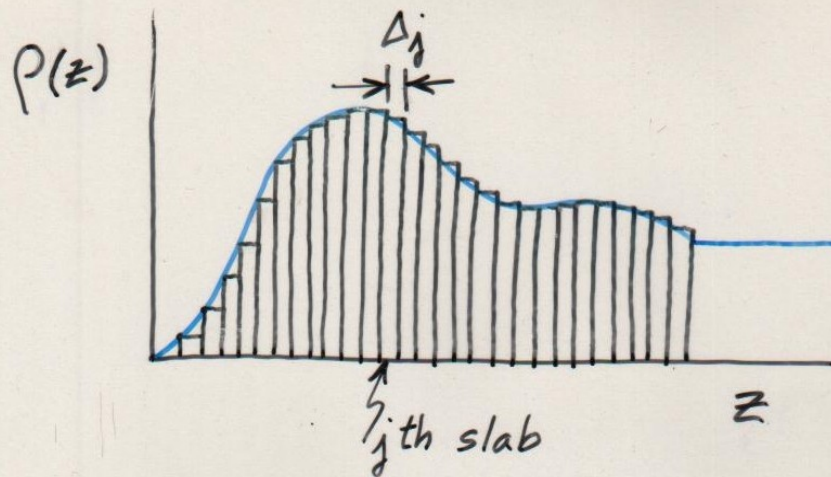


$$\frac{\partial^2 \psi(z)}{\partial z^2} + k_z^2 \psi(z) = 0$$

CONSERVATION OF MOMENTUM  
AND PARTICLE NUMBER  
REQUIRE THAT  $\frac{\partial \psi(z)}{\partial z}$  AND  $\psi(z)$

BE CONTINUOUS AT THE  
BOUNDARIES  $z=0$  &  $z=L$

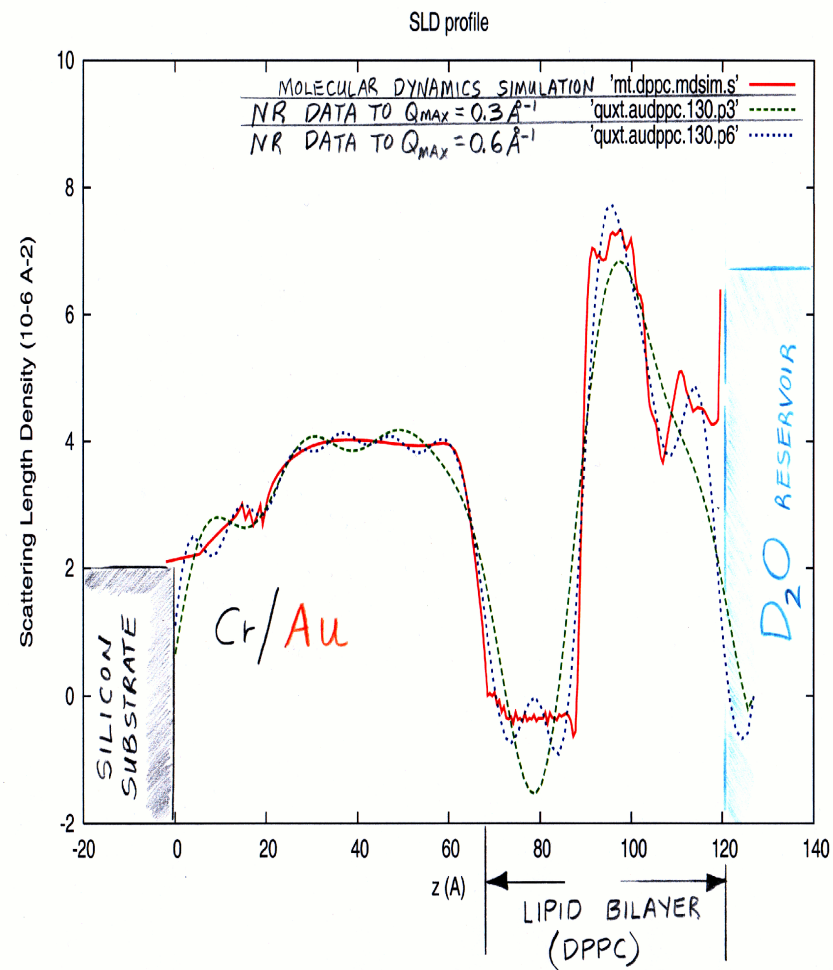
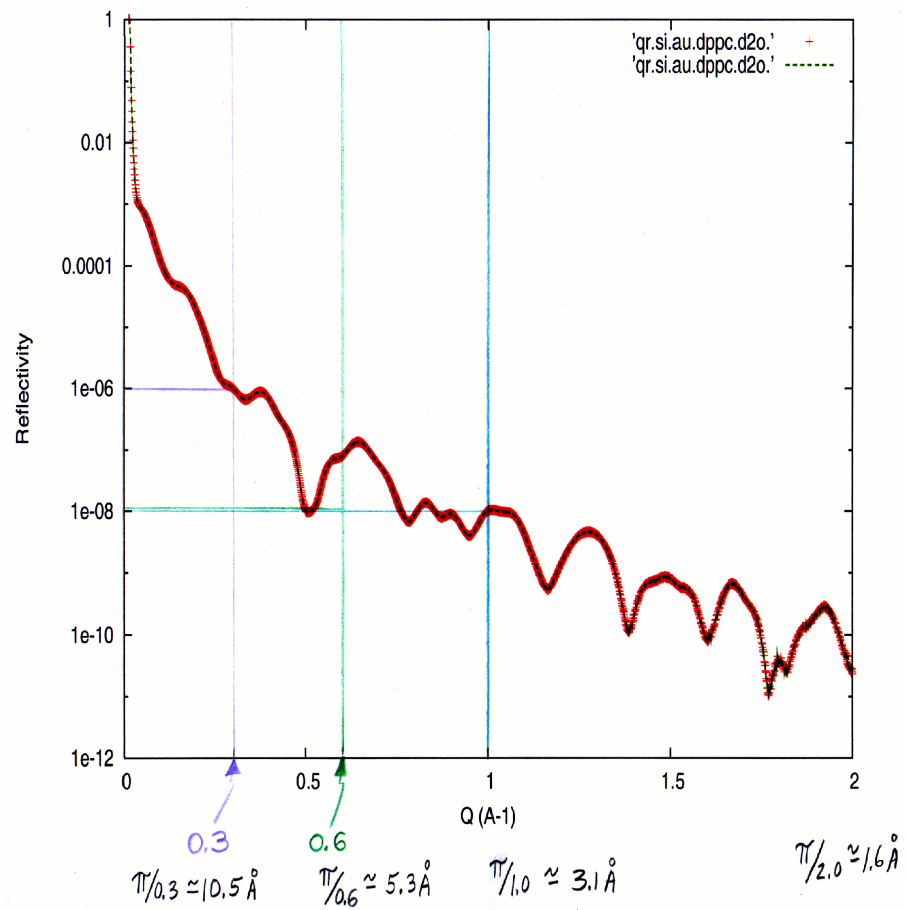
$$\begin{pmatrix} t \\ it \end{pmatrix} e^{ik_0 L} = \begin{pmatrix} A & B \\ C & D \end{pmatrix} \begin{pmatrix} 1+r \\ i(1-r) \end{pmatrix}$$

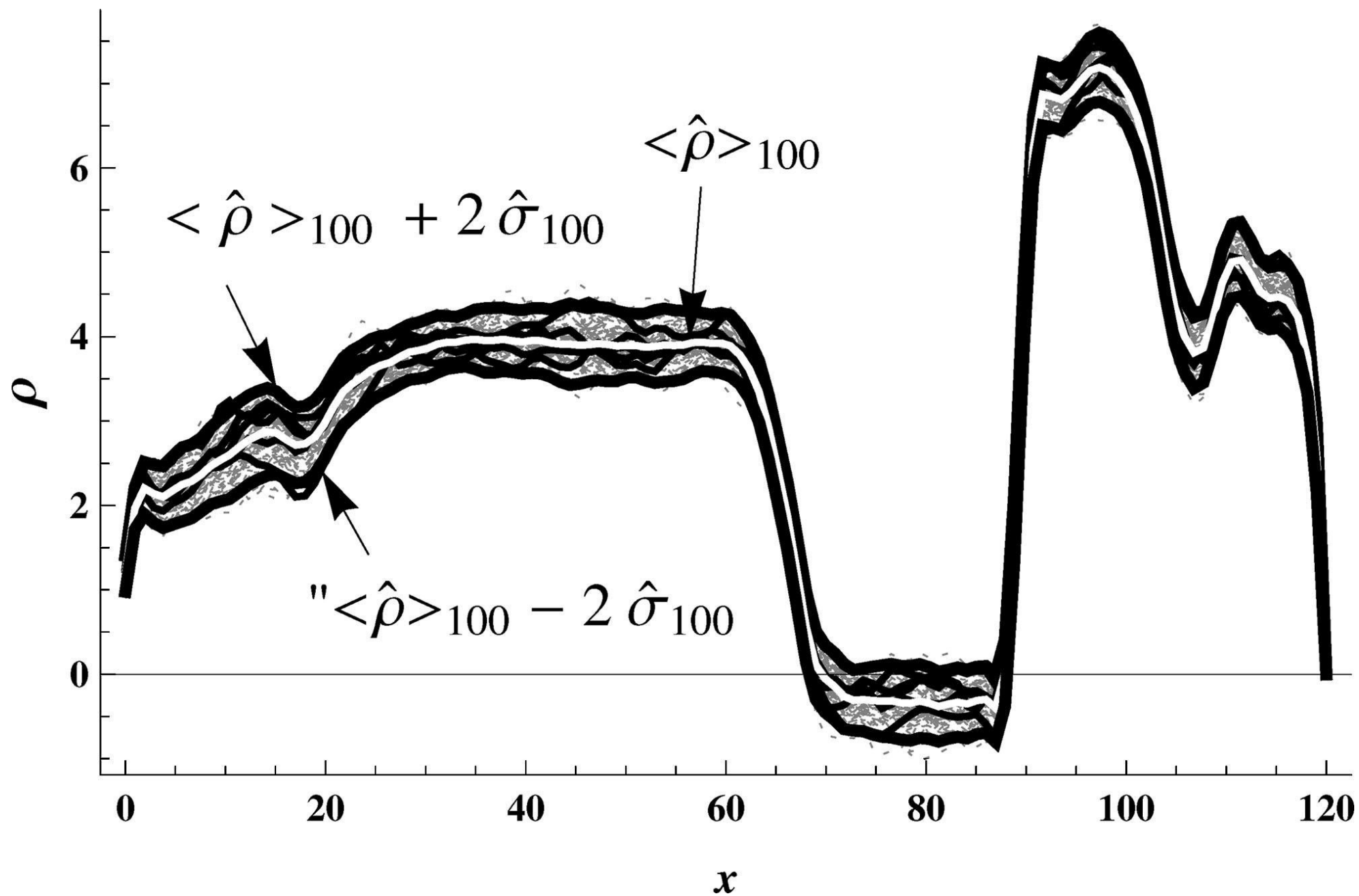


$$\begin{pmatrix} A & B \\ C & D \end{pmatrix} = \begin{pmatrix} a_N & b_N \\ c_N & d_N \end{pmatrix} \begin{pmatrix} a_{N-1} & b_{N-1} \\ c_{N-1} & d_{N-1} \end{pmatrix} \cdots \begin{pmatrix} a_2 & b_2 \\ c_2 & d_2 \end{pmatrix} \begin{pmatrix} a_1 & b_1 \\ c_1 & d_1 \end{pmatrix}$$

$$\begin{pmatrix} a_j & b_j \\ c_j & d_j \end{pmatrix} = \begin{pmatrix} \cos S_j & \frac{1}{n_{zj}} \sin S_j \\ -n_{zj} \sin S_j & \cos S_j \end{pmatrix}$$

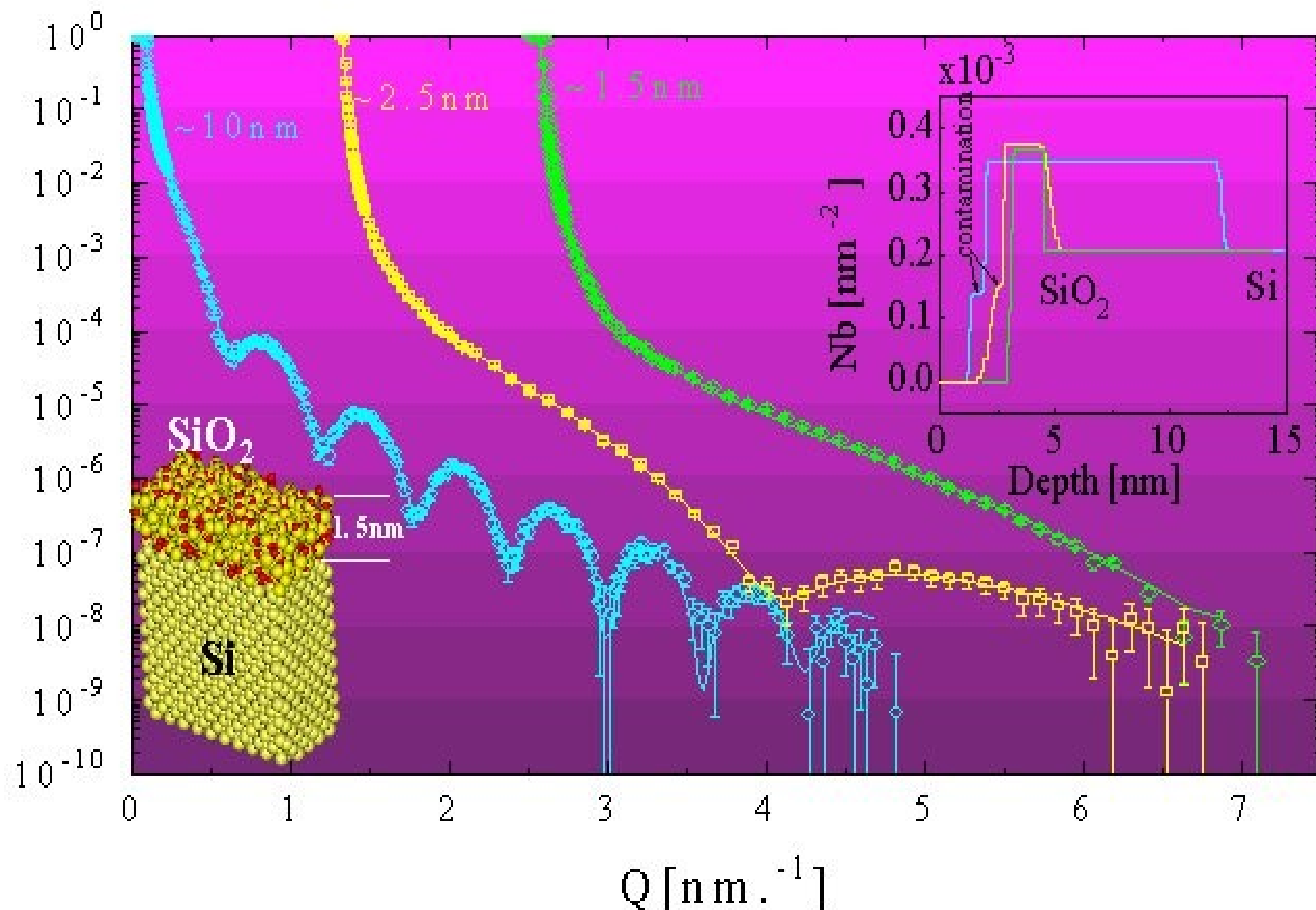
$$\begin{aligned} S_j &= k_0 n_{zj} \Delta_j \\ &= k_{zj} \Delta_j \end{aligned}$$



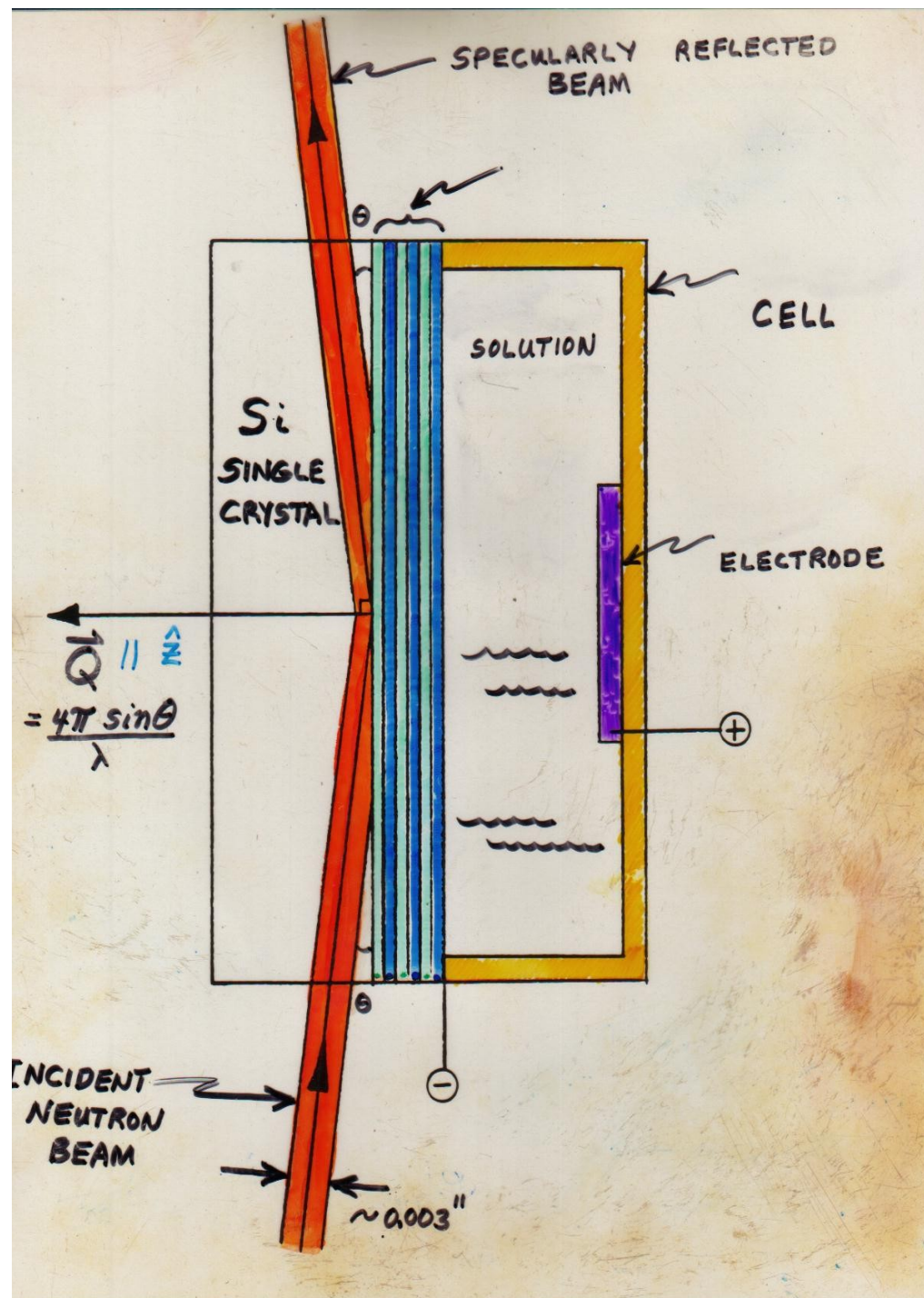


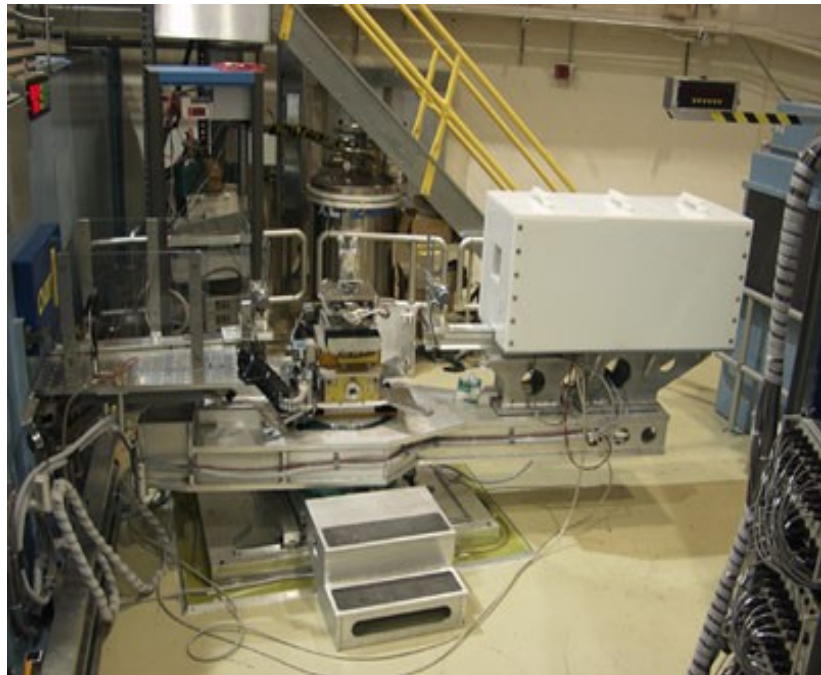
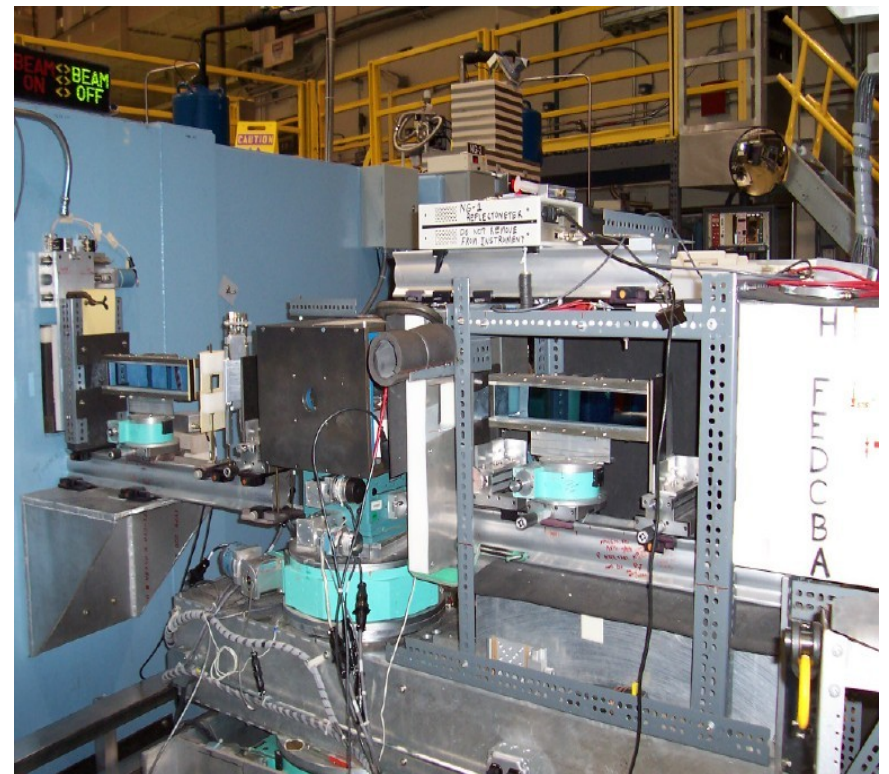
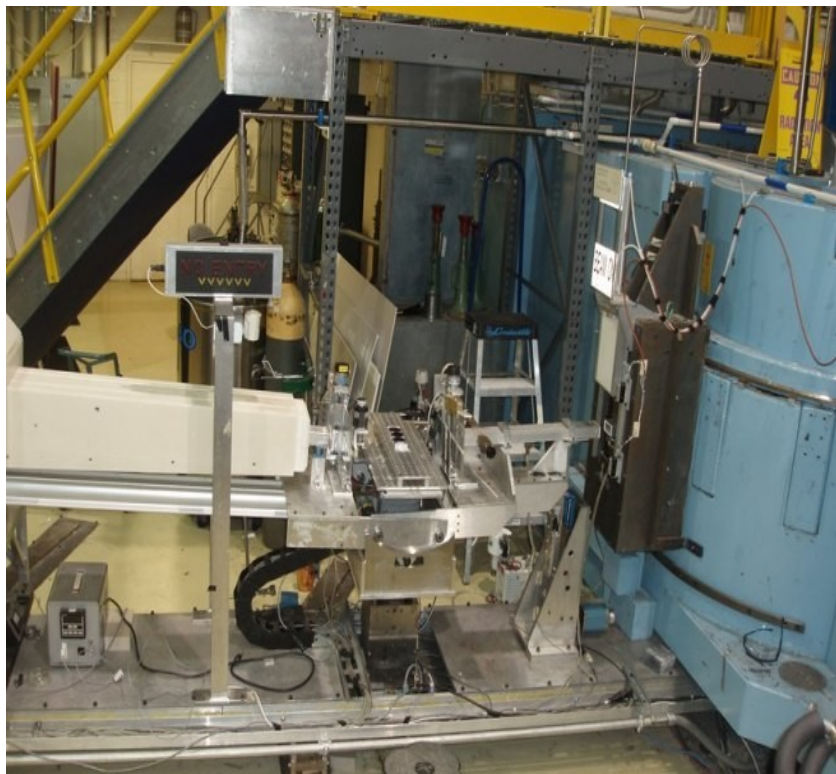
"Statistical Analysis of Phase-Inversion Neutron Specular Reflectivity", N.F.Berk and C.F.Majkrzak, *Langmuir* **25**, 4132 (2009).

Log (Reflectivity)



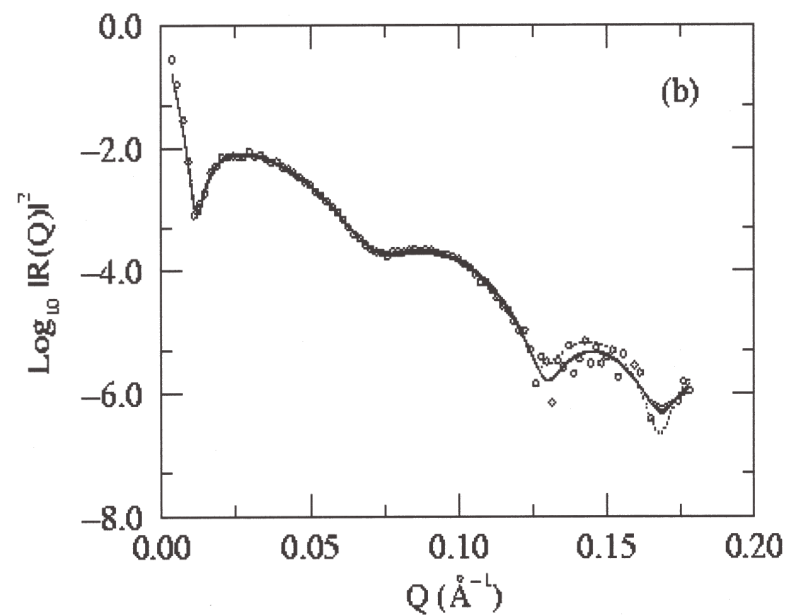
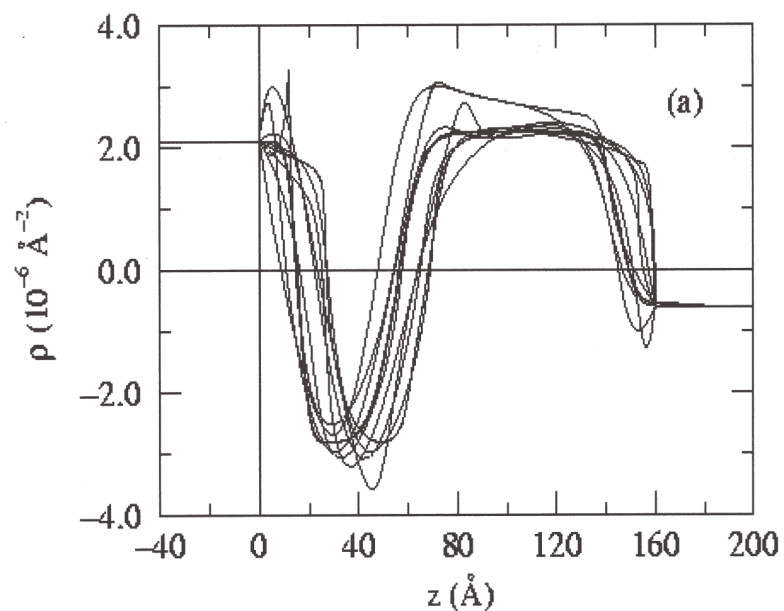
Neutron Reflectivity data and best fits for  $\text{SiO}_2$  films labeled according to thickness. The inset on the right contains the SLD profiles determined by the fits. For clarity the  $\sim 2.5 \text{ nm}$  and  $\sim 1.5 \text{ nm}$  films are shifted to the right by  $1.25 \text{ \AA}^{-1}$  and  $2.5 \text{ \AA}^{-1}$  respectively. The inset on the left is a model of  $1.5 \text{ nm}$  of  $\text{SiO}_2$  on  $\text{Si} (100)$ .





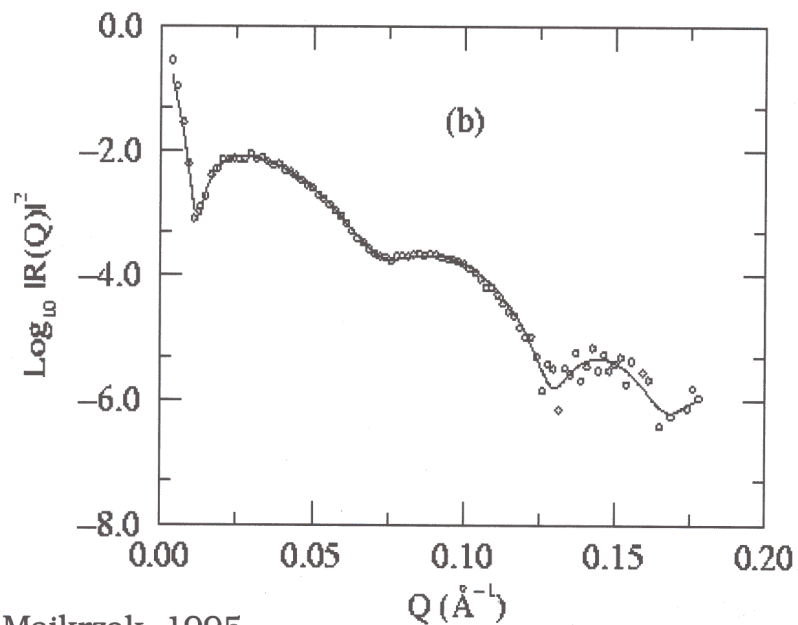
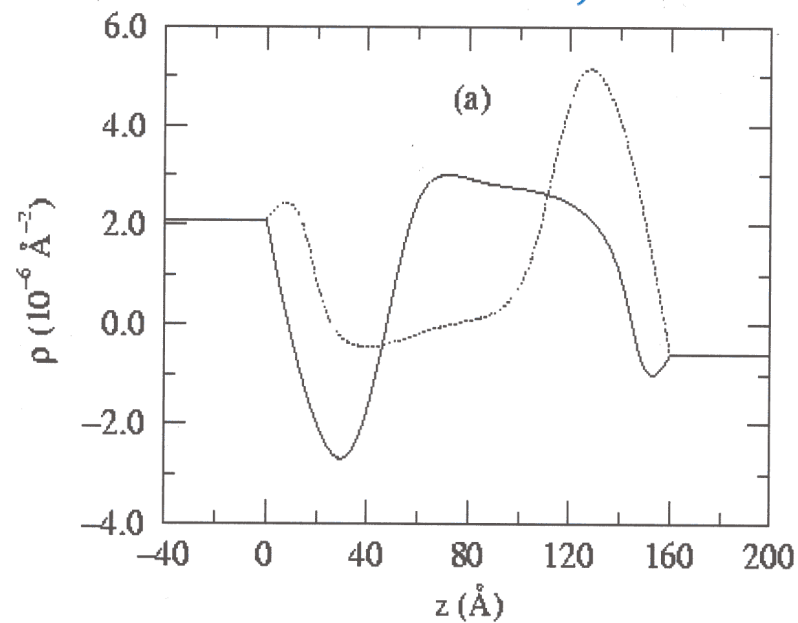
Clockwise from above: NG-1 polarized beam reflectometer, the ANDR instrument, and the NG-7 horizontal reflecting plane machine.

PBS



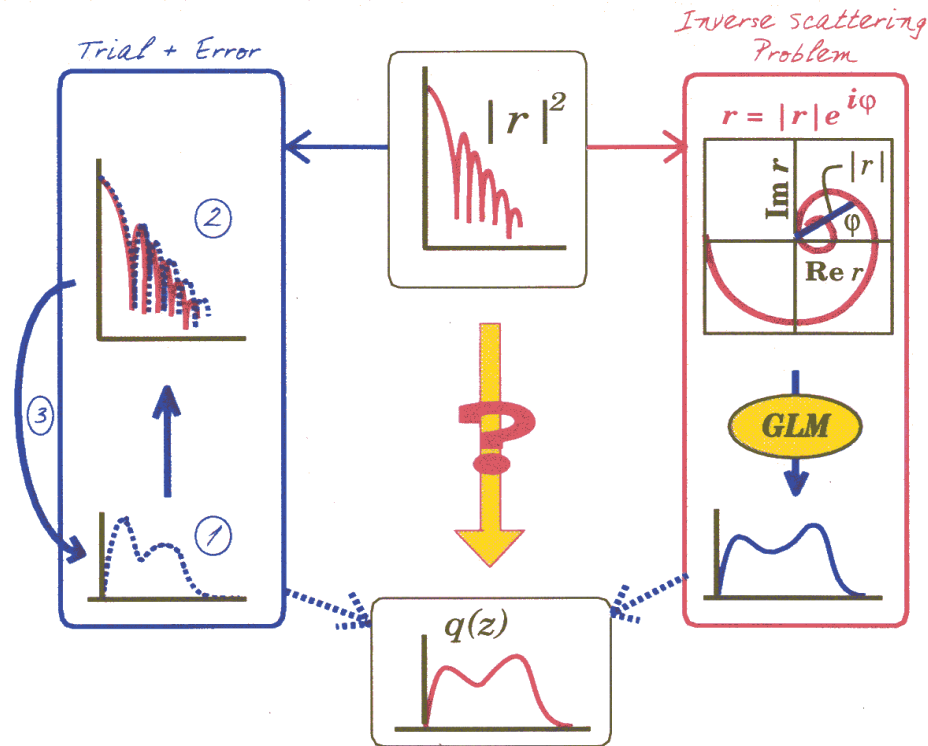
PBS

*TiO in situ: Wiesler, et al.*



Berk & Majkrzak, 1995

# Inverting reflectivity



## Phase determination

C.F. Majkrzak and N.F. Berk, Phys. Rev. B **52**, 10827 (1995).

V.-O. de Haan, et al., Phys. Rev. B **52**, 10830 (1995).

H. Leeb, H.R. Lipperheide and G. Reiss, this conference.

## Logarithmic dispersion

W.L. Clinton, Phys. Rev. B **48**, 1 (1993).

## Tunneling times

H. Fiedeldey, H.R. Lipperheide, et al., Phys. Lett. A **170**, 347 (1992).

## Pseudo-inversion

S.K. Sinha, et al., *Surface X-Ray and Neutron Scattering*, 85 (Springer, 1992).

C.F. Majkrzak, N.F. Berk, et al., SPIE Proc. **1738**, 282 (1992).



At the top of the figure are photographs of Jerome Karle (on the left) and Herb Hauptman (on the right) who together received a Nobel prize for helping solve the phase problem in x-ray diffraction by crystals. If these photos are analyzed as density maps and Fourier transforms are calculated, the phases and amplitudes of the corresponding "structure factors" are obtained. In the lower half of the figure, the picture on the left results from combining the Hauptman phases and Karle amplitudes for the original photos whereas that on the right is obtained vice versa. This demonstrates that the essential information is predominantly contained in the phases. The example above is from R.J.Read, University of Cambridge ([www-structmed.cimr.cam.ac.uk/. . . /Fourier.html](http://www-structmed.cimr.cam.ac.uk/. . . /Fourier.html)).

FOURIER TRANSFORM  
OF THE COMPLEX  
REFLECTION  
AMPLITUDE

$$R(z) = \frac{1}{\pi} \operatorname{Re} \int_0^{\infty} r(k_z) e^{ik_z z} dk_z$$

GELFAND  
LEVITAN  
MARCHENKO  
INTEGRAL  
EQUATION

$$K(z, \gamma) + R(z + \gamma) + \int_{-z}^{+z} K(z, x) R(x + \gamma) dx = 0$$

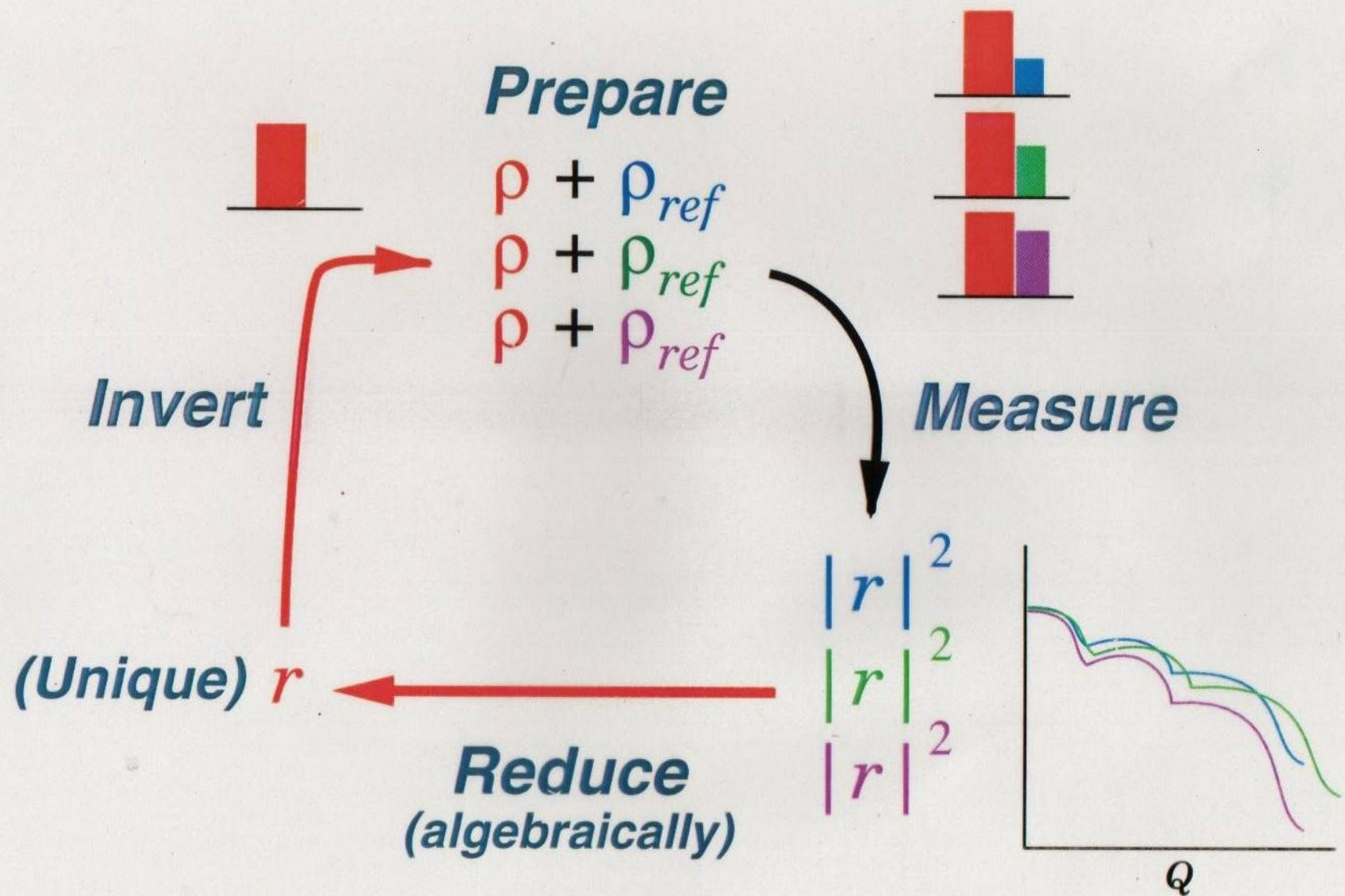
SCATTERING  
LENGTH  
DENSITY

$$\rho(z) = 2 \frac{dK(z, z)}{dz}$$

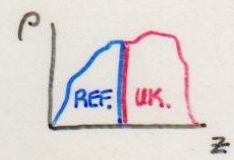
GIVEN THE COMPLEX REFLECTION  
AMPLITUDE, THE SCATTERING  
LENGTH DENSITY  $\rho$  CAN BE  
OBTAINED FROM AN EXACT,  
FIRST PRINCIPLE INVERSION  
FOR A REAL POTENTIAL OF  
FINITE EXTENT — AND THE  
SOLUTION IS UNIQUE!

NO FITTING, NO ADJUSTABLE PARAMETERS

# Phase Determination with 3 References



FORMALISM ALLOWS A COMPOSITE  
POTENTIAL TO BE EXPRESSED AS A PRODUCT:

$$\underbrace{\begin{pmatrix} A & B \\ C & D \end{pmatrix}}_{\text{COMPOSITE (1,2,3)}} = \underbrace{\begin{pmatrix} a & b \\ c & d \end{pmatrix}}_{\text{UNKNOWN}} \underbrace{\begin{pmatrix} w & x \\ y & z \end{pmatrix}}_{\text{REFERENCE (1,2,3)}}$$


$$|R(Q)|^2 = |R_1(Q)|^2, |R_2(Q)|^2, \text{ and } |R_3(Q)|^2$$

$$\Sigma_i \equiv 2 \left[ \frac{1 + |R_i|^2}{1 - |R_i|^2} \right] = A_i^2 + B_i^2 + C_i^2 + D_i^2$$

$$A_i^2 = a^2 w_i^2 + b^2 y_i^2 + 2abw_i y_i$$

$$C_i^2 = c^2 w_i^2 + d^2 y_i^2 + 2cdw_i y_i$$

$$B_i^2 = a^2 x_i^2 + b^2 z_i^2 + 2abx_i z_i$$

$$D_i^2 = c^2 x_i^2 + d^2 z_i^2 + 2cdx_i z_i$$

(INDEPENDENTLY  
AT EACH Q)

$$\Sigma_i = \overbrace{(w_i^2 + x_i^2)}^{\text{REF}} \alpha + \overbrace{(y_i^2 + z_i^2)}^{\text{REF}} \beta + 2 \overbrace{(w_i y_i + x_i z_i)}^{\text{REF}} \gamma$$

$$\alpha = a^2 + c^2$$

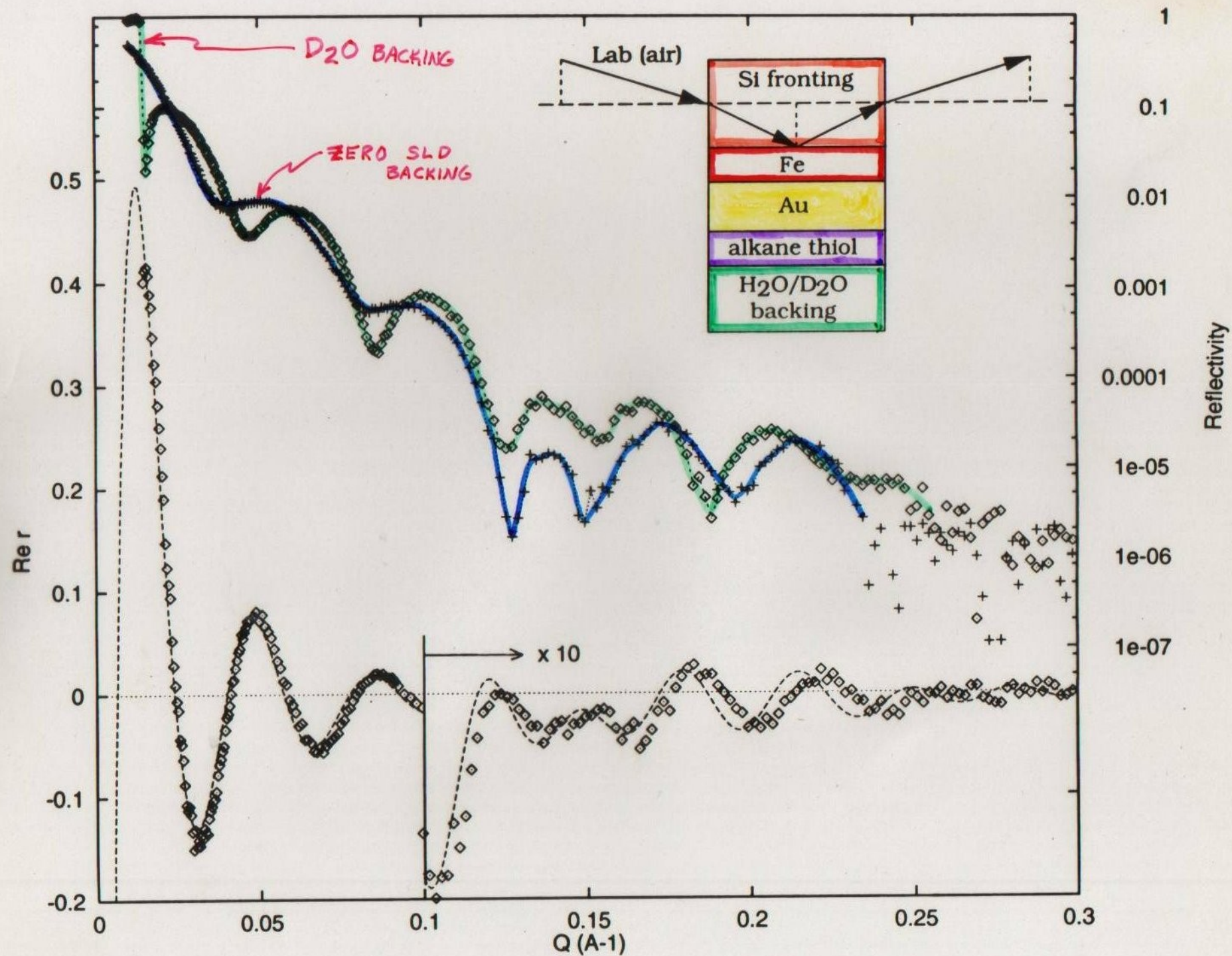
$$\beta = b^2 + d^2$$

$$\gamma = ab + cd$$

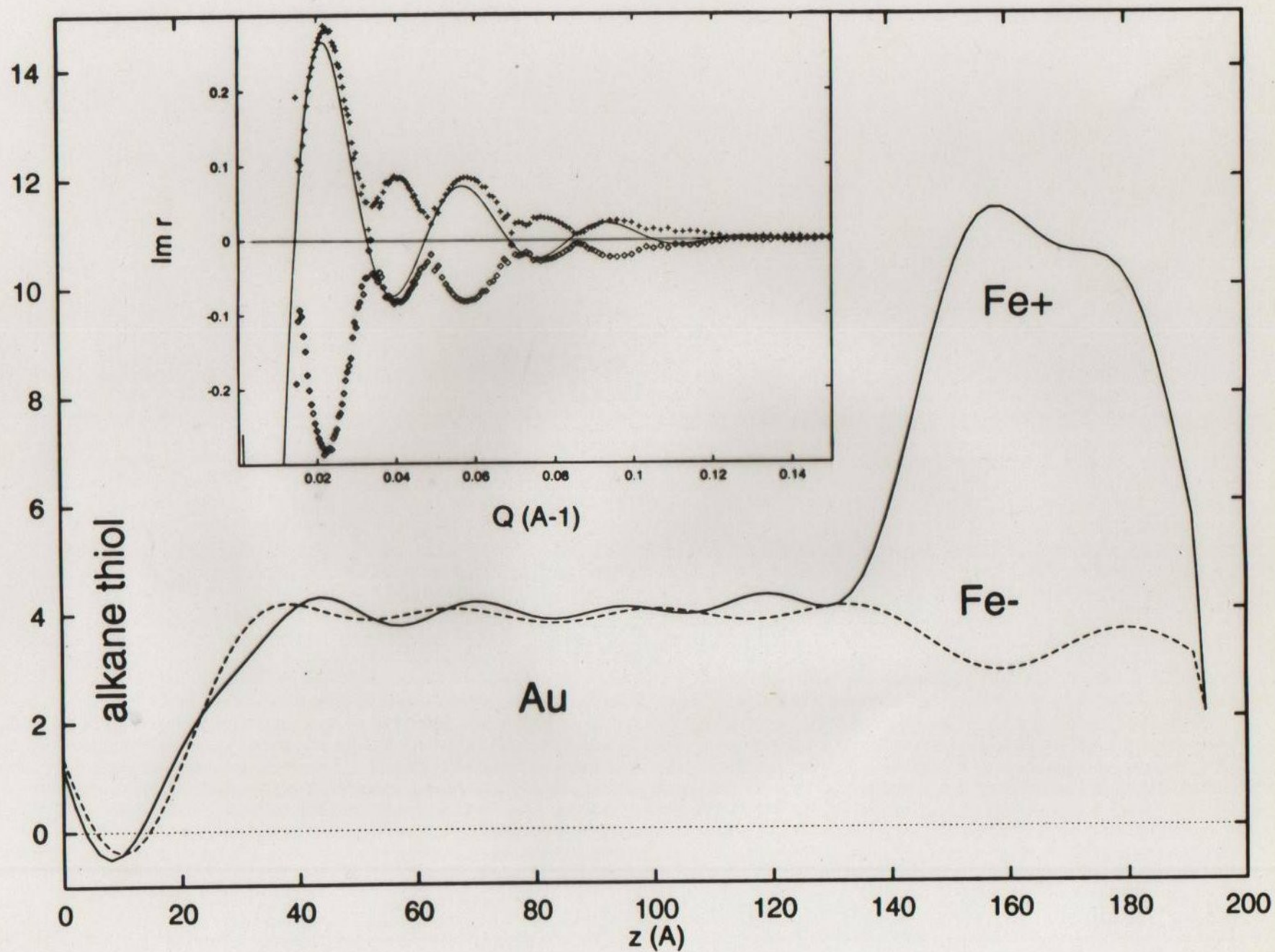
$i = 1, 2, 3$

SOLVE FOR UNKNOWN  
 $\alpha, \beta$ , AND  $\gamma$  TO GET

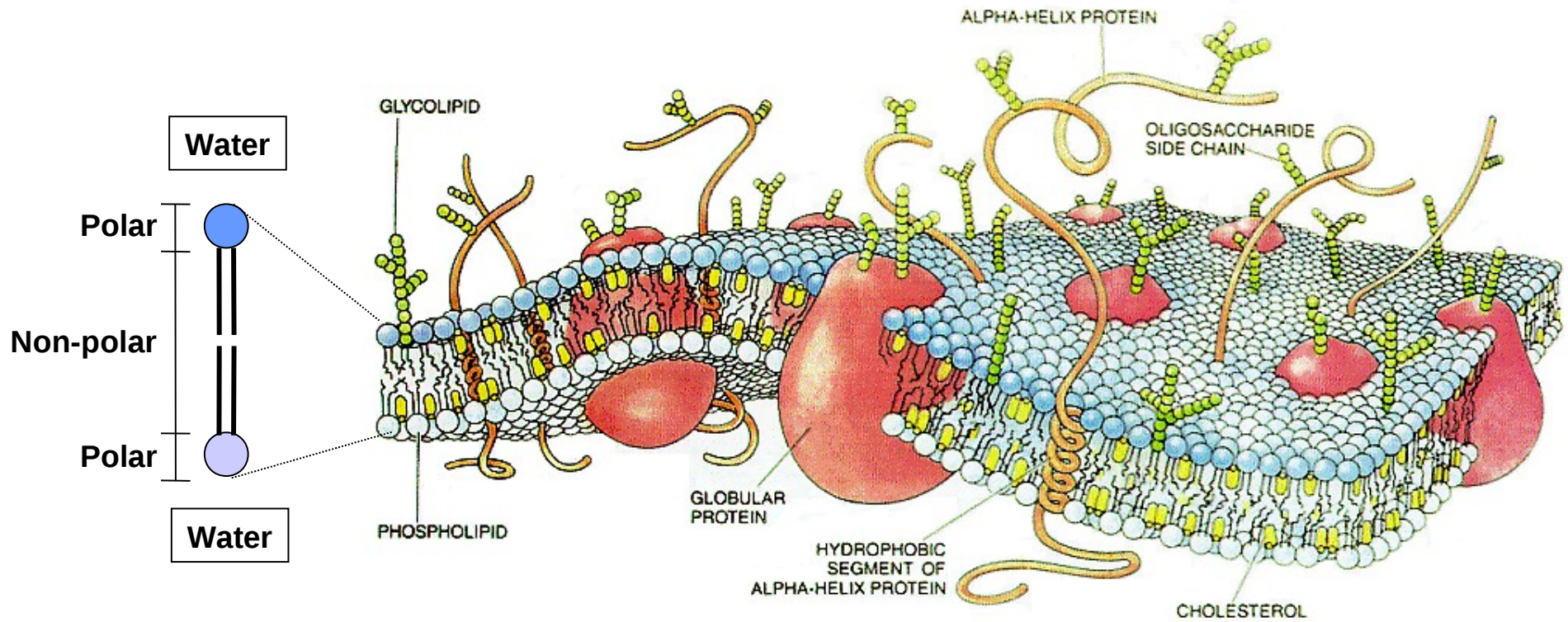
$$R_{\text{UNKNOWN}} = \frac{(\beta - \alpha) - 2i\gamma}{2 + \beta + \alpha}$$



Scattering Length Density ( $10^{-6} \text{ \AA}^{-2}$ )



# The Cell Membrane



## Essential Biological Functions

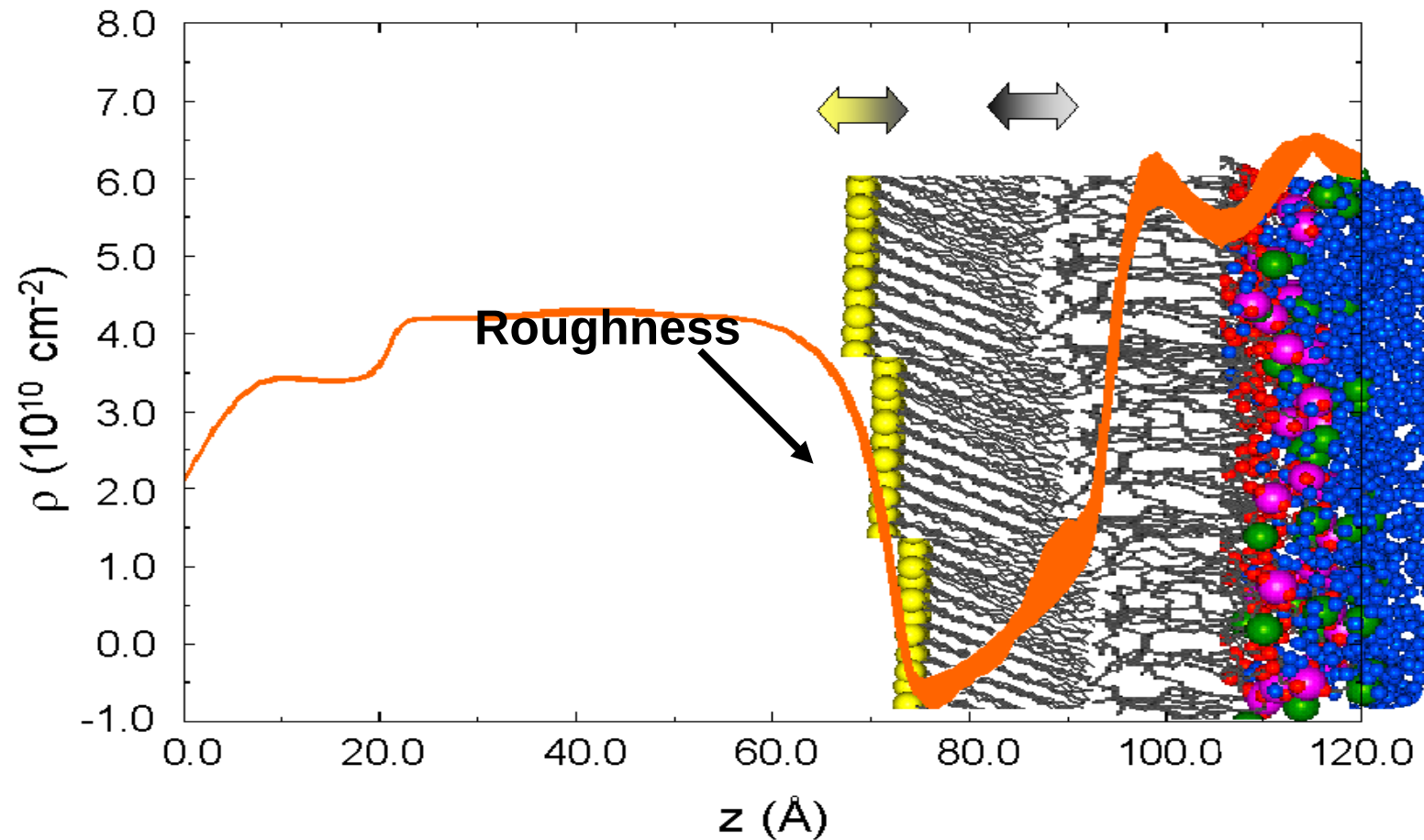
Immune response  
Cell metabolism  
Neurotransmission  
Photosynthesis  
Cell adherence  
Cell growth and differentiation

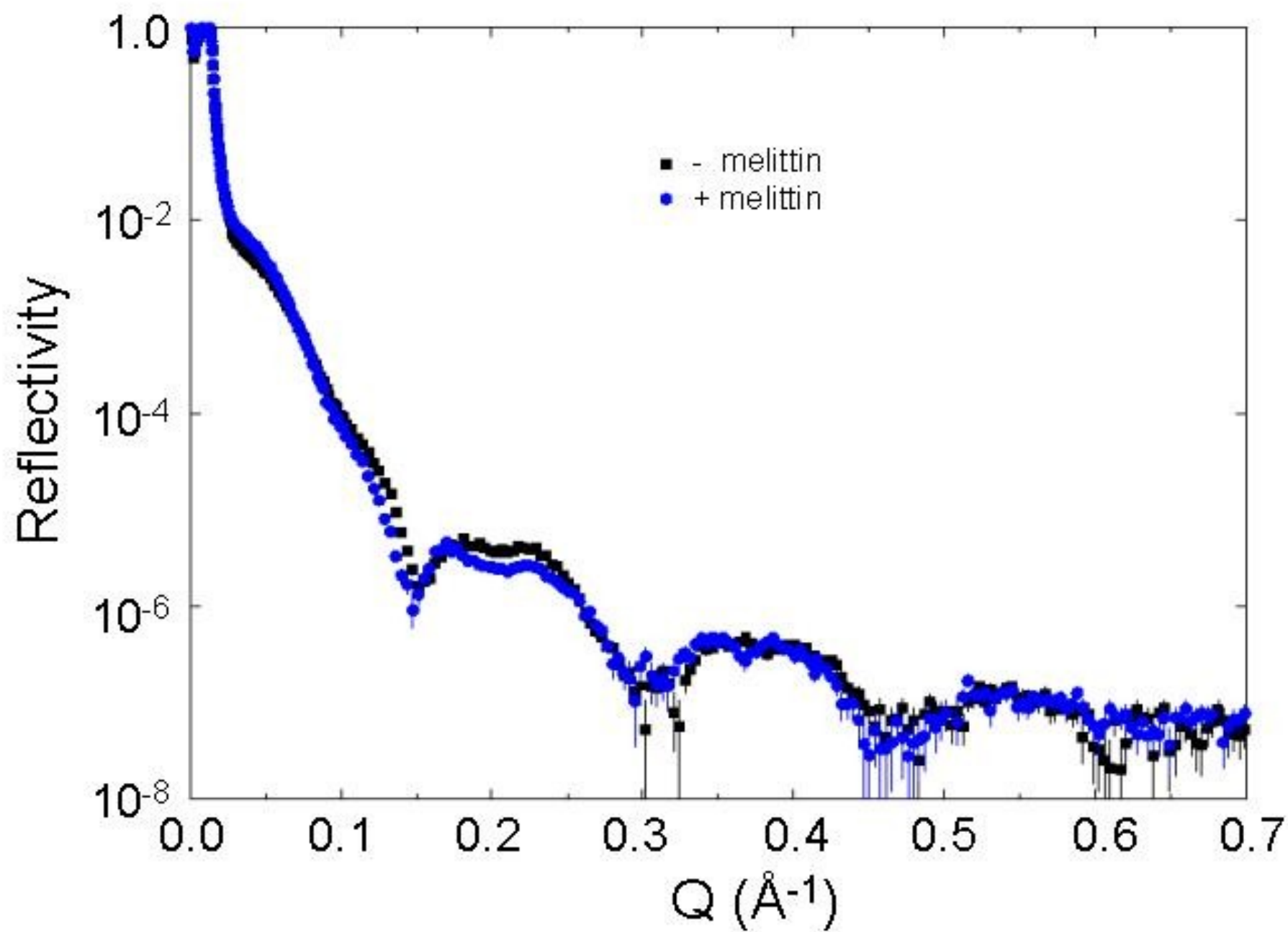
## Potential Commercial Applications

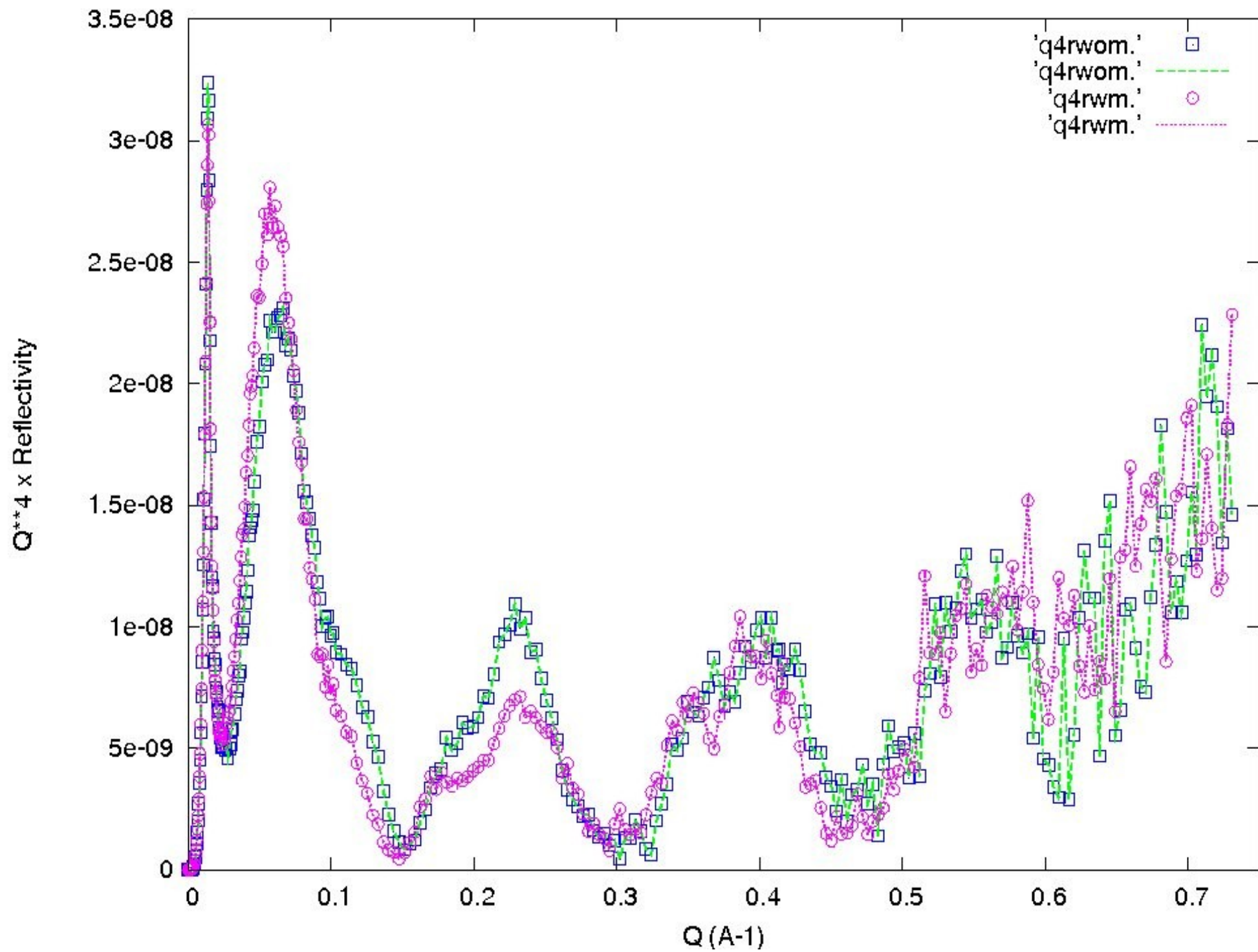
Drug response monitoring  
Chemical manufacturing  
Biosensing  
Energy conversion  
Tissue engineering

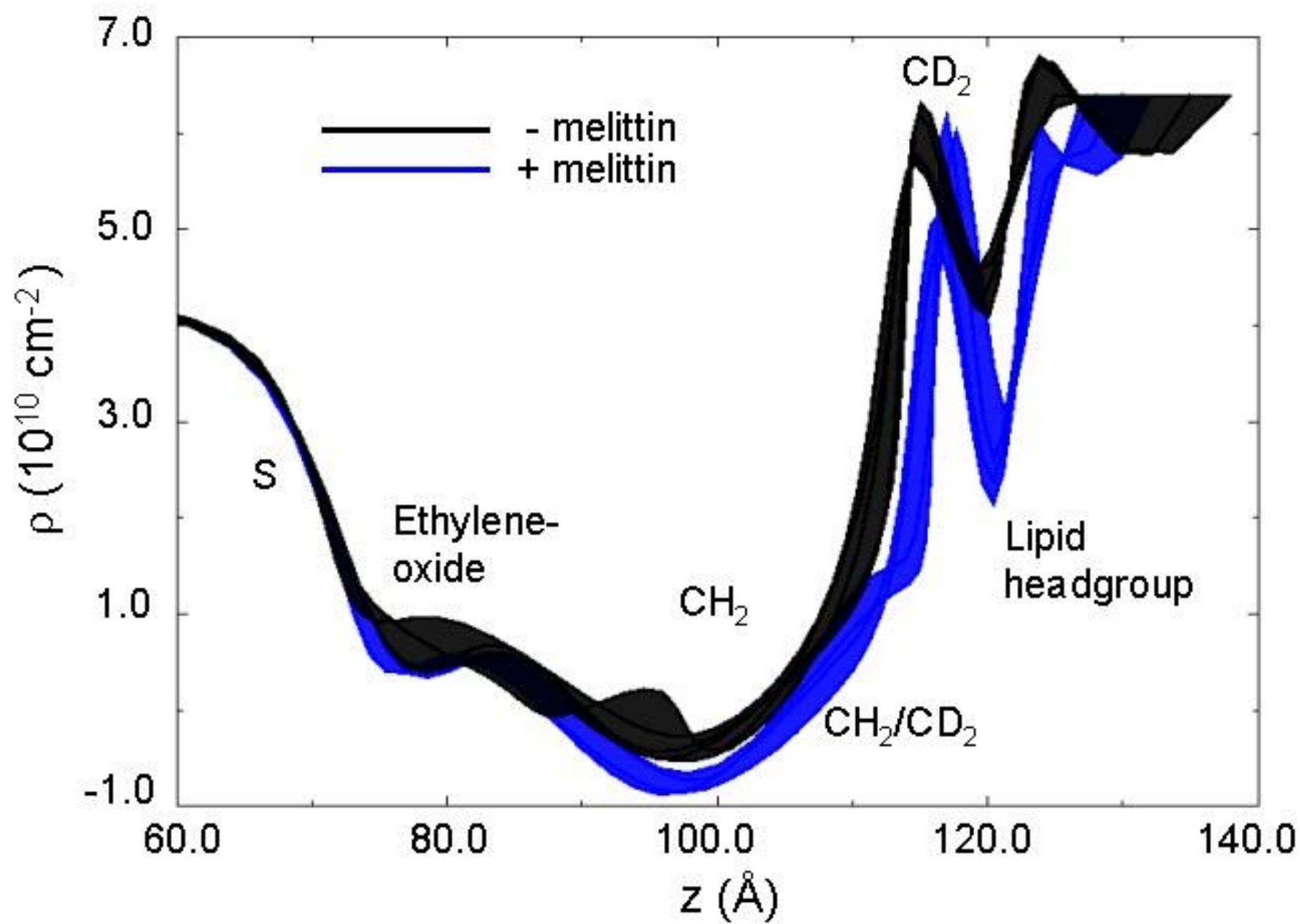
# Models of Hybrid Bilayer Membranes

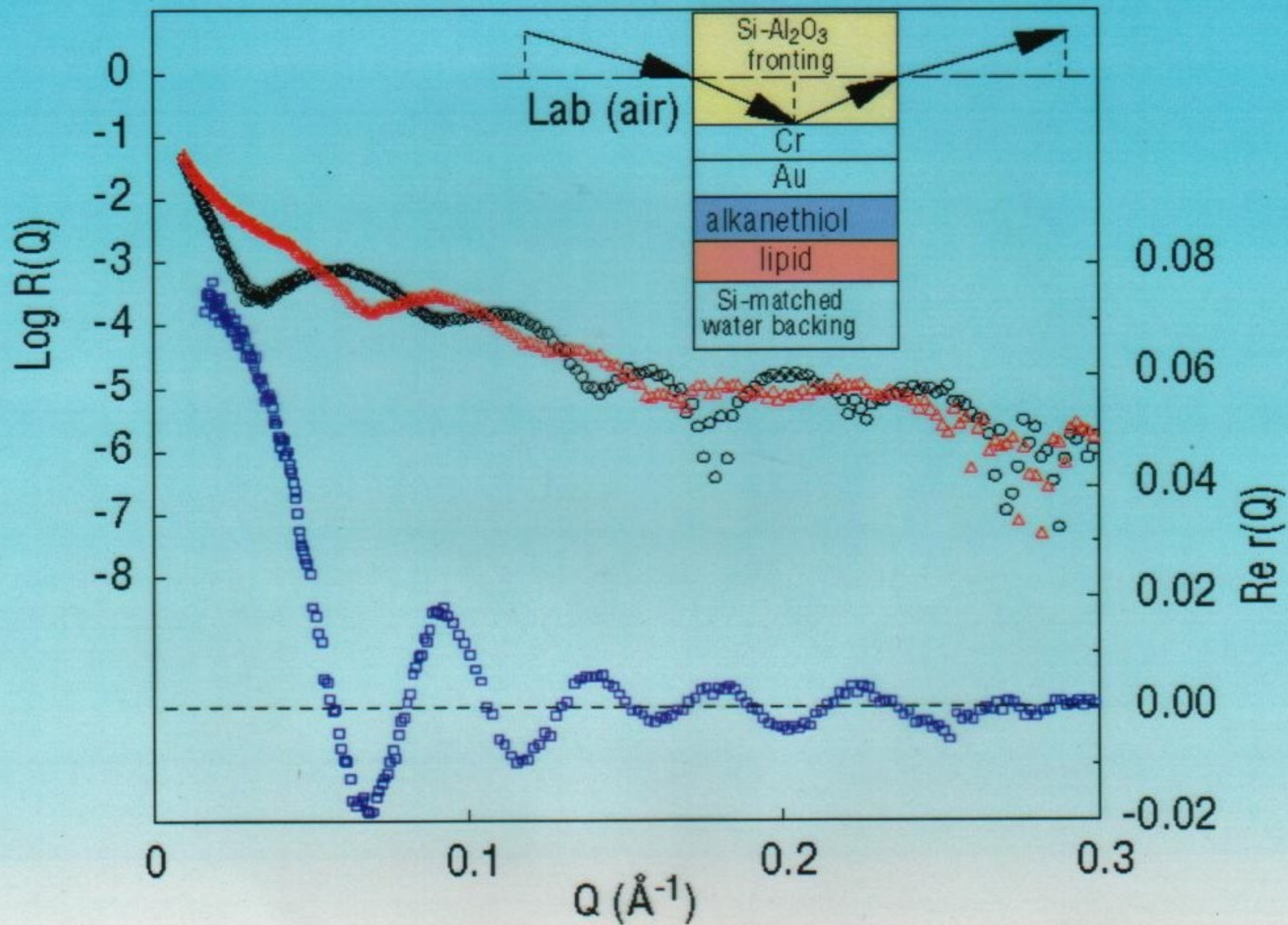
with M. Tarek, [NIST NCNR](#)

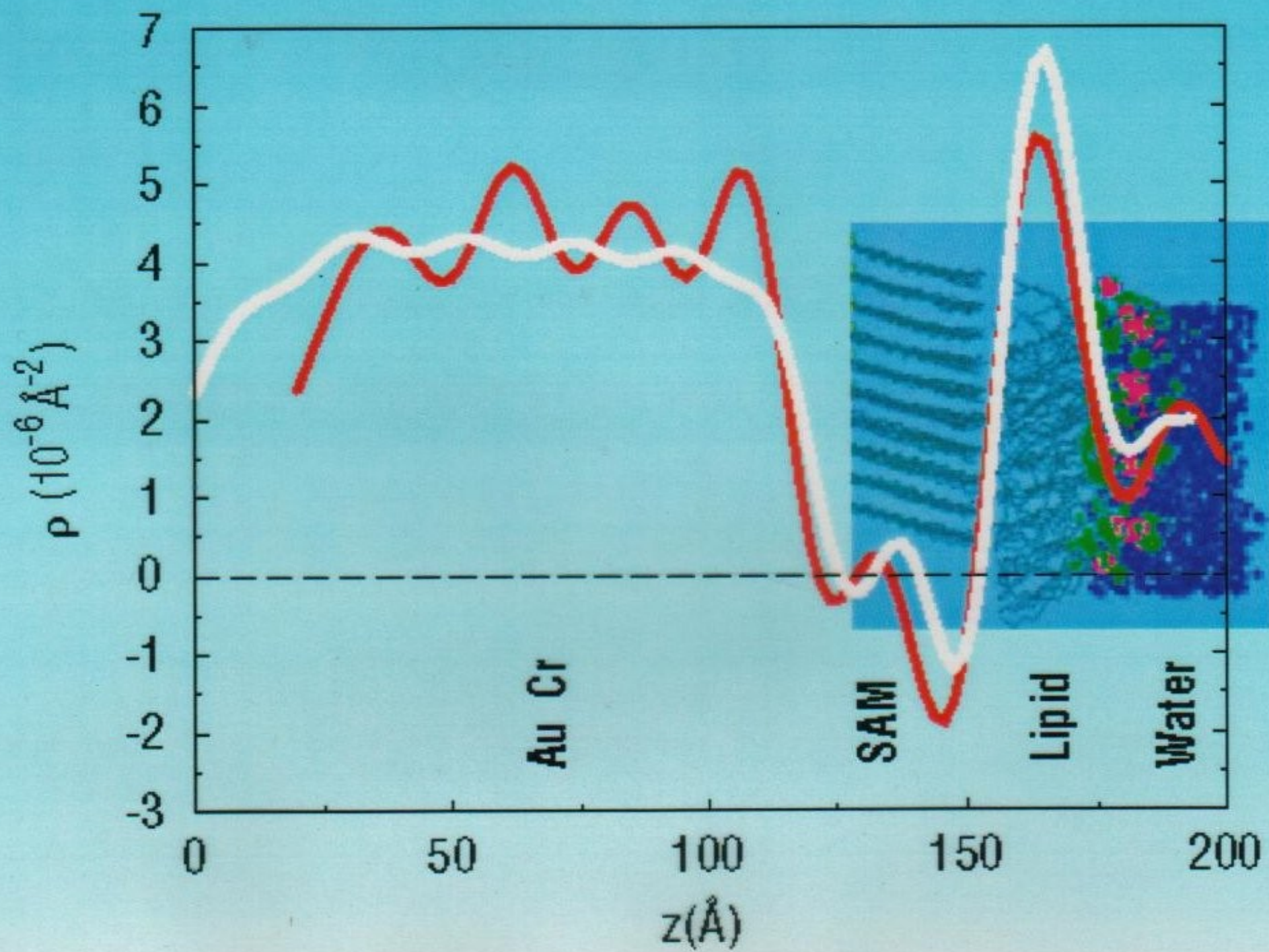


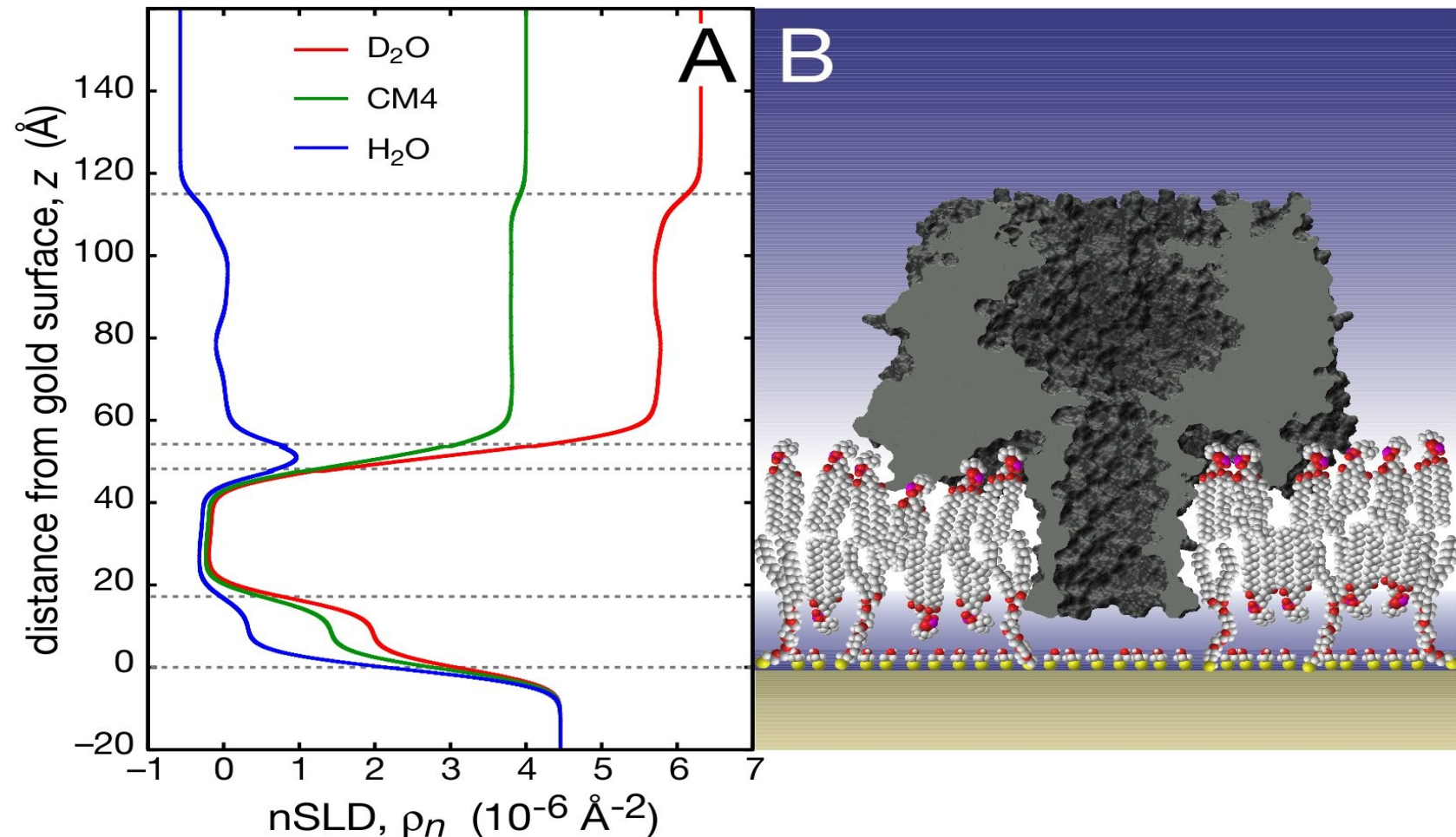












D.J.McGillivray et al., "Structure of Functional Staphylococcus Aureus Alpha Hemolysin Channels in Tethered Bilayer Lipid Membranes", *Biophysical Journal* **96**,1547 (2009).

F.Heinrich et al., "Composition-Space Model for the Investigation of Complex Molecular Architectures near Interfaces with Scattering techniques", *J. Chem. Phys.: BioChemical Physics*, (Submitted 2010).

## Reflection and Transmission of Polarized Neutrons Involving Magnetic Potentials

Given the existence of two different spin states of the neutron, a general magnetic interaction potential must be able to account for two qualitatively different types of possible scattering processes -- one which results in a change of the initial spin state, and another which does not. Consequently, the description of specular reflection from a flat magnetic film structure requires a pair of coupled, one-dimensional wave equations (the spin quantization axis is taken to be  $z$  whereas the direction of propagation of the wave is along the  $x$ -axis):

$$\left[ \frac{-\hbar^2}{2m} \frac{\partial^2}{\partial x^2} \begin{pmatrix} 1 & 0 \\ 0 & 1 \end{pmatrix} + \begin{pmatrix} V_{++} & V_{+-} \\ V_{-+} & V_{--} \end{pmatrix} - E \begin{pmatrix} 1 & 0 \\ 0 & 1 \end{pmatrix} \right] \begin{pmatrix} \psi_+ \\ \psi_- \end{pmatrix} = 0$$

The interaction potentials can be, in general, spin-dependent and derive from both nuclear and magnetic interactions between neutron and matter. As shown in detail in the quantum mechanics text by Merzbacher (Chapters 12 & 13, pages 251 to 293), the magnetic interaction must be represented by an operator appropriate for the quantum spinor nature of the neutron magnetic moment:

$$\begin{aligned} \check{V}_M &= \check{\mu} \cdot \vec{B} = -\mu \check{\sigma} \cdot \vec{B} = -\mu (\check{\sigma}_x B_x + \check{\sigma}_y B_y + \check{\sigma}_z B_z) \\ &= -\mu \left[ \begin{pmatrix} 0 & 1 \\ 1 & 0 \end{pmatrix} B_x + \begin{pmatrix} 0 & -i \\ i & 0 \end{pmatrix} B_y + \begin{pmatrix} 1 & 0 \\ 0 & -1 \end{pmatrix} B_z \right] = -\mu \begin{bmatrix} B_z & B_x - iB_y \\ B_x + iB_y & -B_z \end{bmatrix} \end{aligned}$$

where  $\mu$  is the magnitude of the magnetic moment of the neutron,  $\check{\sigma}$  is the Pauli spin operator, and  $\vec{B}$  is the magnetic field. Previously, the scalar, non-spin-dependent nuclear potential was written as

$$V_N = \frac{2\pi\hbar^2}{m} N b = \frac{2\pi\hbar^2}{m} \rho_N$$

The magnetic potential can also be expressed in terms of scattering length densities as

$$\check{V}_M = \frac{2\pi\hbar^2}{m} \begin{pmatrix} \rho_{Mz} & \rho_{Mx} - i\rho_{My} \\ \rho_{Mx} + i\rho_{My} & -\rho_{Mz} \end{pmatrix}$$

Combining nuclear and magnetic potentials we obtain

$$V_N + \check{V}_M = \frac{2\pi\hbar^2}{m} \begin{pmatrix} \rho_N + \rho_{Mz} & \rho_{Mx} - i\rho_{My} \\ \rho_{Mx} + i\rho_{My} & \rho_N - \rho_{Mz} \end{pmatrix} = \frac{2\pi\hbar^2}{m} \begin{pmatrix} \rho_{++} & \rho_{+-} \\ \rho_{-+} & \rho_{--} \end{pmatrix}$$

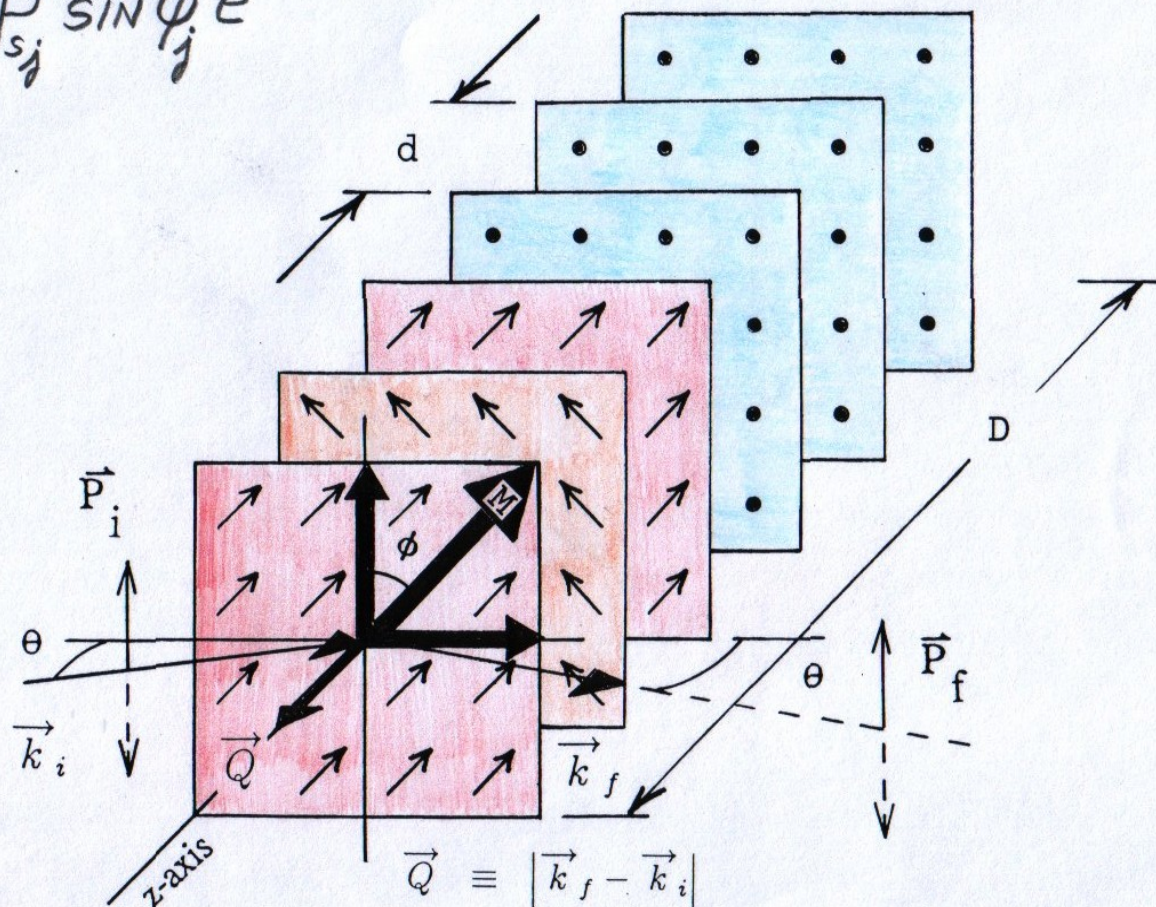
In terms of the scattering length densities, the coupled wave equations of motion are

$$\begin{aligned} \left[ \frac{\partial^2}{\partial x^2} + k_{0x}^2 - 4\pi\rho_{++} \right] \psi_+ - 4\pi\rho_{+-} \psi_- &= 0 \\ \left[ \frac{\partial^2}{\partial x^2} + k_{0x}^2 - 4\pi\rho_{--} \right] \psi_- - 4\pi\rho_{-+} \psi_+ &= 0 \end{aligned}$$

In the special case where all magnetic fields are taken to be along the defined  $z$ -axis of quantization,  $\rho_{+-} = \rho_{-+} = 0$  and the wave equations become decoupled, each describing one of the two pure spin eigenstates independently. The expressions for the reflection and transmission amplitudes associated with each of the two uncoupled equations then become essentially equivalent to those derived for the nonmagnetic case in Figure 3. For the time being, this is all we should need.

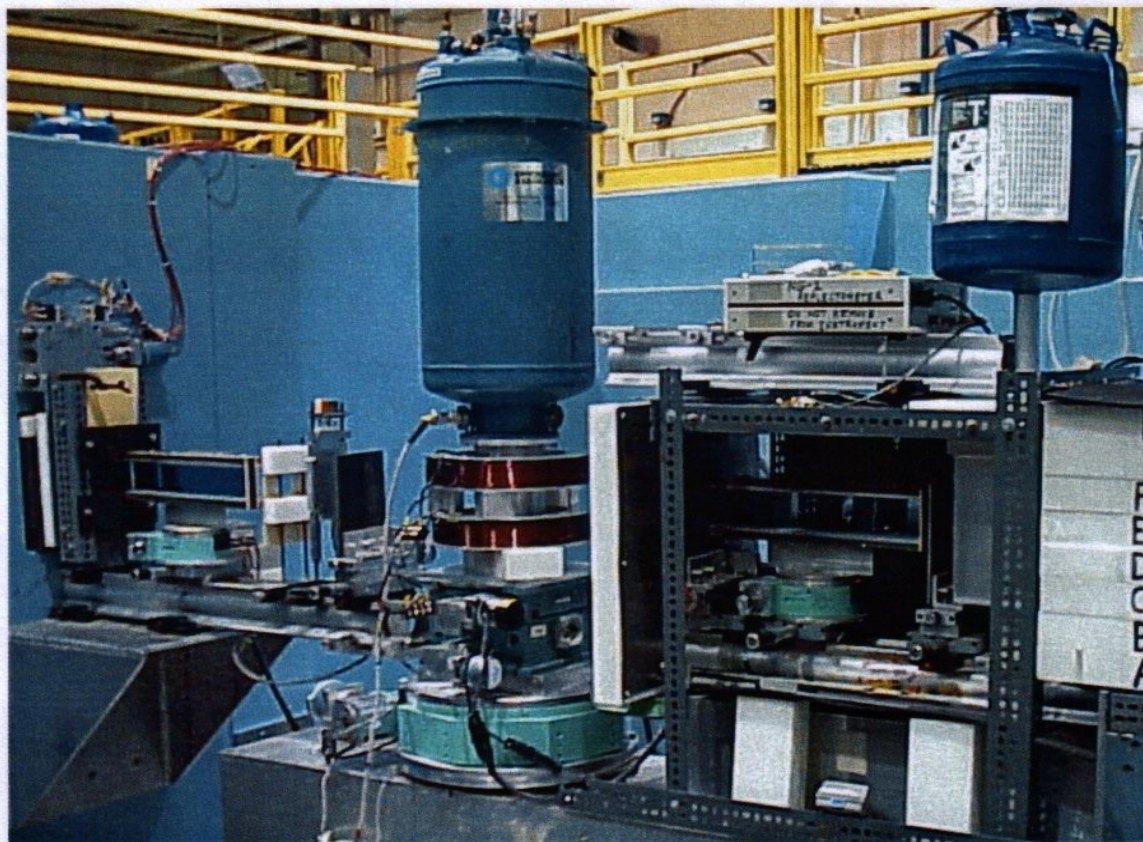
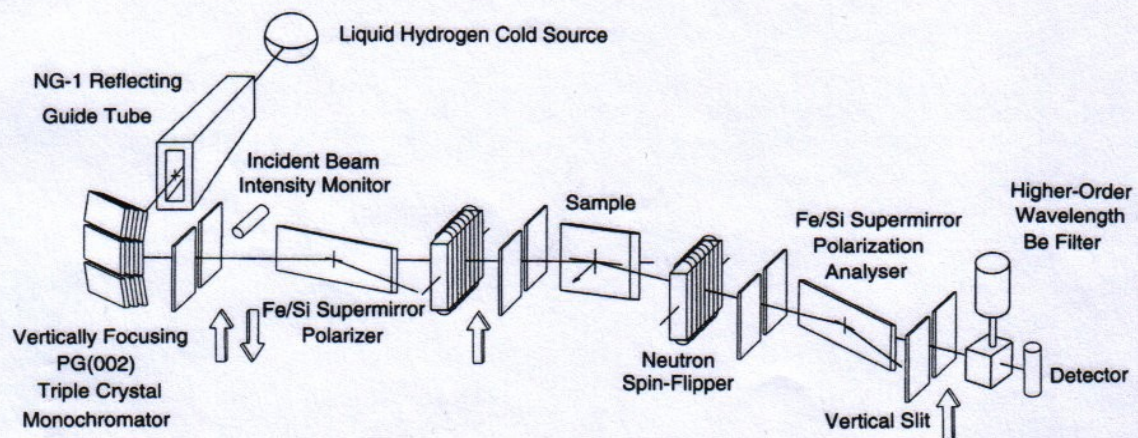
$$F^{\pm\pm} \propto \sum_{j=1}^N [b_{sj} \pm p_{sj} \cos \phi_j] e^{iQ u_j}$$

$$F^{\pm\mp} \propto \sum_{j=1}^N p_{sj} \sin \phi_j e^{iQ u_j}$$



# Polarized Neutron Reflectometry

at the NCNR NG-1 Reflectometer

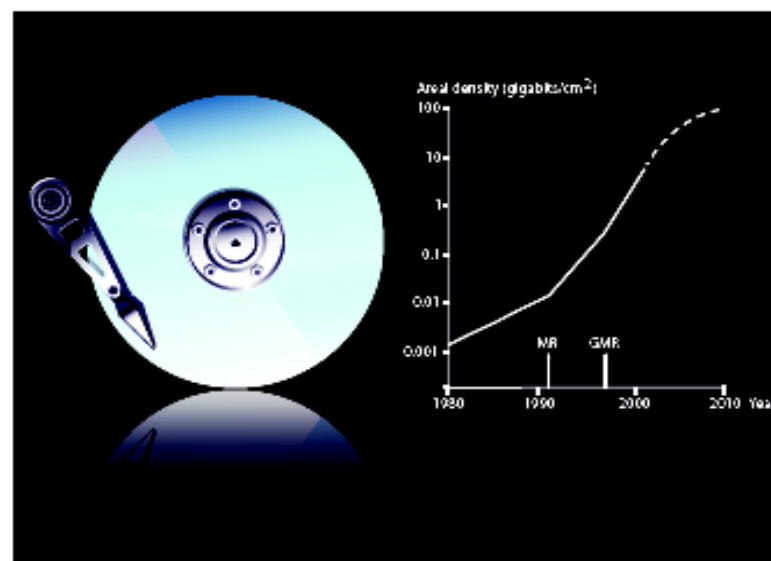


## The Nobel Prize in Physics 2007

*This year's Nobel Prize in Physics is awarded to ALBERT FERT and PETER GRÜNBERG for their discovery of Giant Magnetoresistance. Applications of this phenomenon have revolutionized techniques for retrieving data from hard disks. The discovery also plays a major role in various magnetic sensors as well as for the development of a new generation of electronics. The use of Giant Magnetoresistance can be regarded as one of the first major applications of nanotechnology.*

### Better read-out heads for pocket-size devices

Constantly diminishing electronics have become a matter of course in today's IT-world. The yearly addition to the market of ever more powerful and lighter computers is something we have all started to take for granted. In particular, hard disks have shrunk – the bulky box under your desk will soon be history when the same amount of data can just as easily be stored in a slender laptop. And with a music player in the pocket of each and everyone, few still stop to think about how many cds' worth of music its tiny hard disk can actually hold. Recently, the maximum storage capacity of hard disks for home use has soared to a terabyte (a thousand billion bytes).



Diagrams showing the accelerating pace of miniaturization might give a false impression of simplicity – as if this development followed a law of nature. In actual fact, the ongoing IT-revolution depends on an intricate interplay between fundamental scientific progress and technical fine tuning. This is just what the Nobel Prize in Physics for the year 2007 is about.

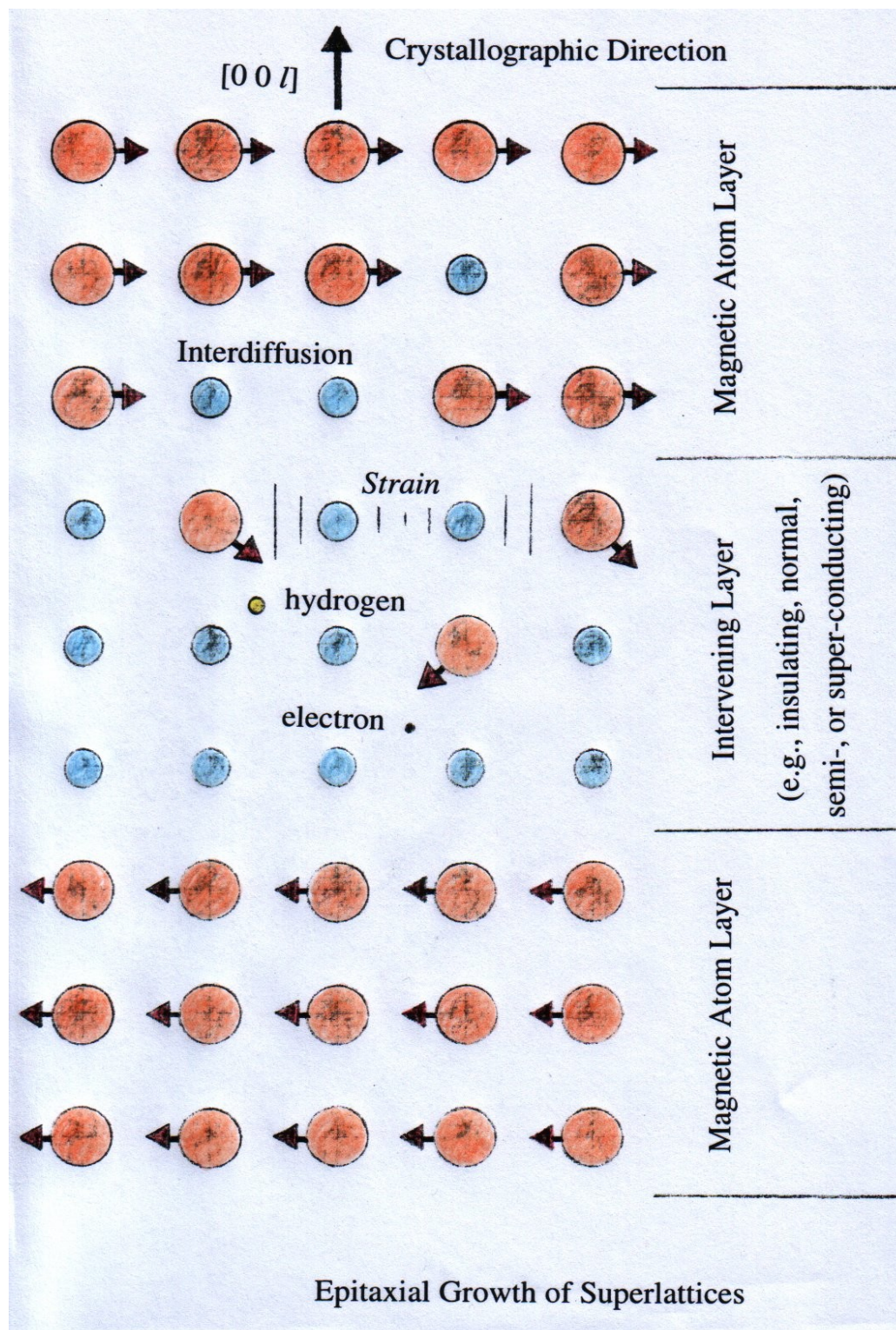


Scientific Background on the Nobel Prize in Physics 2007

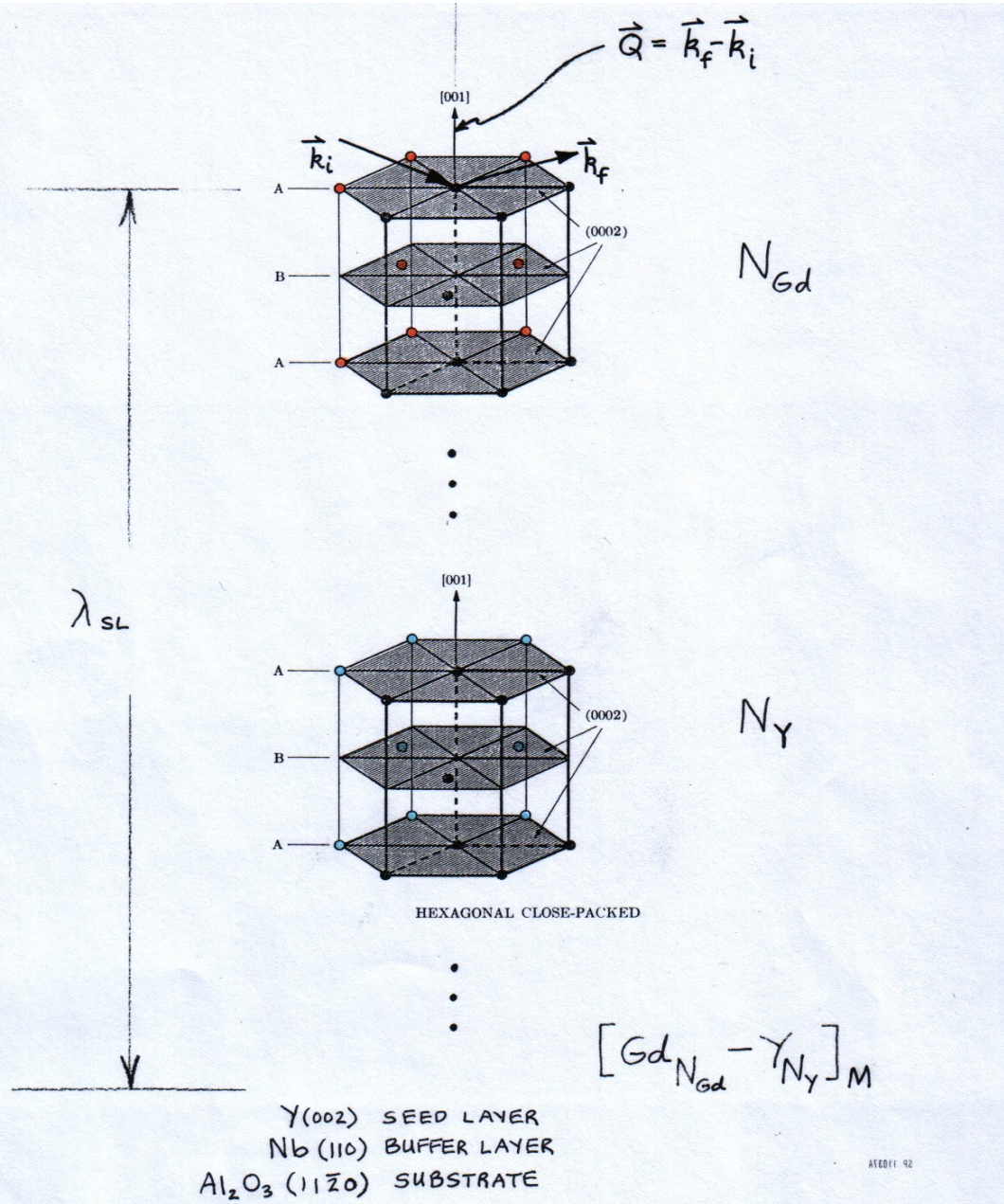
## The Discovery of Giant Magnetoresistance

compiled by the Class for Physics of the Royal Swedish Academy of Sciences

As recounted in the “Scientific Background” material referred to on the left side of the page, prior to the discovery of the GMR effect by Gruenberg, polarized neutron diffraction studies of magnetic superlattices revealed an unambiguous coupling between magnetic layers across intervening nonmagnetic spacers. The interlayer coupling (IEC) observed in this neutron diffraction work was explained in terms of long-range exchange interactions, for example, the RKKY (Ruderman Kittel Kasuya Yosida) interaction. Interestingly, the underlying mechanism responsible for GMR was thus known about before the effect itself was discovered! Much of the original neutron diffraction work was performed at the NIST (then NBS) neutron scattering facility by scientists including James Rhyne, Ross Erwin, and Julie Borchers, some of whom continue related forefront research today at the NCNR. This is an example of the continuing importance of neutron scattering as a fundamental probe of condensed matter.



Epitaxial Growth of Superlattices



Gd<sub>10</sub>-Y<sub>10</sub> T=79.K H=2.kOe

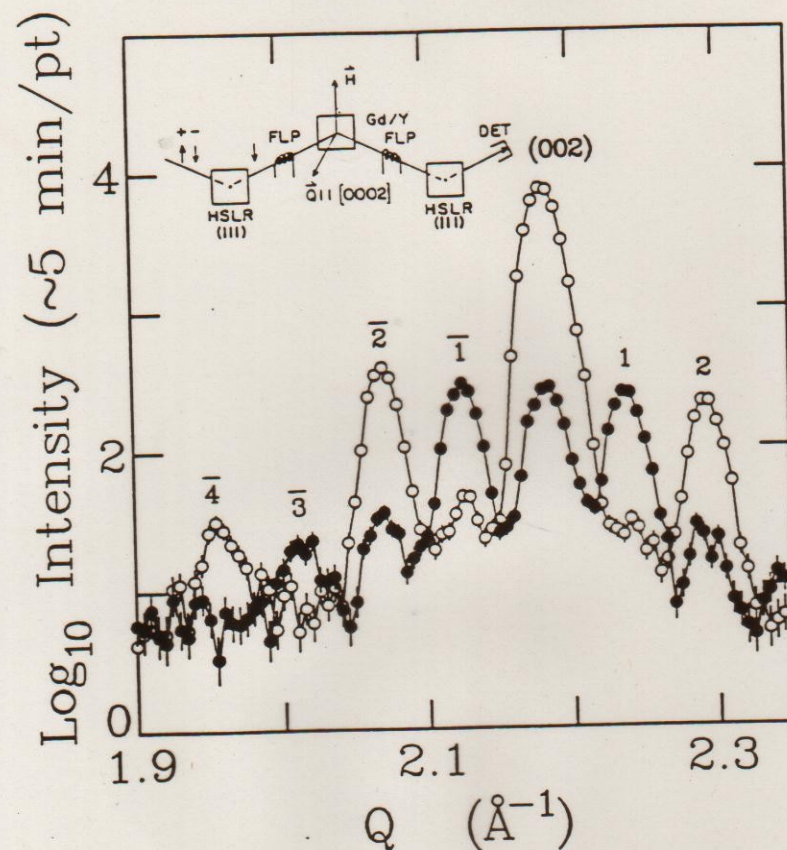


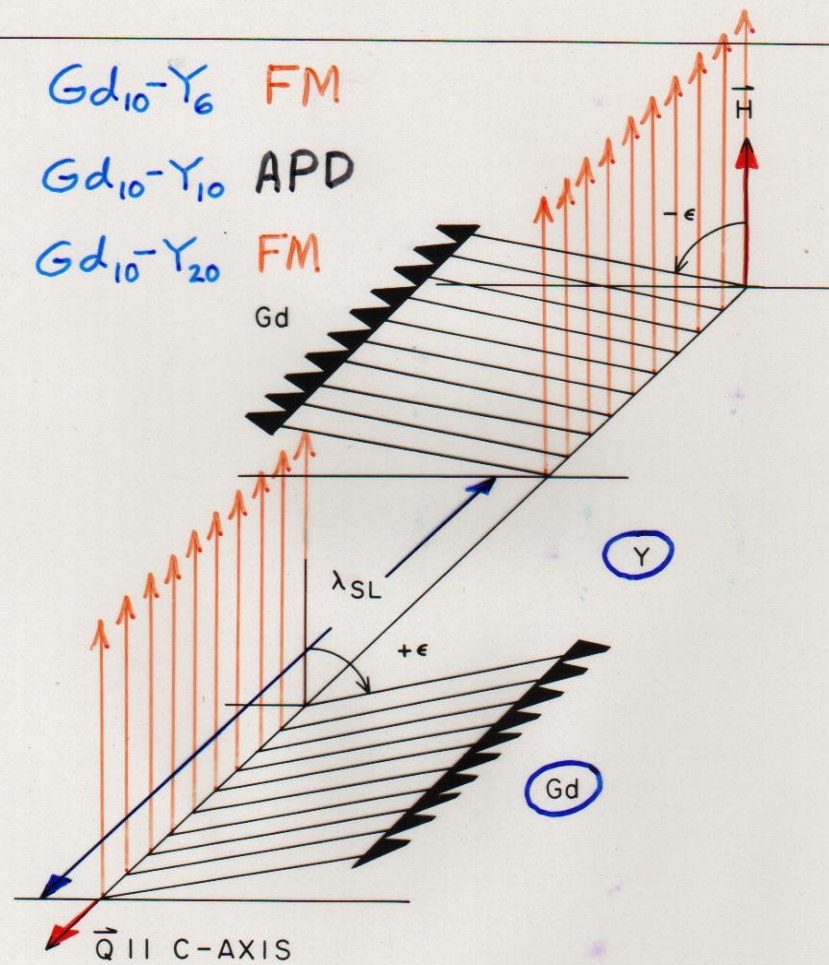
Fig. 7-1

Figure 7-1. NSF (open circles) and SF (filled circles) scattering from a  $[\text{Gd}_{10} - \text{Y}_{10}]$  superlattice as described in the text. The data have not been corrected for instrumental polarizing and flipping efficiencies (the SF scattering at the (002) position is predominantly, if not entirely, instrumental in origin). The SF scattering which appears at values of  $Q$  corresponding to a doubling of the chemical bilayer spacing (odd-numbered satellites) is consistent with an antiferromagnetic alignment (for an applied field approaching zero) of neighboring ferromagnetic Gd layers as depicted schematically in Figure 7-2. (After Majkrzak et al. (1986)).

$Gd_{10}-Y_6$  FM

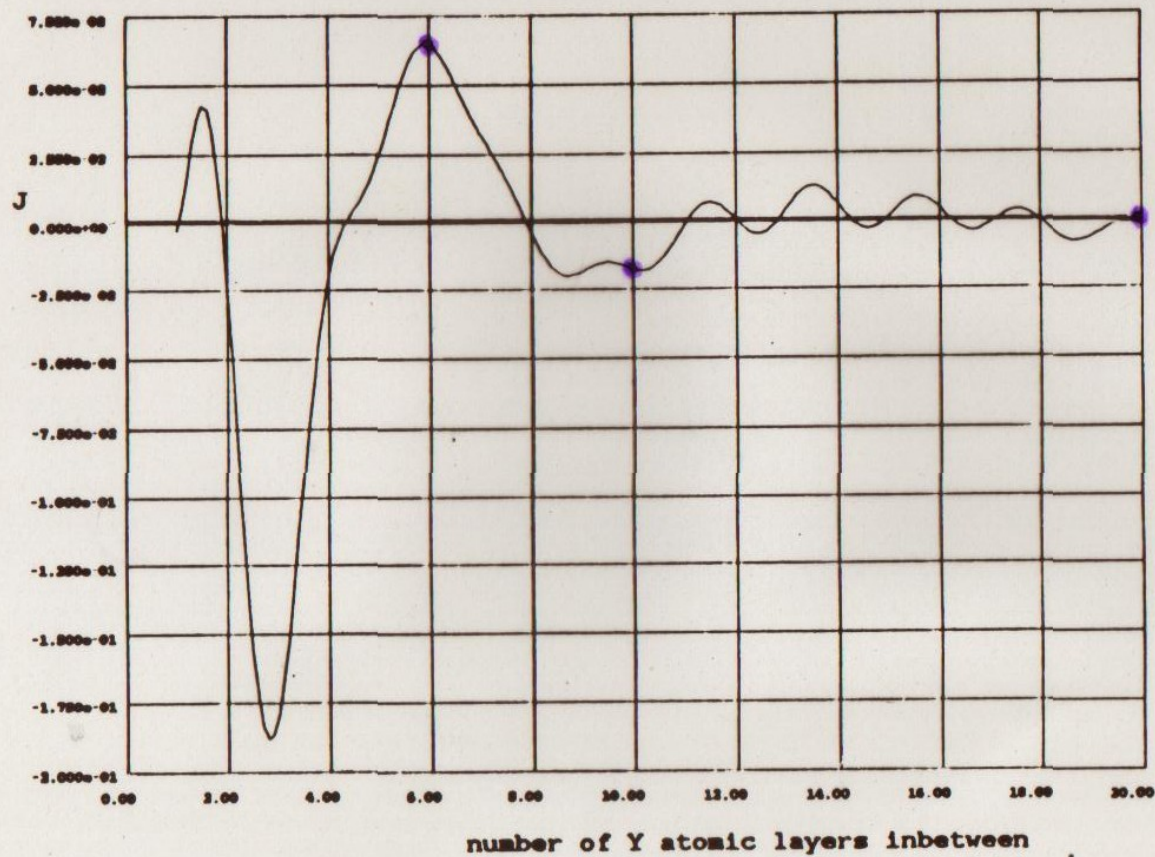
$Gd_{10}-Y_{10}$  APD

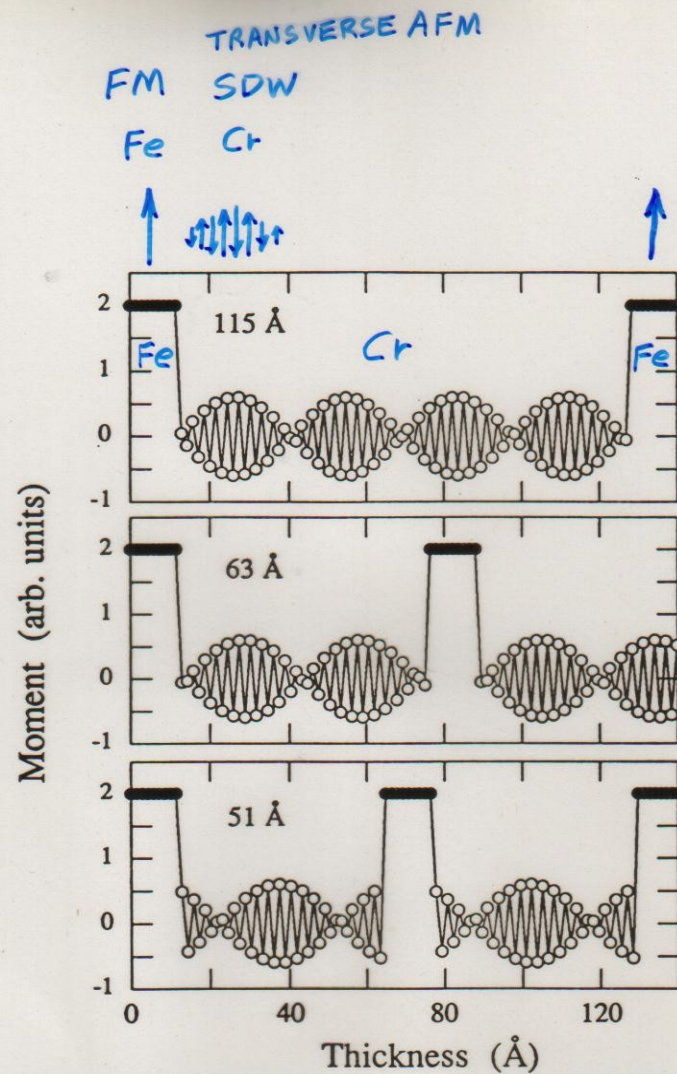
$Gd_{10}-Y_{20}$  FM



• n-diff. meas.

Gd in Y, Range Function,  $q_{\max} = .28 \cdot 2\pi/c$





Fe/Cr SUPERLATTICES

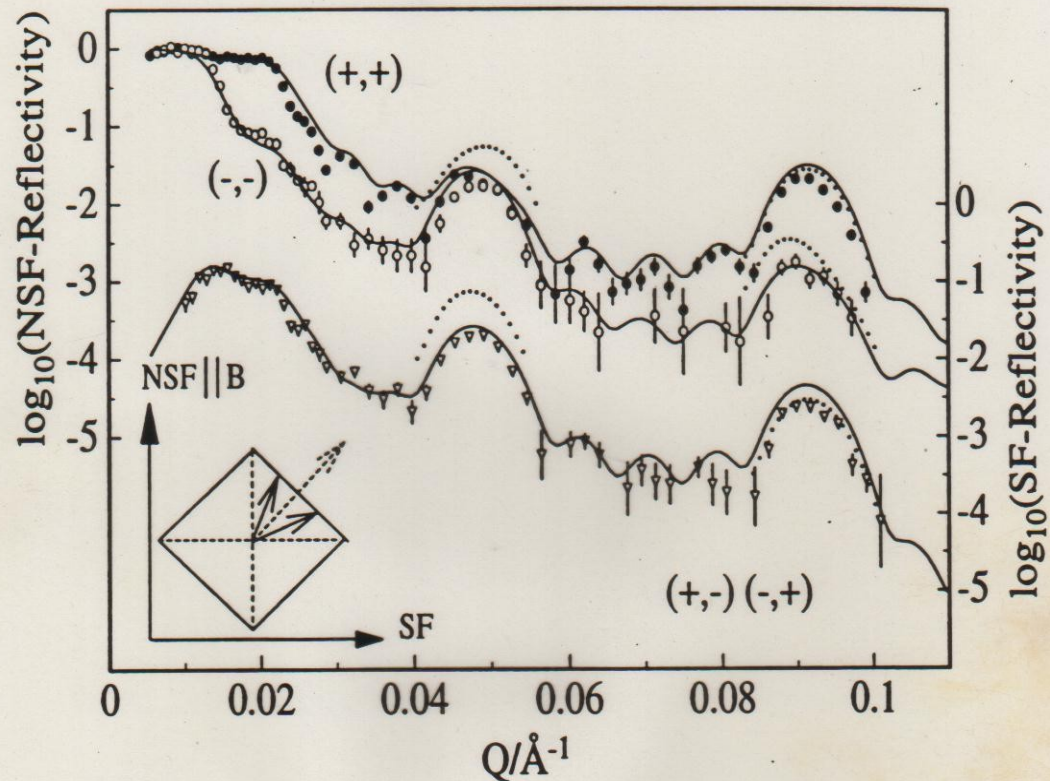
(GMR)

FULLERTON, BADER, & ROBERTSON

Figure 3

SCHREYER, ZEIDLER, ZABEL, ANKNER, MAJKREK,  
SCHÄFER, & GRÜNBERG, THIS CONFERENCE

# NONCOLLINEAR Fe/Cr(001)

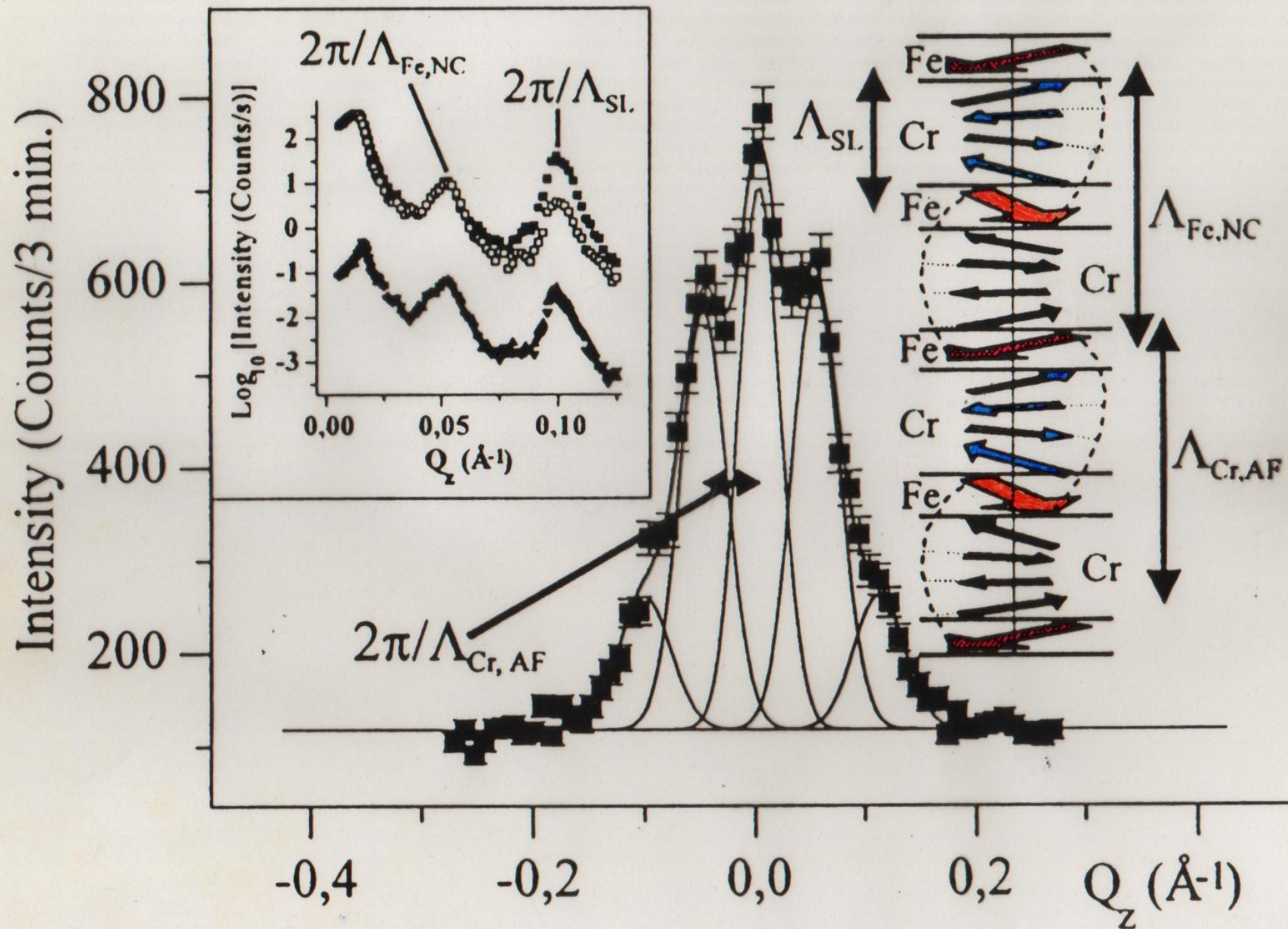


..... 90°

— 50°

$$E = \underbrace{-J_1 \frac{\vec{M}_1 \cdot \vec{M}_2}{|\vec{M}_1| |\vec{M}_2|}}_{\text{EXCHANGE COUPLING BILINEAR}} - \underbrace{J_2 \left( \frac{\vec{M}_1 \cdot \vec{M}_2}{|\vec{M}_1| |\vec{M}_2|} \right)^2}_{\text{BIQUADRATIC}}$$

*A. Schreyer et al.*



# Pinpointing Chiral Structures with Front/Back Polarized Neutron Reflectometry

We have developed a new method of using polarized neutron reflectometry (PNR) to extract the structure of buried magnetic spirals in magnetic films. This technique improves upon earlier methods by being particularly sensitive to the presence of magnetic twists vis-à-vis structures in which the magnetization direction does not vary appreciably. Tracking the formation and growth of twists may solve a number of puzzles that hamper the development of magnetic thin film devices.

In collaboration with IBM scientists, we have applied the technique to a thin-film exchange-spring magnet and confirmed that the results may violate the current theory regarding the behavior of such magnets. It has been predicted that exchange-spring magnets, comprised of soft and hard ferromagnets in close proximity, are a composite that has a strong moment and does not readily demagnetize [1]. Therefore, exchange-spring magnets should give industry the ability to make much smaller permanent magnets for use in the magnetic recording devices, and elsewhere. As a side effect, when a small external magnetic field is opposed to that of the magnet, the portion of the soft ferromagnet farthest from the hard ferromagnet may twist into alignment with the field. When the field is removed, the soft ferromagnet untwists. The film provided by IBM consists of the hard ferromagnet  $\text{Fe}_{55}\text{Pt}_{45}$  topped by the soft ferromagnet  $\text{Ni}_{80}\text{Fe}_{20}$  [2].

Figure 1 shows a simplified diagram of the behavior predicted by current theories [1]. A magnetic field of 0.890 T, provided by an electromagnet, is sufficient to align both the soft and the hard layers of our exchange-spring magnet, as shown on the left. When a modest reverse field (on the order of 0.025 T) is applied to the exchange spring magnet, only the top of the soft layer will realign with the magnetic field. The hard layer remains pinned in the original direction, and a continuous twist is induced in the soft layer, as the direction of magnetization changes smoothly between the reverse field direction to the aligning field direction.

Although there are many alternatives to PNR to measure the magnetization, typically they measure only the average orientation of the magnetic spins, and cannot readily distinguish a spiral from a structure in which all the spins are canted with respect to an external field. PNR can extract the

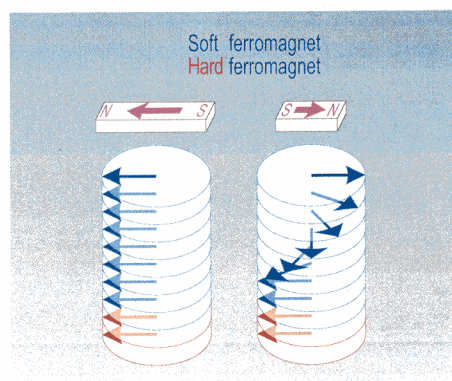


FIGURE 1. Model for field behavior of exchange-spring magnets. On the left the magnet has been aligned by a large external magnetic field. On the right a smaller field opposed to the first field causes a twist to form in the soft ferromagnet, while the hard ferromagnet remains aligned.

depth-dependence of the magnetic and chemical structure. We have studied the sample over a wide range of external magnetic fields, and can track the development of the spiral with field [3].

A PNR experiment begins with neutrons whose magnetic moments are aligned parallel (+) or opposite (−) to the external magnetic field. When the magnetization of the sample is perpendicular to this magnetic field, the neutron moment precesses as it interacts with the sample. When this happens the spin-flip (SF) reflectivities  $R^{+-}$  and  $R^{-+}$  are strong. If the magnetization of the sample is parallel to the external magnetic field, no precession occurs, but the non-spin-flip (NSF) reflectivities  $R^{++}$  and  $R^{--}$  will differ. The NSF reflectivities also provide information about the chemical structure of the film.

Our new modification of the PNR method greatly enhances the contrast between colinear and certain non-colinear magnetic structures [4]. We first measure the reflectivity with neutrons glancing off the front surface of the material, and then repeat with neutrons glancing off the back surface. The experiment is akin to holding the plane of the film up to a “magnetic mirror” to see whether the mirror image is the same as the original structure. In a colinear structure, all the spins are aligned along a common direction, and the mirror image is very much like the original structure.

K. V. O'Donovan, J. A. Borchers, and C. F. Majkrzak  
NIST Center for Neutron Research  
National Institute of Standards and Technology  
Gaithersburg, MD 20899-8562

O. Hellwig, E. E. Fullerton  
IBM Almaden Research Facility  
San Jose, CA 95120-6001

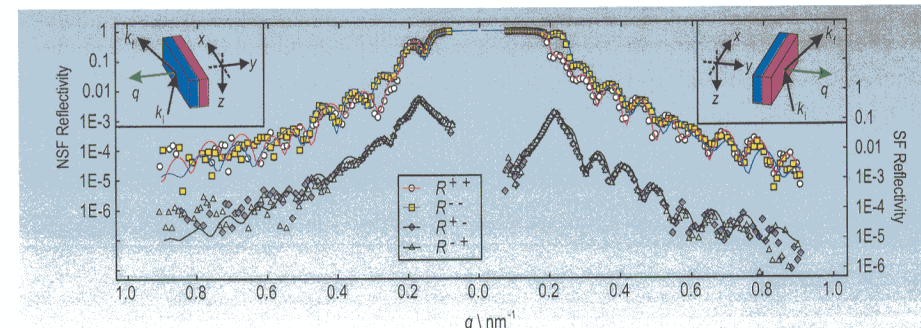


FIGURE 2. Reflectivity of a  $\text{Ni}_{80}\text{Fe}_{20}/\text{Fe}_{55}\text{Pt}_{45}$  bilayer. The front reflectivity is plotted on the right while the back reflectivity is plotted on the left. The SF reflectivities  $R^{+-}$  and  $R^{-+}$  are plotted against the right ordinate axis. The NSF reflectivities  $R^{++}$  and  $R^{--}$  are plotted against the left ordinate axis.

But the mirror image of a magnetic twist to the right is a magnetic twist to the left. Therefore, if the front and back reflectivities are significantly different, we can deduce the presence of a spiral. Fitting the data confirms the spiral's existence.

Figure 2 shows data collected at 0.026 T after aligning in -0.89 T. Fits to the data are shown as solid lines. The data from the front reflectivity are shown on the right, and the data from the back reflectivity are shown on the left. The spin-flip (SF) reflectivities  $R^{+-}$  and  $R^{-+}$  are plotted against the right-hand axis, which have been shifted relative to the NSF reflectivities  $R^{++}$  and  $R^{--}$  plotted against the left axis. At  $q = 0.2 \text{ nm}^{-1}$ , there is a splitting in the front NSF reflectivity that is much more pronounced than that of the back reflectivity at the same  $q$ . This is a hallmark of the spiral structure.

Figure 3 shows the magnetic structure that gives the excellent fit to the data plotted in Fig. 2. The location of the hard/soft interface is marked in Fig. 3. Surprisingly, we discover the spiral invades the hard ferromagnet even at extremely low fields. Current theory predicts that when this occurs, the soft ferromagnet will not be able to untwist fully. Yet, other magnetic studies show that our exchange-spring magnet does untwist when this field is removed. Thus, our PNR measurements have identified a shortcoming of current theory.

With this new technique, NIST is now able to better characterize the magnetic properties of thin films, which can improve the capability and reliability of industrial devices for magnetic recording and sensing.

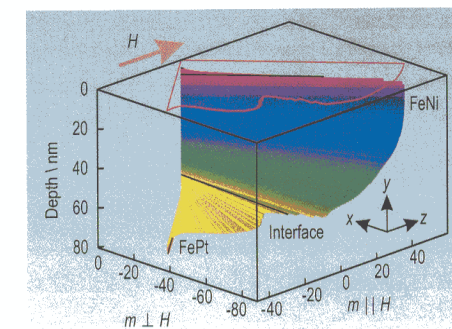
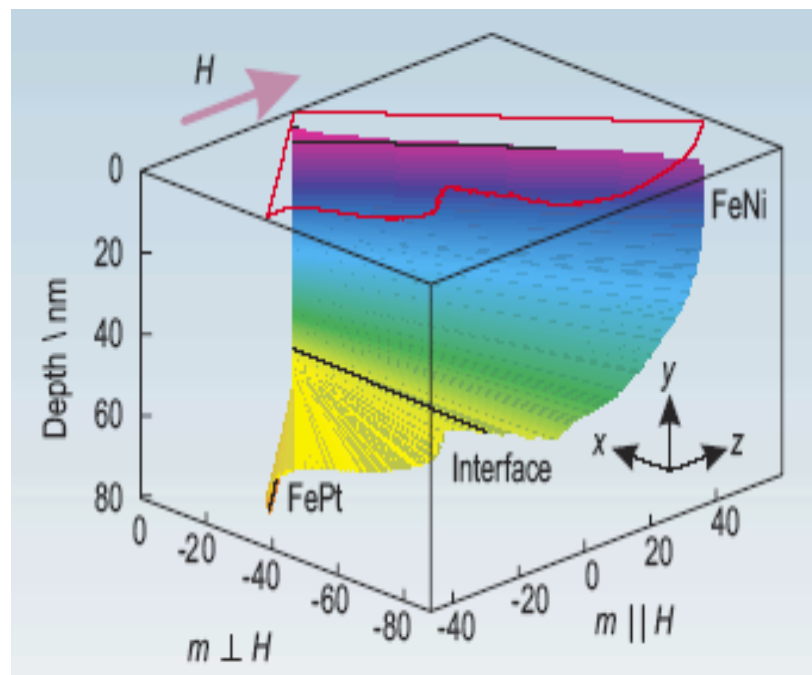
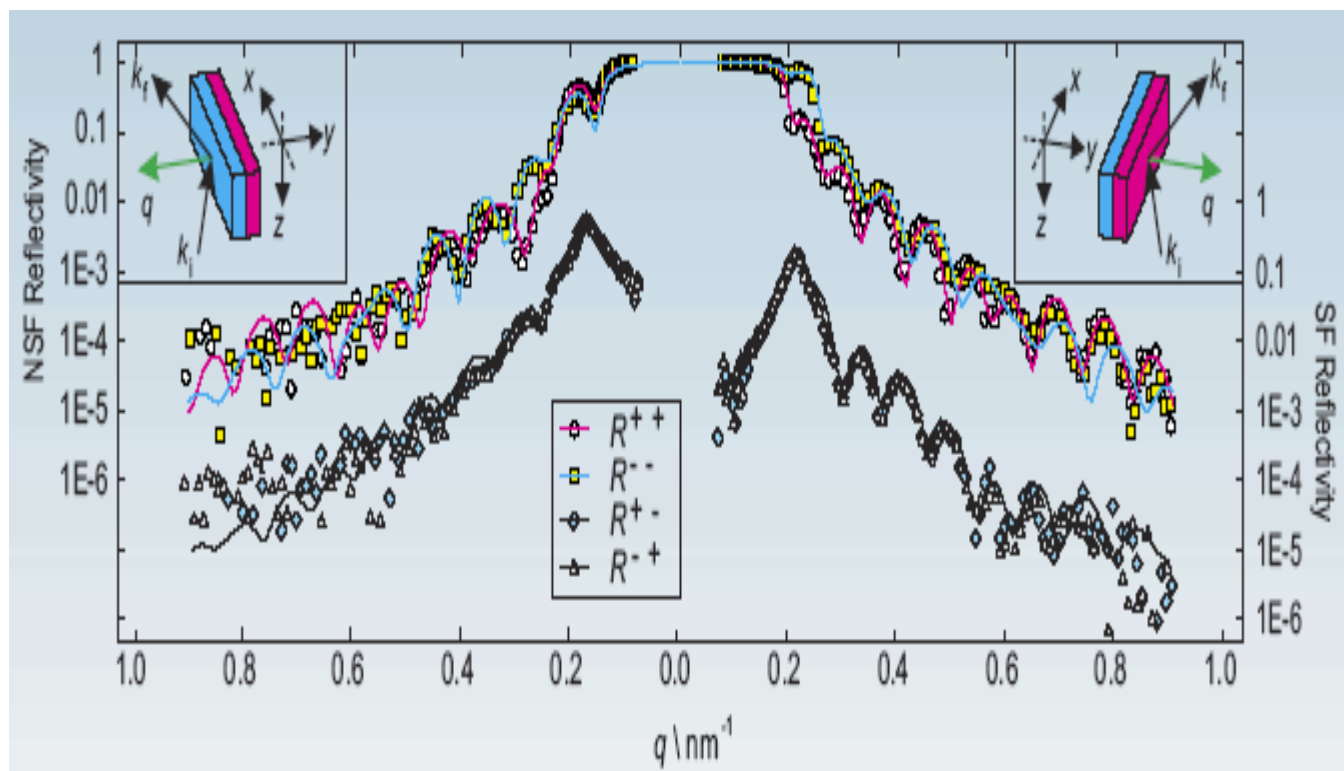


FIGURE 3. Fitted magnetization of the data presented in Fig. 2. The front of the sample is at a depth of 0 nm and the back is at a depth of 70 nm. The red curve is a projection of the magnetic structure into the plane of the front surface.

## References

- [1] E. F. Kneller and R. Hawig, *IEEE Trans. Magn.* **27**, 3588 (1991).
- [2] O. Hellwig, J. B. Kortright, K. Takano, and E. E. Fullerton, *Phys. Rev. B* **62**, 11694 (2000).
- [3] K. V. O'Donovan, *et al.*, in preparation.
- [4] K. V. O'Donovan, *et al.*, submitted to *Applied Physics A*.



Example of polarized neutron reflectometry.  
(After Kevin O'Donovan et al.)

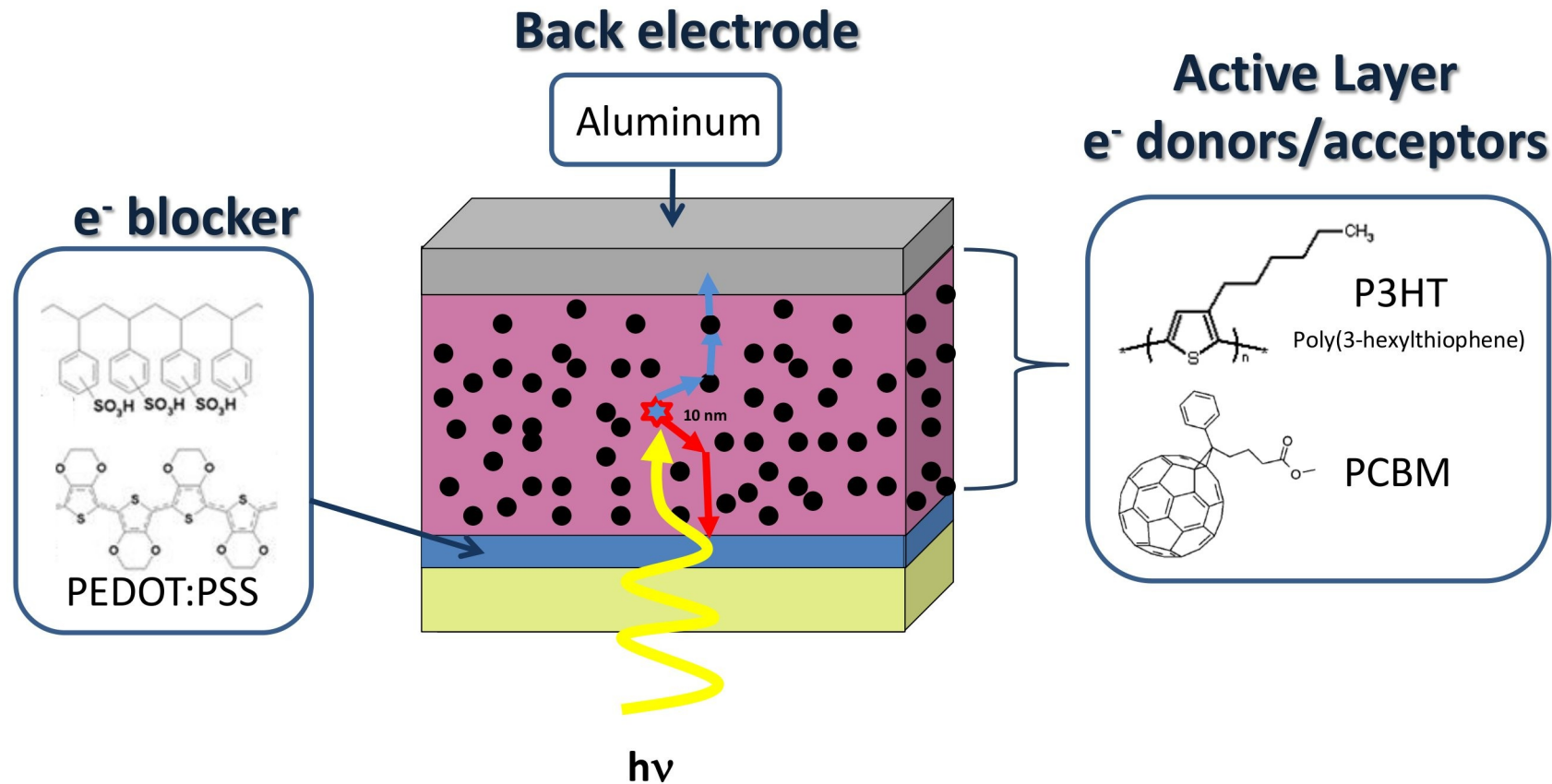
# Nanoparticle distribution in polymer-based solar cells affects solar cell performance: A neutron reflectivity study

Jonathan Kiel<sup>1</sup>, Brian Kirby<sup>2</sup>, Charles Majkrzak<sup>2</sup>,  
Brian Maranville<sup>2</sup>, Michael Mackay<sup>3</sup>

Thursday, August 20th, 2009

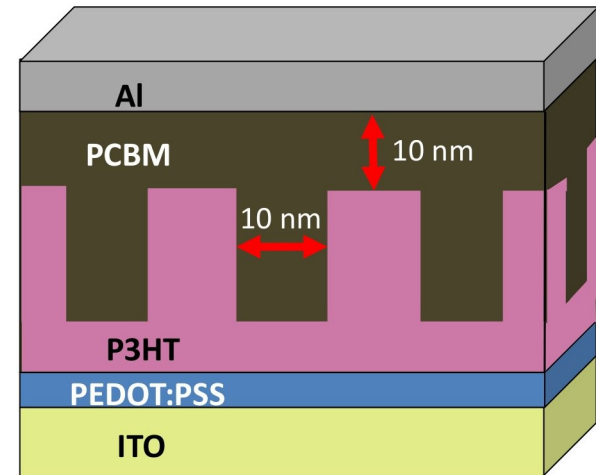
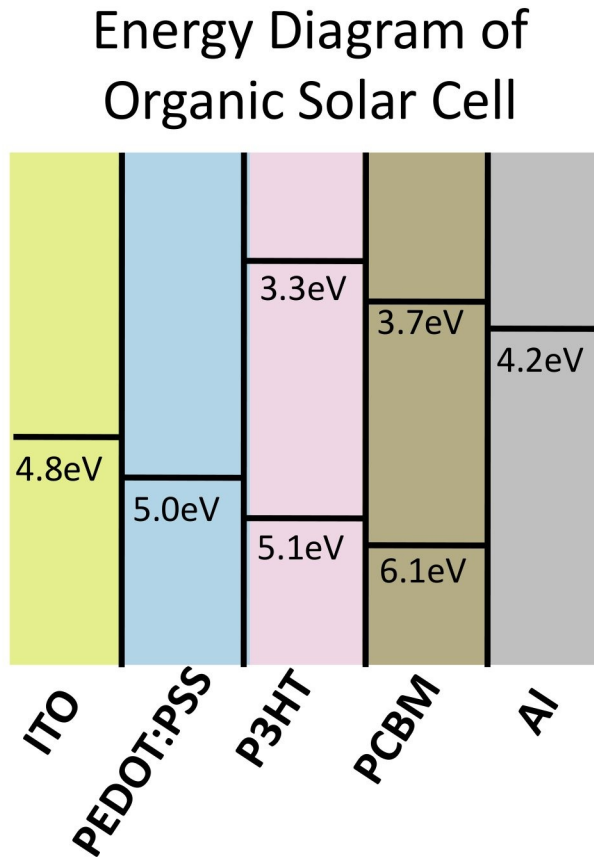
- 1) Michigan State University, Department of Chemical Engineering and Materials Science
- 2) National Institute of Standards and Technology, Center for Neutron Research
- 3) University of Delaware, Materials Science and Engineering

# Components of organic solar cells

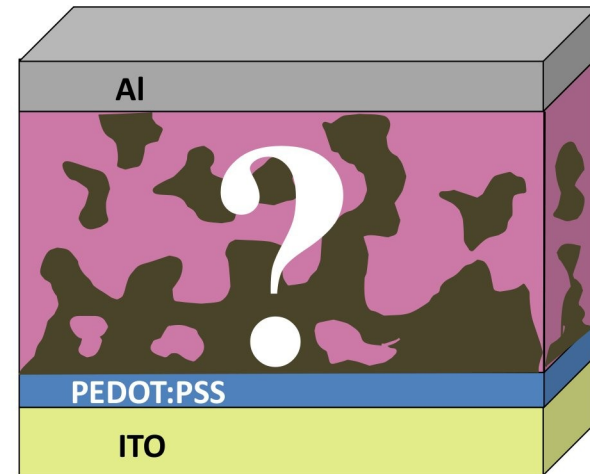


- Exciton diffusion length  $\sim 10$  nm
- PCBM:P3HT morphology very important

# What is the morphology of the active layer

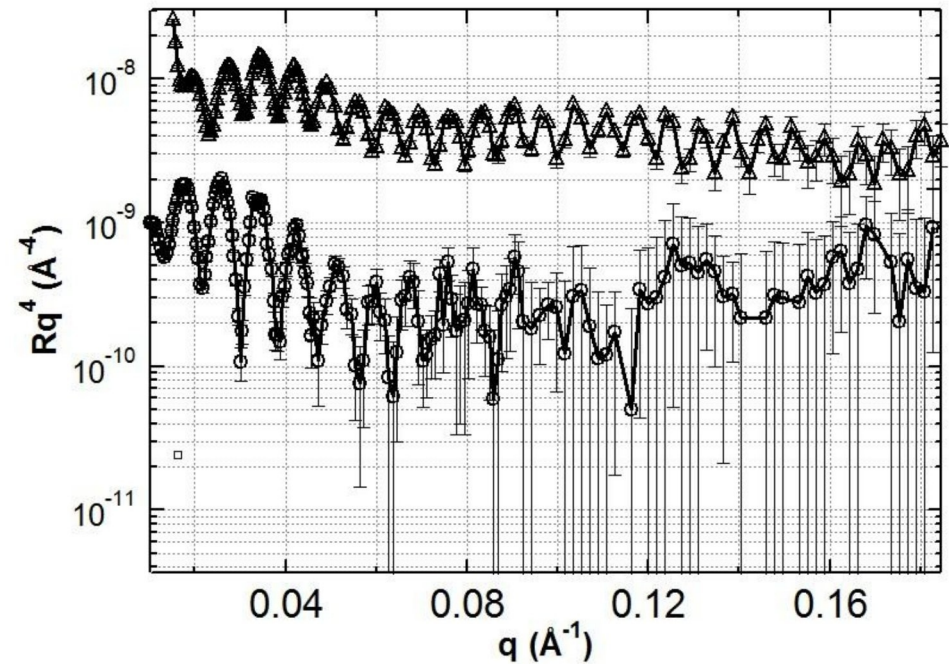
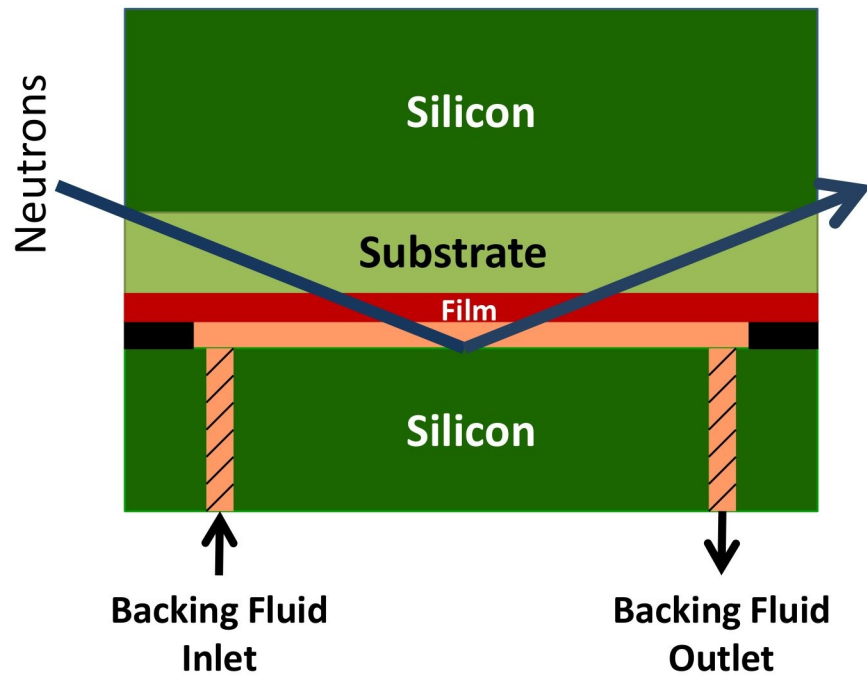


Idealized morphology

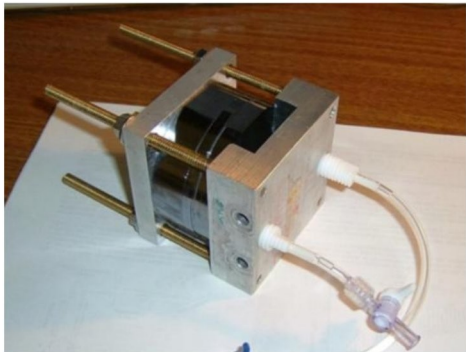


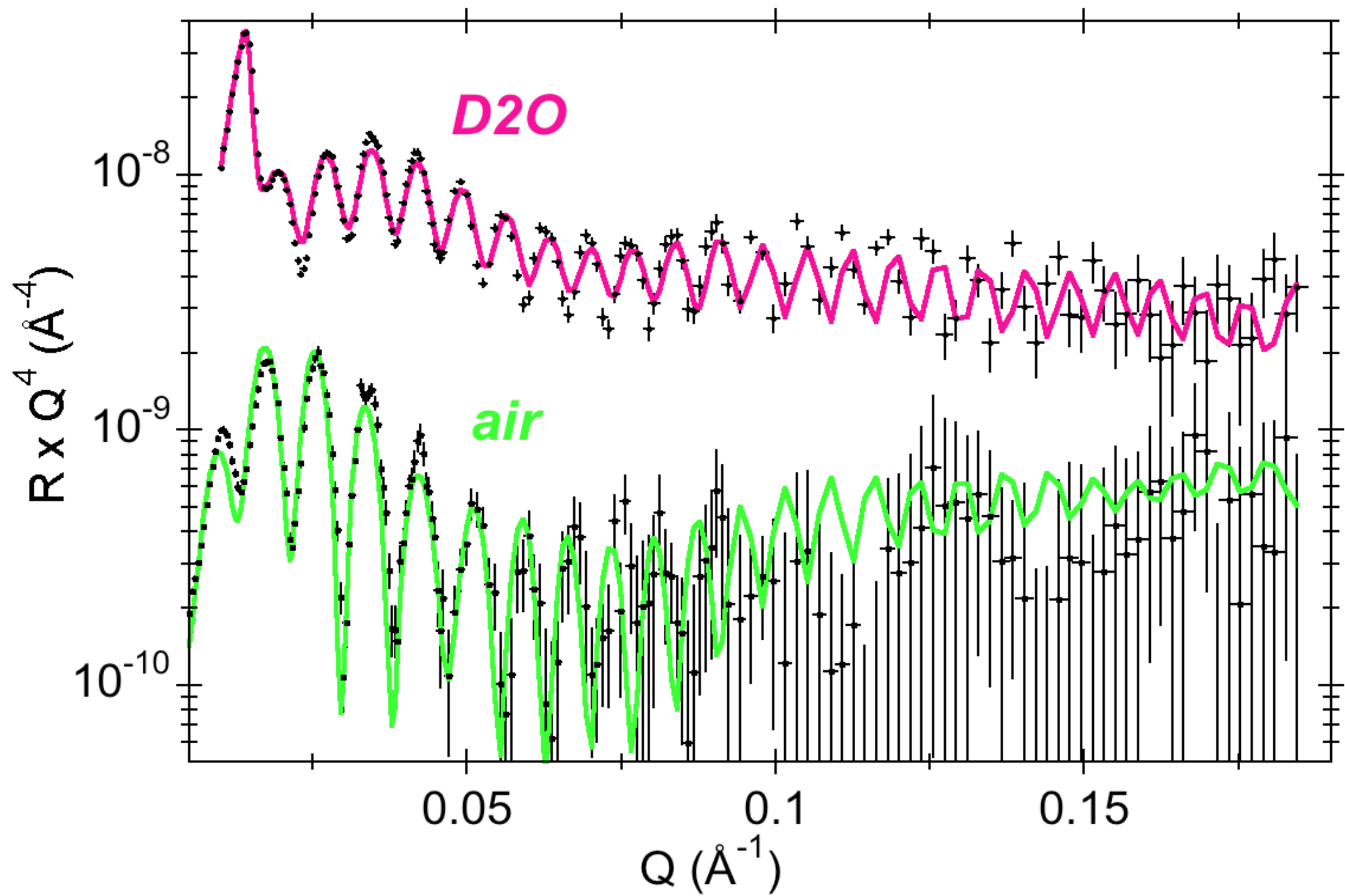
Actual morphology

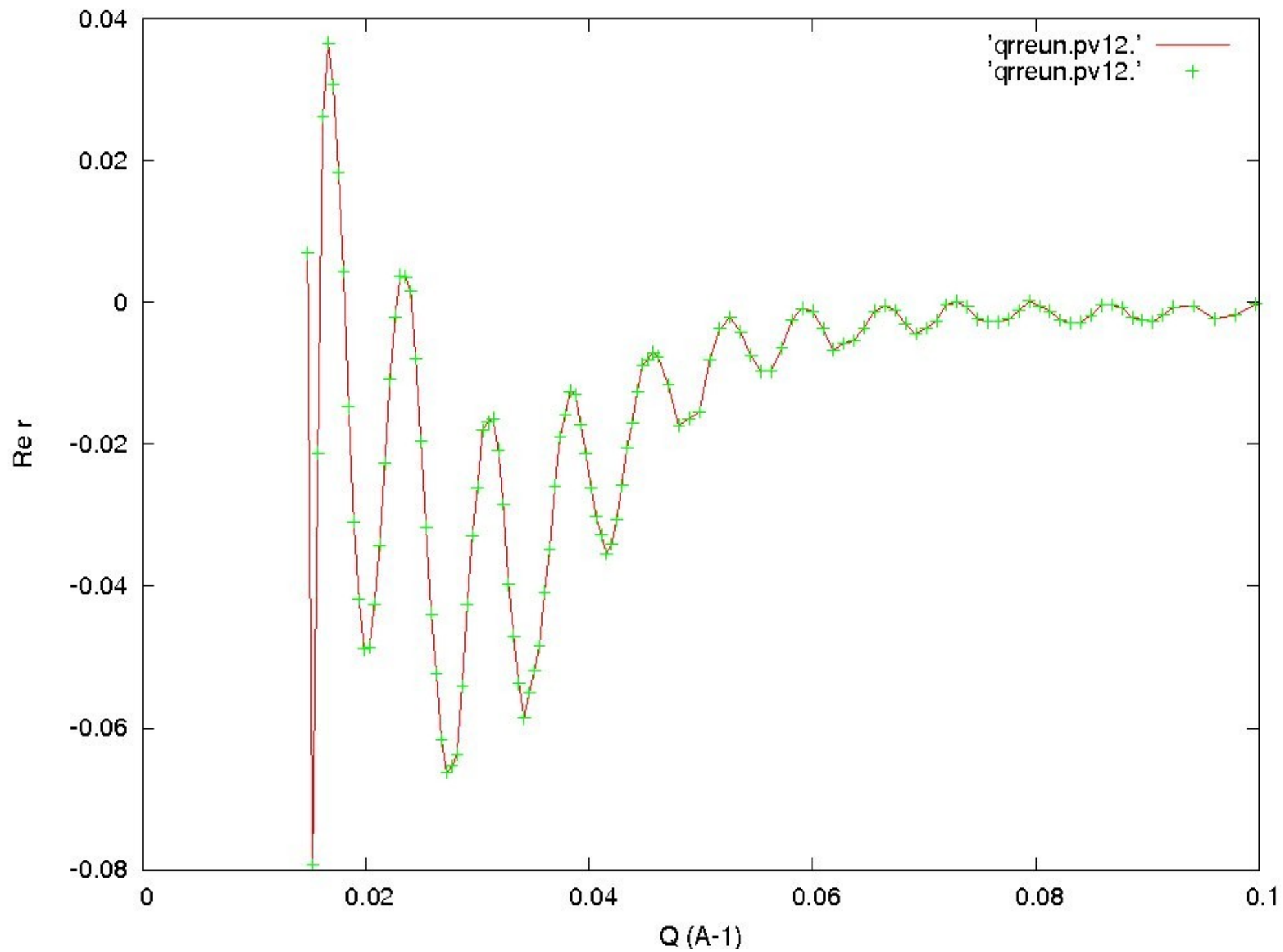
# Wet Cell Holder – Deuterated Backing Media

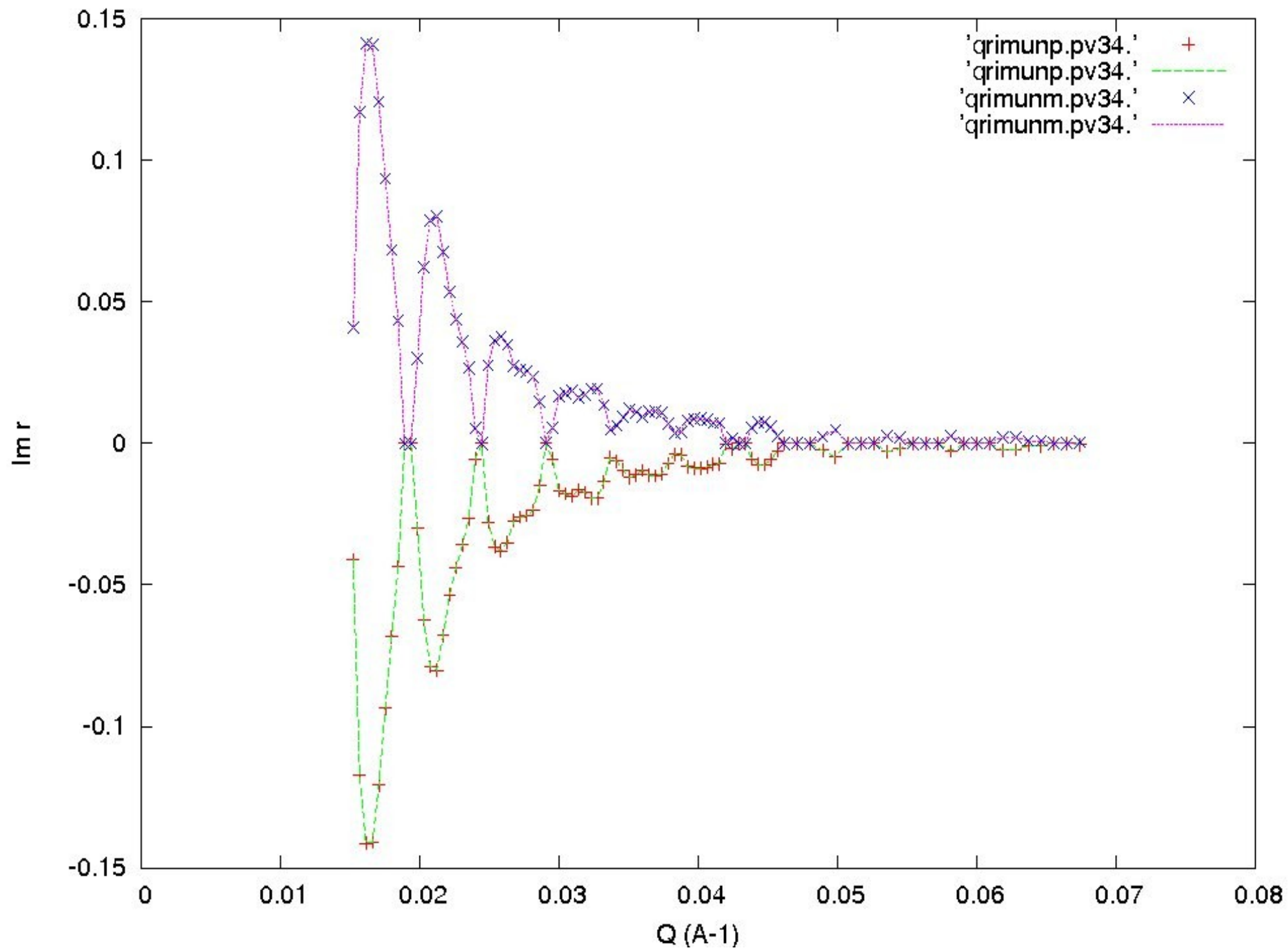


Addition of high SLD backing media greatly enhances scattering intensity and statistics

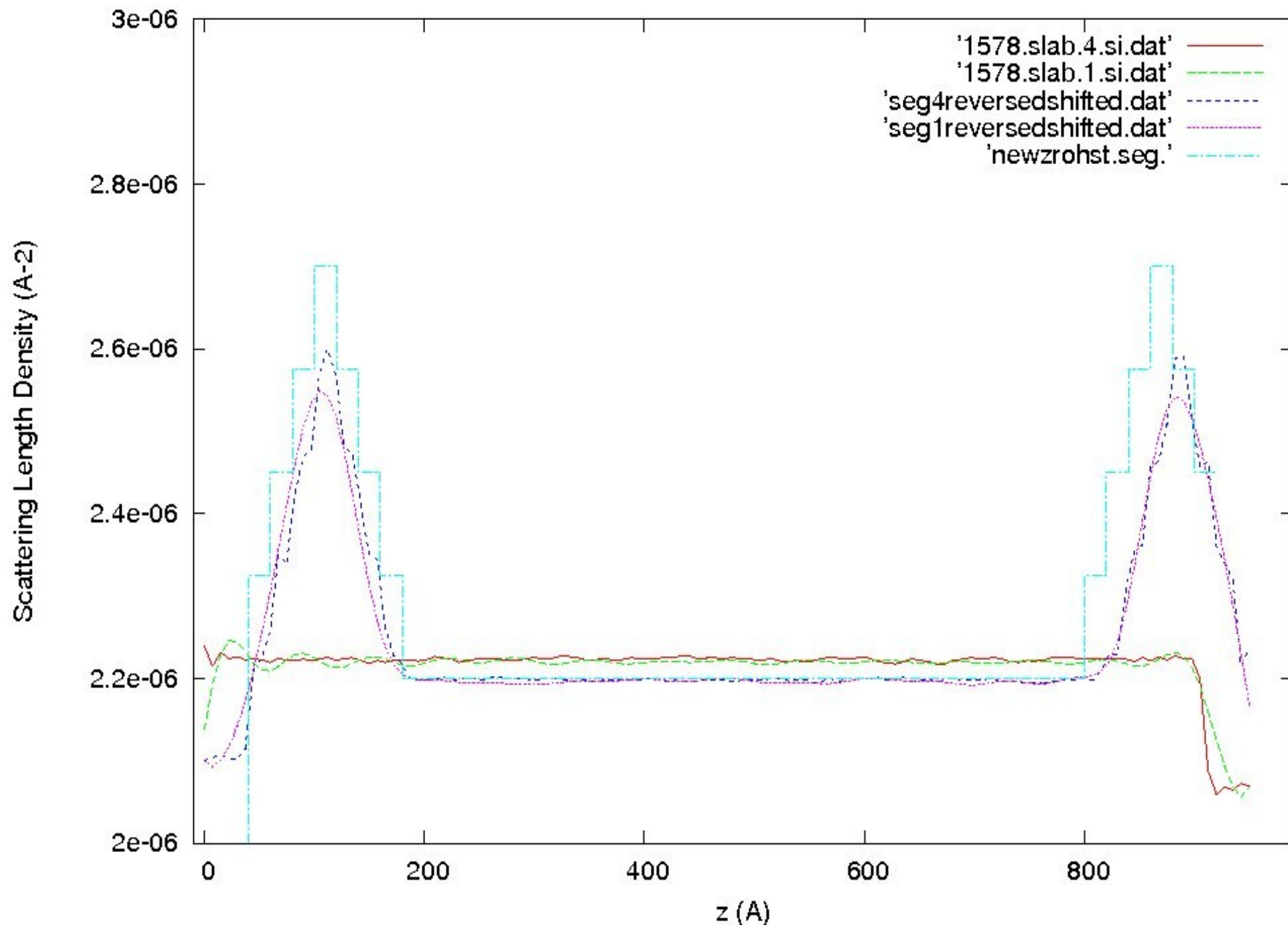


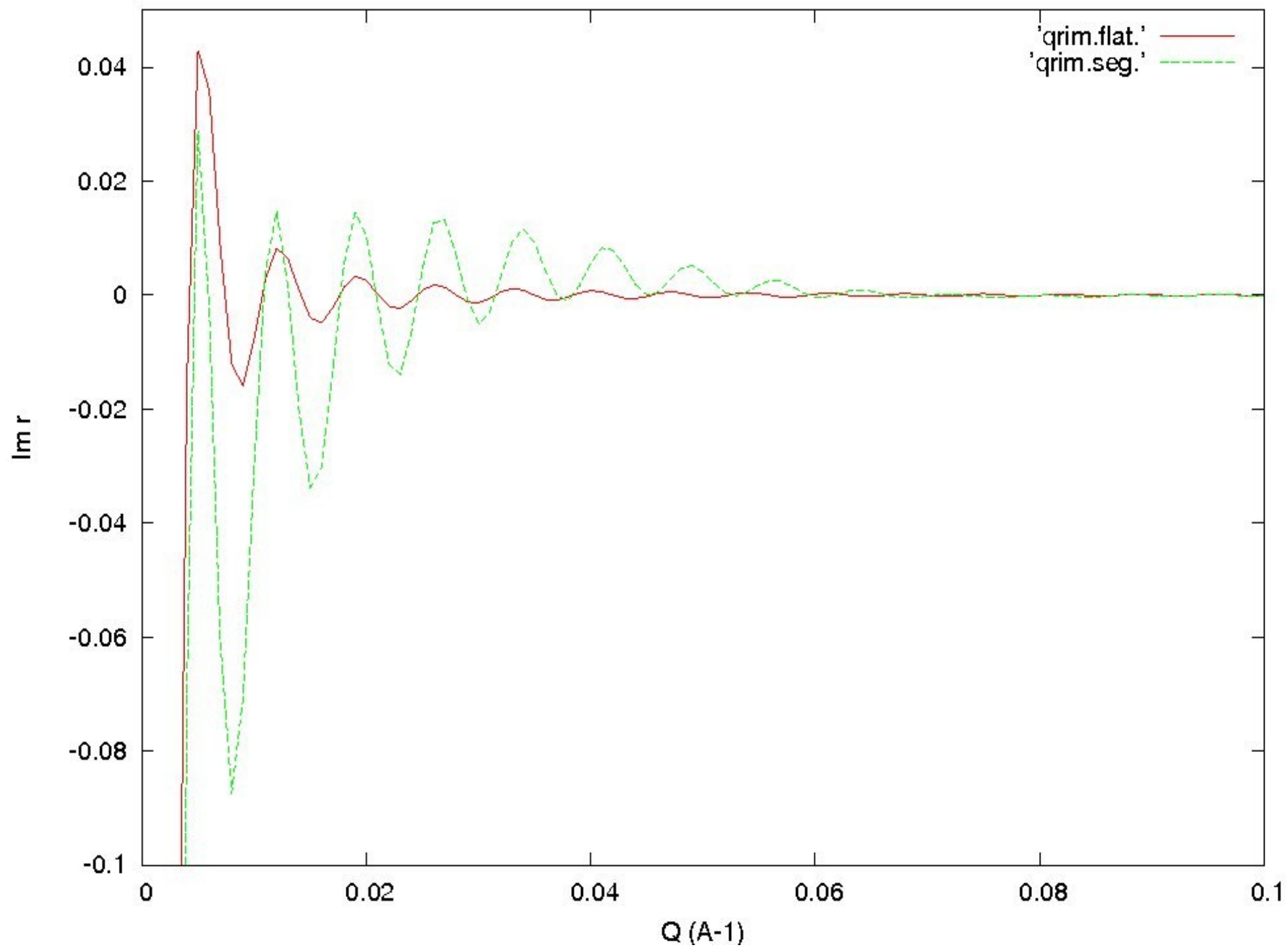




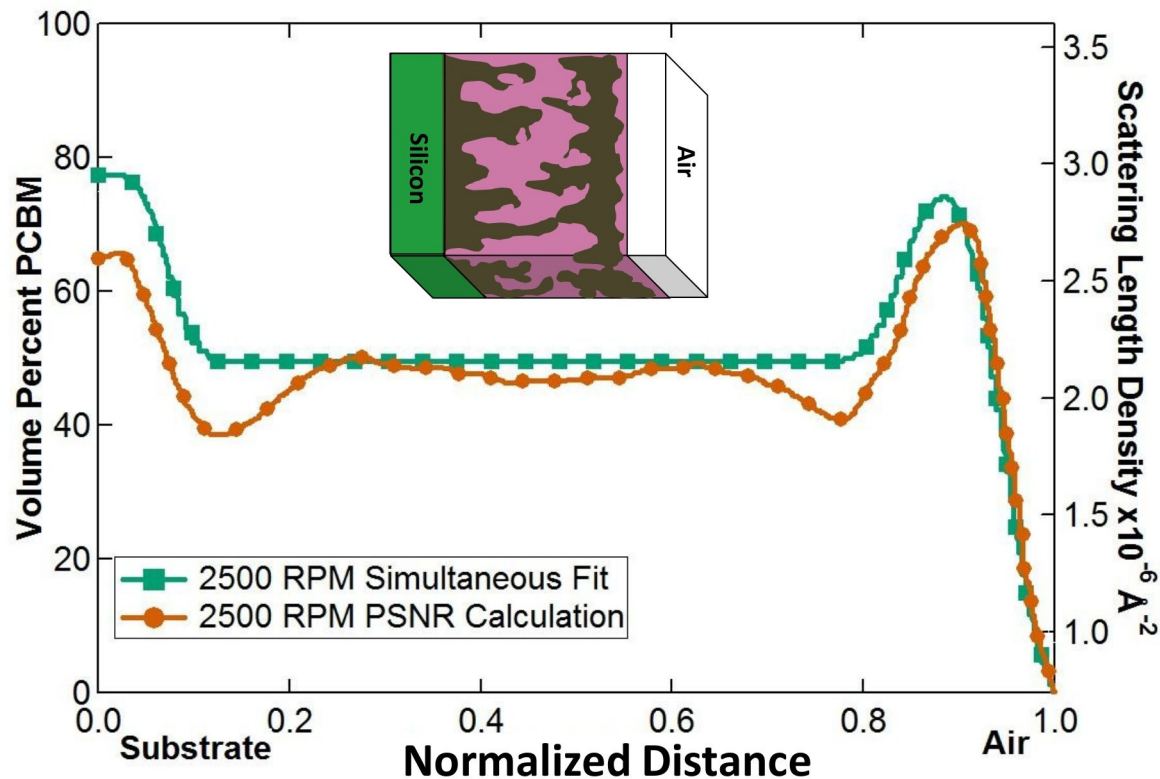


# SLD Depth Profile



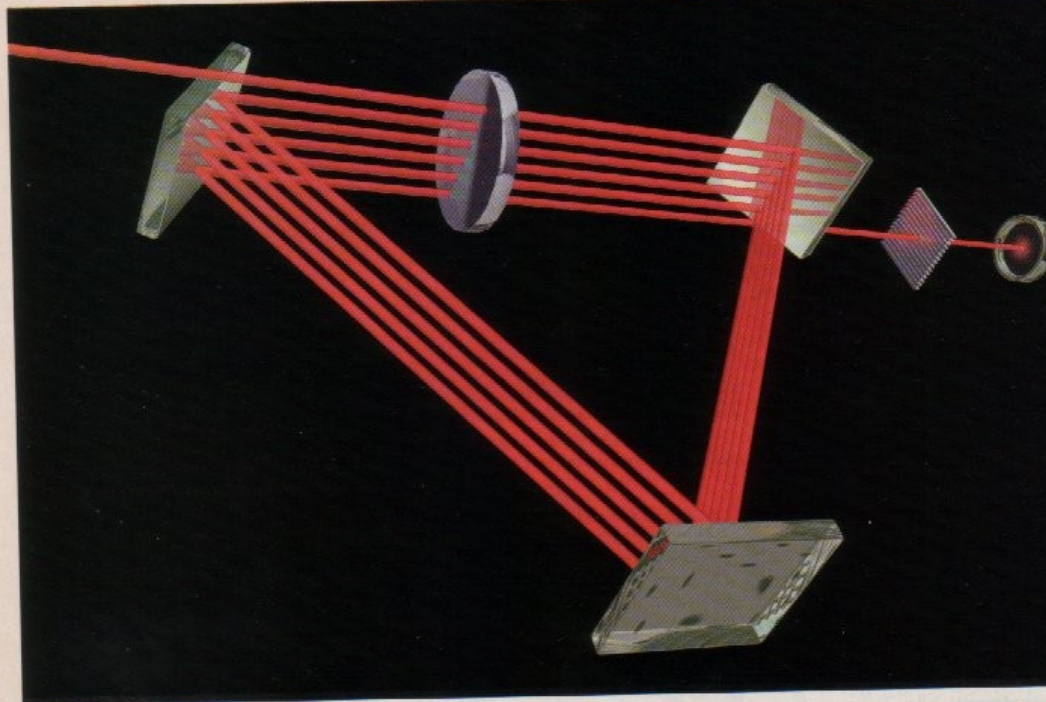


# PCBM Volume % Comparison



- Simultaneous fitting and PSNR calculations show great agreement
- High PCBM concentration at substrate
- High PCBM concentration near air interface

$$\text{Vol\% PCBM} = \frac{\text{SLD}_{\text{measured}} - \text{SLD}_{\text{P3HT}}}{\text{SLD}_{\text{PCBM}} - \text{SLD}_{\text{P3HT}}}$$



# Quantum Seeing in the Dark

*Quantum optics demonstrates the existence of interaction-free measurements: the detection of objects without light—or anything else—ever hitting them*

by Paul Kwiat, Harald Weinfurter and Anton Zeilinger

**I**n Greek mythology, the hero Perseus is faced with the unenviable task of fighting the dreaded Medusa. The snake-haired beast is so hideous that a mere glimpse of her immediately turns any unlucky observer to stone. In one version of the story, Perseus avoids this fate by cleverly using his shield to reflect Medusa's image back to the creature herself, turning *her* to stone. But what if Perseus did not have well-polished armor? He presumably would have been doomed. If he closed his eyes, he would have been unable to find his target. And the smallest peck would

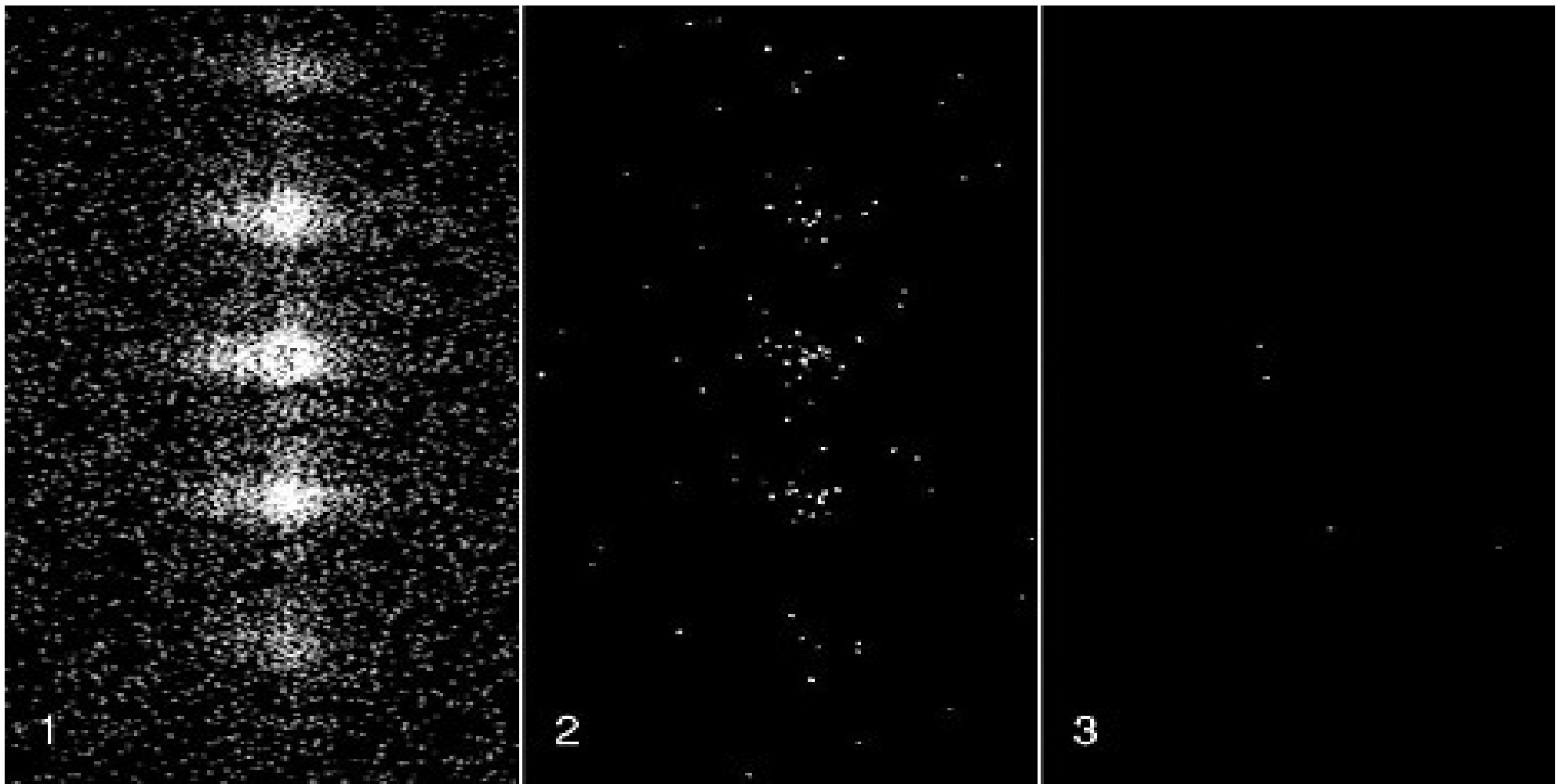
have allowed some bit of light striking Medusa to reflect into his eye; having thus "seen" the monster, he would have been finished.

In the world of physics, this predicament might be summed up by a seemingly innocuous, almost obvious claim made in 1962 by Nobelist Dennis Gabor, who invented holography. Gabor asserted, in essence, that no observation can be made with less than one photon—the basic particle, or quantum, of light—striking the observed object.

In the past several years, however, physicists in the increasingly bizarre

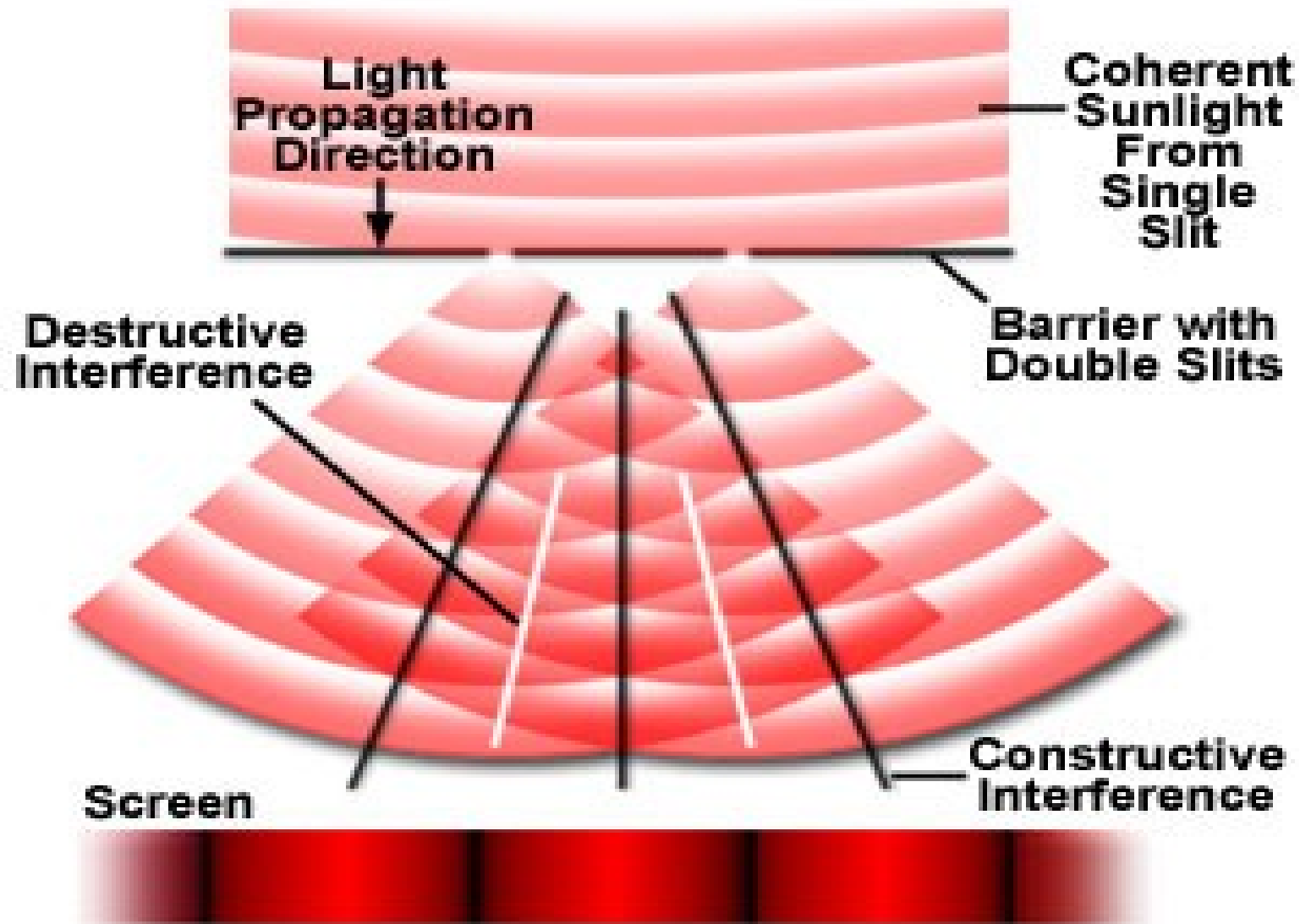
field of quantum optics have learned that not only is this claim far from obvious, it is, in fact, incorrect. For we now know how to determine the presence of an object with essentially no photons having touched it.

Such interaction-free measurement seems to be a contradiction—if there is no interaction, how can there be a measurement? That is a reasonable conundrum in classical mechanics, the field of physics describing the motions of footballs, planets and other objects that are not too small. But quantum mechanics—the science of electrons, photons and



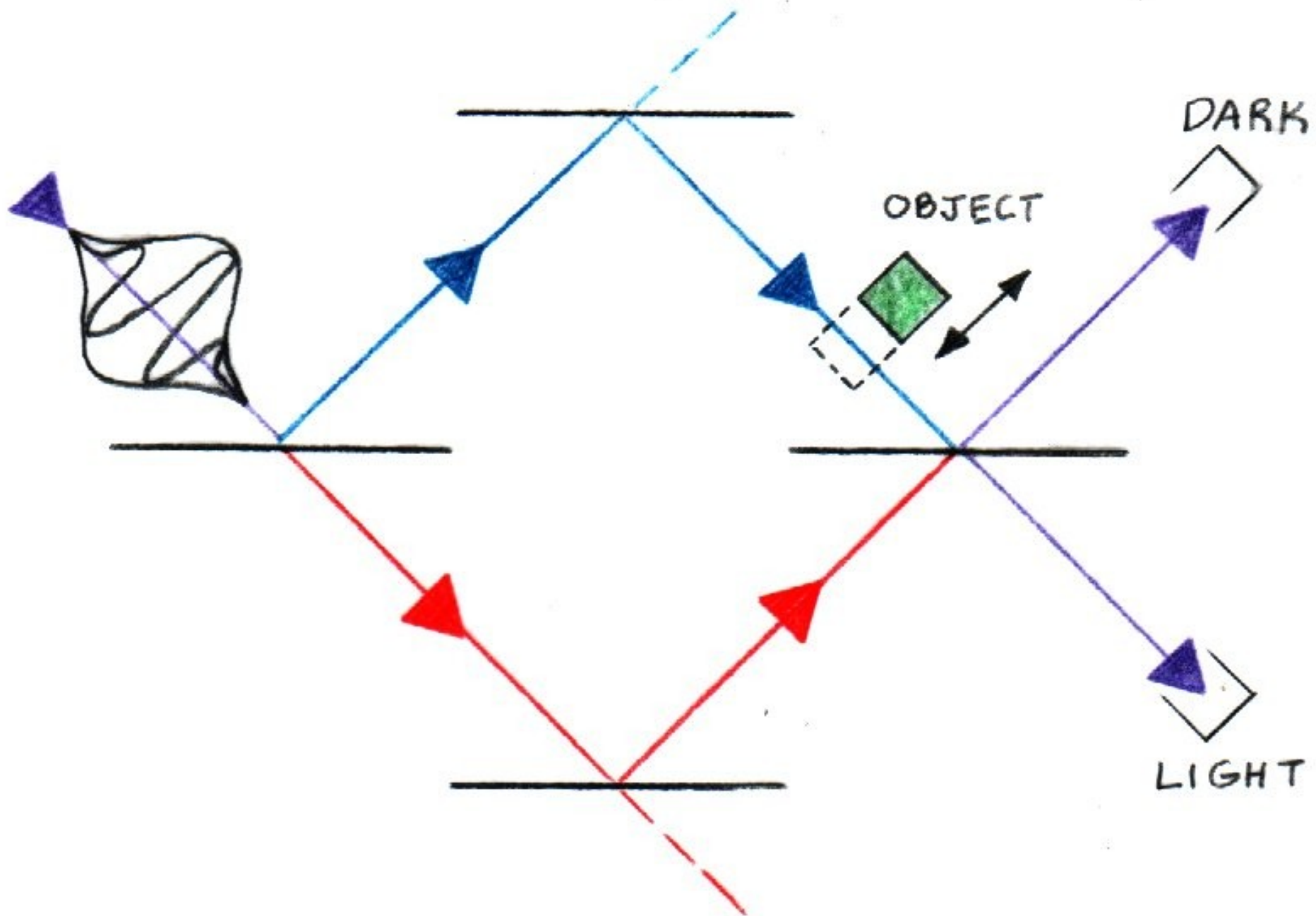
Wave interference patterns produced by monochromatic laser light diffracting through a triple slit aperture for various intensities – L.Page ([www.vias.org/physics](http://www.vias.org/physics)). This is a dramatic illustration of wave-particle duality.

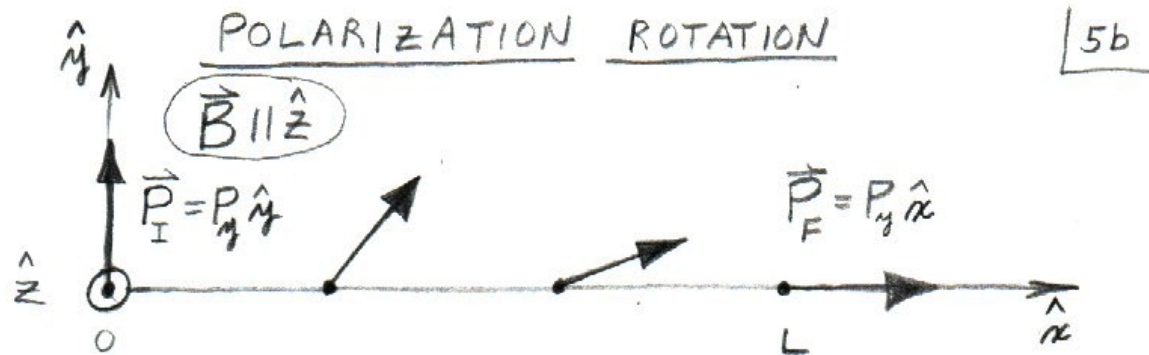
# Young's Double Slit Experiment



**Figure 6**

**Intensity Distribution of Fringes**





$$\psi = \underbrace{C_+ e^{i m_{x+} k_{0x} x}}_{C_+} \begin{pmatrix} 1 \\ 0 \end{pmatrix} + \underbrace{C_- e^{i m_{x-} k_{0x} x}}_{C_-} \begin{pmatrix} 0 \\ 1 \end{pmatrix}$$

$$C_{\pm}(x) = C_{\pm} [\cos(m_{x\pm} k_{0x} x) + i \sin(m_{x\pm} k_{0x} x)]$$

$\frac{1}{\sqrt{2}}$

$$P_x(x) = 2 \operatorname{Re}(C_+^* C_-) = \cos[(m_{x-} - m_{x+}) k_{0x} x]$$

$$P_y(x) = 2 \operatorname{Im}(C_+^* C_-) = \sin[(m_{x-} - m_{x+}) k_{0x} x]$$

$$P_z(x) = |C_+|^2 - |C_-|^2 = 0$$

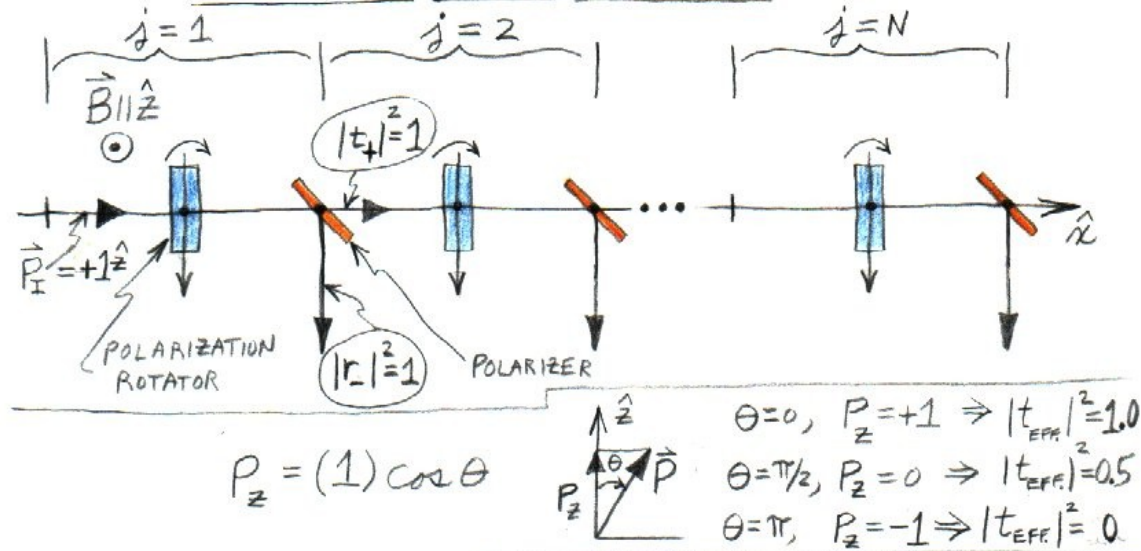
(Note that the  $z$  component of the polarization — along the quantization axis — remains unchanged at zero value through this rotation.)

$$(m_{x-} - m_{x+}) k_{0x} x =$$

$$\left[ \sqrt{1 - \frac{2m\mu B}{(\hbar k_{0x})^2}} - \sqrt{1 + \frac{2m\mu B}{(\hbar k_{0x})^2}} \right] k_{0x} x$$

$$\approx \frac{2m\mu B}{(\hbar k_{0x})^2} k_{0x} x$$

# QUANTUM ZENO EFFECT



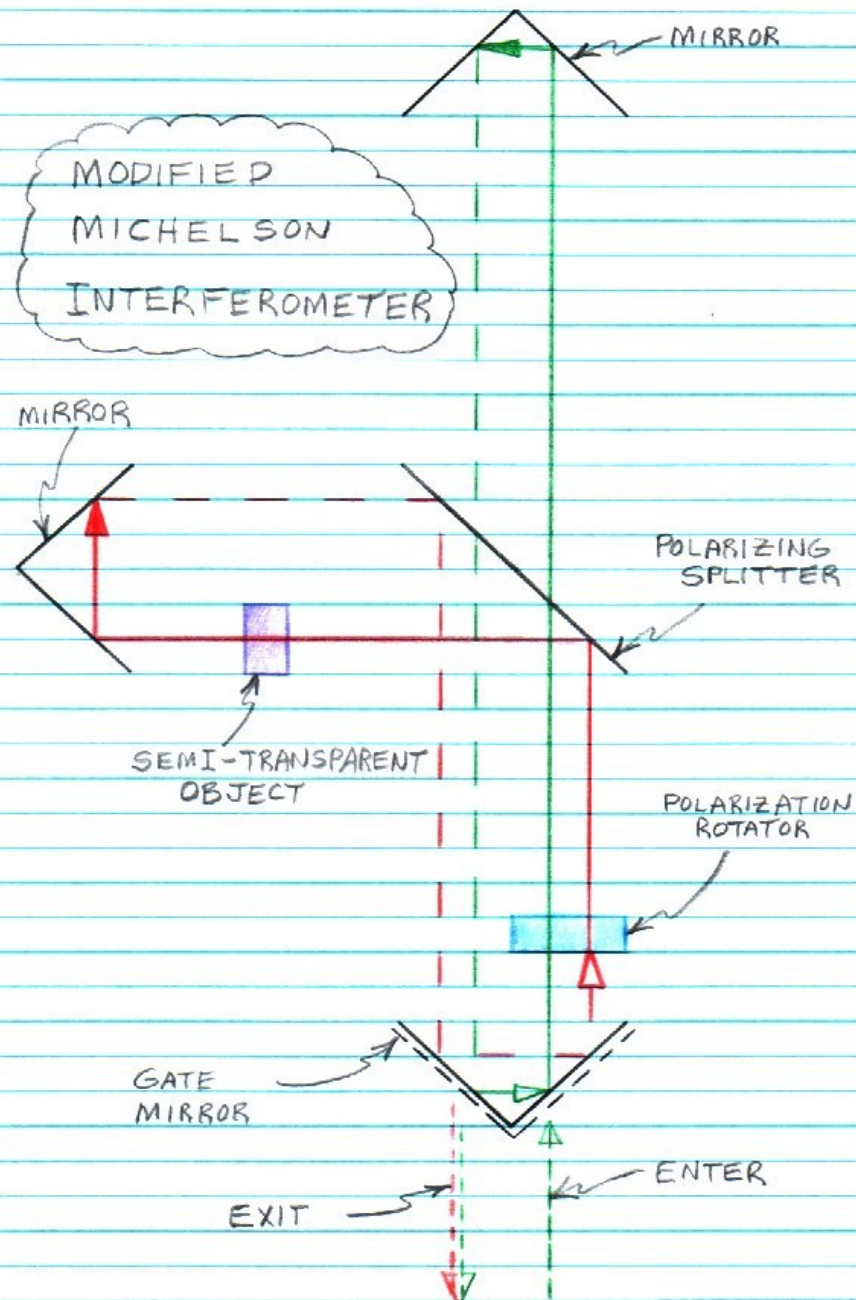
$$P_z = |C_+|^2 - |C_-|^2 ; \quad |C_+|^2 + |C_-|^2 = 1$$

$$\text{THEREFORE, } P_z = |C_+|^2 - [1 - |C_+|^2] = 2|C_+|^2 - 1$$

$$\text{BUT } P_z = \cos \theta$$

$$\text{THUS } |C_+|^2 = \left[ \frac{1 + \cos \theta}{2} \right] = \text{EFFECTIVE TRANSMISSION FOR ONE PAIR}$$

NET ANGLE ALWAYS $180^\circ$	$\theta$	$N$	$\left[ \frac{1 + \cos \theta}{2} \right]^N = \text{EFFECTIVE TRANSMISSION FOR } N \text{ PAIRS IN SERIES}$
	$180^\circ$	1	0
	$90^\circ$	2	0.25
	$30^\circ$	6	0.66
	$15^\circ$	12	0.81
	$5^\circ$	36	0.93
	$1^\circ$	180	0.98



$$T_c \equiv |t_c|^2 = N_F / N_I$$

$$\frac{\partial T_c}{\partial N_F} = \frac{1}{N_I} \quad ; \quad \frac{\partial T_c}{\partial N_I} = \frac{-N_F}{N_I^2}$$

$$\therefore, \text{ USING, AGAIN, } \Delta N_F = \sqrt{N_F} \text{ AND } \Delta N_I = \sqrt{N_I},$$

$$\left( \frac{\Delta T_c}{T_c} \right)^2 = \frac{N_I + N_F}{N_F N_I}$$

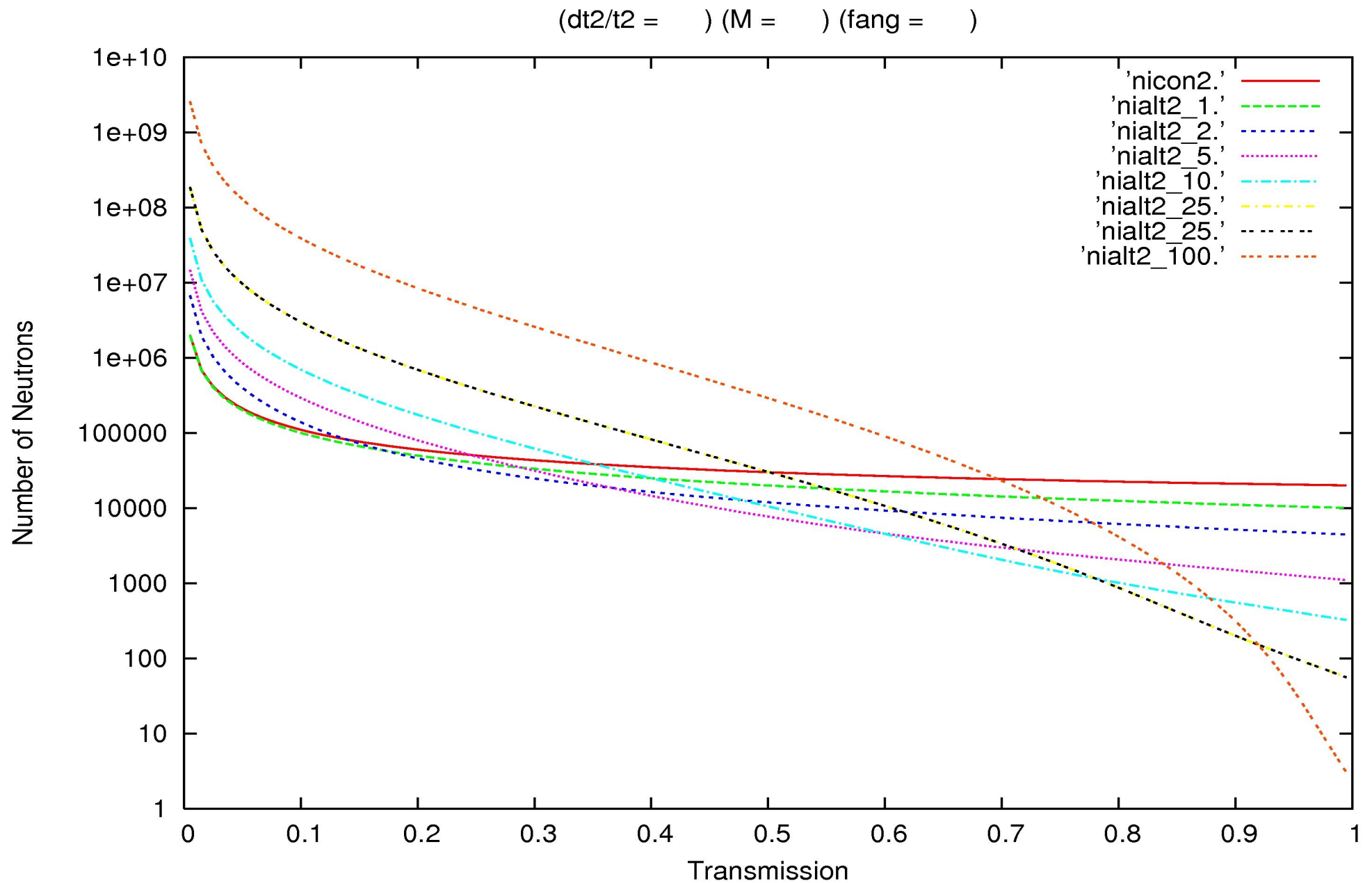
$$\text{USING } N_F = T_c N_I$$

$$N_I = \frac{T_c (1 + T_c)}{(\Delta T_c)^2}$$

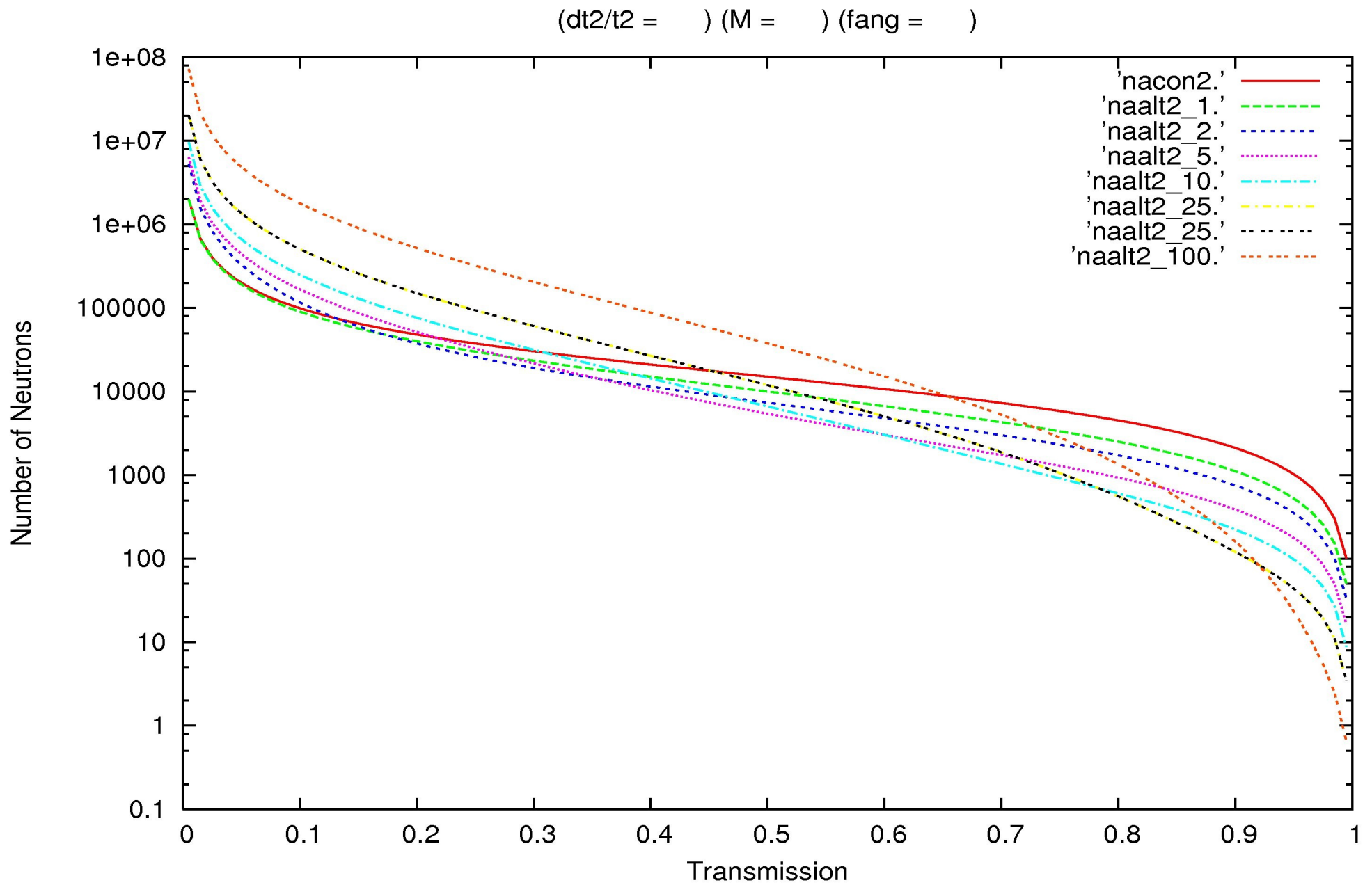
Number of neutrons required to obtain a given transmission  $T$  and corresponding uncertainty  $dT$  in a conventional measurement.

TABLE II.

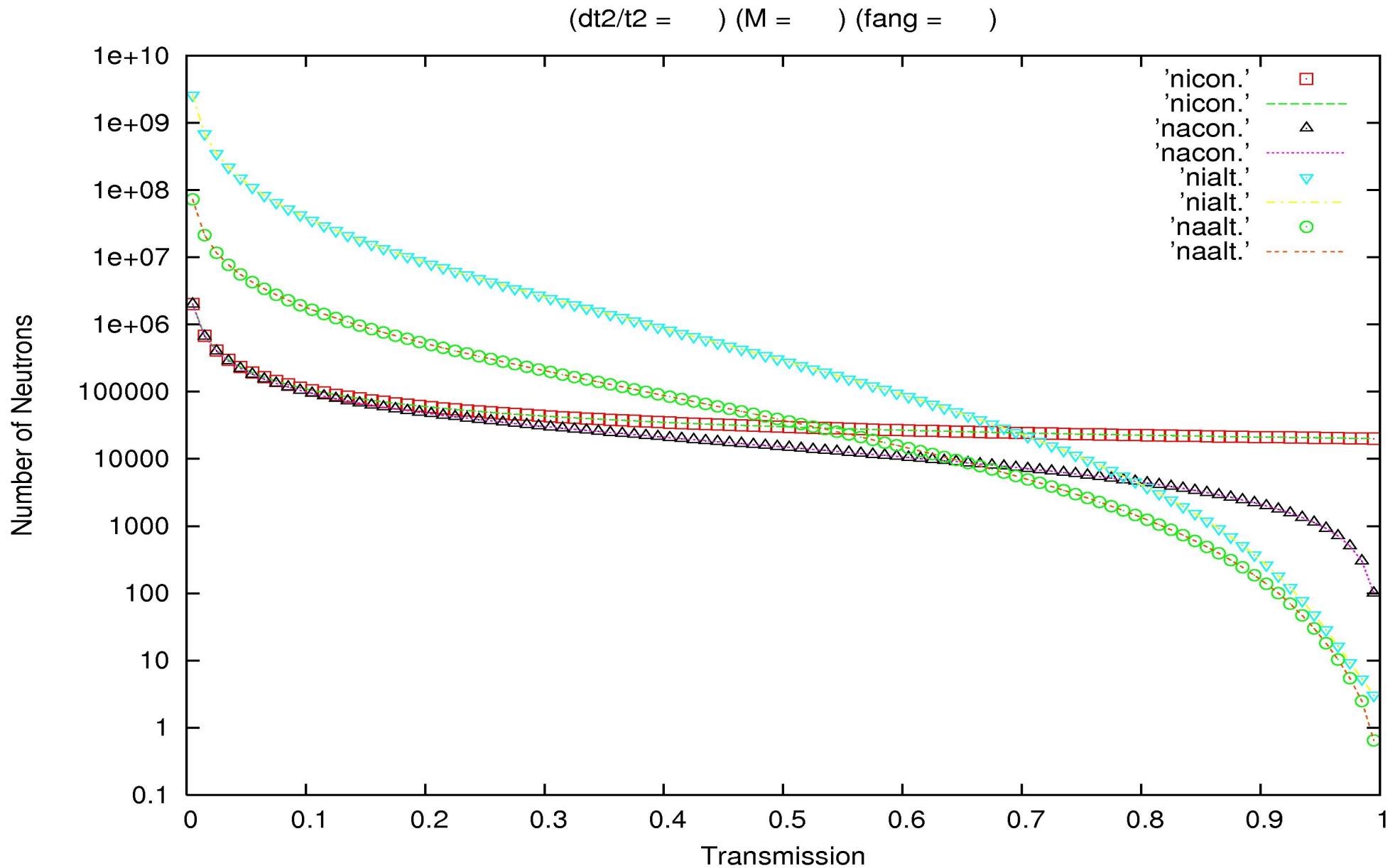
FIRST CYCLE	BEFORE ROTATION (INITIAL) $\psi_{Ij=1} = (1)\begin{pmatrix} 1 \\ 0 \end{pmatrix} + (0)\begin{pmatrix} 0 \\ 1 \end{pmatrix}$
	AFTER ROTATION $\psi_{ARj=1} = C\begin{pmatrix} 1 \\ 0 \end{pmatrix} + S\begin{pmatrix} 0 \\ 1 \end{pmatrix}$
	FINAL (END OF CYCLE) $\psi_{Fj=1} = C\begin{pmatrix} 1 \\ 0 \end{pmatrix} + tS\begin{pmatrix} 0 \\ 1 \end{pmatrix}$
SECOND CYCLE	$\psi_{Ij=2} = C\begin{pmatrix} 1 \\ 0 \end{pmatrix} + tS\begin{pmatrix} 0 \\ 1 \end{pmatrix}$
	$\psi_{ARj=2} = (C^2 - S^2t)\begin{pmatrix} 1 \\ 0 \end{pmatrix} + (SC + SCT)\begin{pmatrix} 0 \\ 1 \end{pmatrix}$
	$\psi_{Fj=3} = (C^2 - S^2t)\begin{pmatrix} 1 \\ 0 \end{pmatrix} + t(SC + SCT)\begin{pmatrix} 0 \\ 1 \end{pmatrix}$
THIRD CYCLE	$\psi_{Ij=3} = (C^2 - S^2t)\begin{pmatrix} 1 \\ 0 \end{pmatrix} + (SCt + SCT^2)\begin{pmatrix} 0 \\ 1 \end{pmatrix}$
	$\psi_{ARj=3} = [(C^3 - CS^2t) - (CS^2t + CS^2t^2)]\begin{pmatrix} 1 \\ 0 \end{pmatrix} + [(SC^2 - S^3t) + (SC^2t + SC^2t^2)]\begin{pmatrix} 0 \\ 1 \end{pmatrix}$
	$\psi_{Fj=3} = (C^3 - 2CS^2t - CS^2t^2)\begin{pmatrix} 1 \\ 0 \end{pmatrix} + t(SC^2 - S^3t + SC^2t + SC^2t^2)\begin{pmatrix} 0 \\ 1 \end{pmatrix}$
WHERE $C \equiv \cos\left(\frac{\epsilon}{2}\right)$ $S \equiv \sin\left(\frac{\epsilon}{2}\right)$ $t \equiv  t e^{i\phi_{t,0}}$	
& USING $\left\{ \begin{array}{l} C_{F+} = CC_{I+} - SC_{I-} \\ C_{F-} = SC_{I+} + CC_{I-} \end{array} \right\}$ FOR POLARIZATION ROTATION	



Number of incident neutrons required in an IFM to achieve  $dT/T = 0.01$  for various cycles  $m$ : red curve is for conventional transmission measurement.



Number of neutrons absorbed in an IFM required to achieve  $dT/T = 0.01$  for various cycles  $m$ : red curve is for conventional transmission measurement.



Transmission measurement with  $dT/T = 0.01$ : number of neutrons incident and absorbed in:  
a) IFM for  $m = 100$  cycles (blue and green curves respectively; b) conventional measurement (red and black curves, respectively).

# Summary and Conclusions

<> Phase-sensitive neutron specular reflectometry (NSR), employing references, enables direct inversion of composite reflectivity data sets to yield a unique scattering length density depth profile for an “unknown” film of interest, without fitting or any adjustable parameters. In a sense, phase-sensitive NSR with direct inversion is effectively a type of imaging.

<> Neutron reflectometry is a valuable probe of the structure of both hard and soft condensed matter in thin film or multilayered form -- particularly for hydrogenous and magnetic materials. NR can see *beneath* the surface and provide quantitative structural information from *everywhere within* the film on a nanometer scale.

<> “Interaction-Free Measurement” (IFM) is an interesting quantum phenomenon which might find application in NR -- further investigation, however, is needed.